On some control and observation issues related to high-precision positioning tables

Jérémy Malaizé

ED n°431: ICMS

N° attribué par la bibliothèque

THÈSE

pour obtenir le grade de
Docteur de l'École des Mines de Paris
Spécialité "Mathématiques et Automatique"

présentée et soutenue publiquement par
Jérémy MALAIZÉ

le 20 décembre 2007

Sur certains problèmes de commande et d'observation pour des tables de positionnement de haute précision

Directeur de thèse: Jean LÉVINE

Jury

M. BASTIN Georges	Président
M. EL GHAOUI Laurent	Rapporteur
M. STEINBUCH Maarten	Rapporteur
M. DESAILLY Roger	Examinateur
Mme. DURIEU Cécile	Examinatrice
M. LÉVINE Jean	Examinateur

Jérémy Malaizé

On Some Control and Observation Issues Related to High-Precision Positioning Tables

A mes parents.
Voyez ici le fruit de votre éducation.

Remerciements

Avant de commencer les travaux présentés dans ce manuscrit, j'imaginais naïvement qu'un directeur de thèse gérait tout, orientait tout, bref, que le thèsard suivait un guide. Trois ans et quelques mois plus tard, je suis ravi que les choses ne se soient pas du tout passées de la sorte. C'est une relation de travail qui s'est établie avec Jean. Une relation tout au long de laquelle j'ai pu faire preuve d'autonomie et de créativité. Je lui suis très reconnaissant d'avoir su, au cours de nos échanges, susciter la curiosité mais aussi recentrer mes activités. Je suis également redevable d'une ardoise d'expressos, que je ne serai jamais en mesure de rembourser. Puisse-t-il l'effacer, pour peu que je reconnaisse la supériorité des Mac.

Ces travaux répondent à des problématiques industrielles émises par Micro-Controle. J'y ai trouvé des personnes ouvertes au dialogue et en recherche d'innovation. Je pense évidemment à Roger Desailly pour la confiance, la liberté d'action et de pensée qu'il m'a accordées. Arnaud Deleu a su répondre de façon très réactive à mes besoins matériels, il m'a aussi apporté un œil extérieur bien utile lors de certaines phases expérimentales où l'enlisement guettait.

Je tiens également à souligner la disponibilité de Max et Caroline, pour m'avoir guidé dans les entrailles de la programmation, un domaine que je suis loin de connaître aussi bien que l'automatique. Je pense aussi au formidable enthousiasme de Laurent Praly, jamais réfractaire à s'impliquer dans mes réflexions ou à jeter sur un tableau des idées suscitant parfois plusieurs jours d'incrédulité.

En écrivant ces quelques lignes, j'ai une pensée très forte pour ma famille, et une émotion encore plus particulière pour mes proches qui, malheuresement, n'ont pu assister au dénouement de ces trois années de travail. Je ne remercie pas mes parents pour avoir contribué au contenu de ce manuscrit qui doit leur sembler bien mystérieux. Je les remercie pour m'avoir appris à ne pas baisser les bras et perséver, c'est ce qui leur donne à lire ces quelques lignes aujourd'hui.

Et une pensée amoureuse pour Alex...

Résumé — Dans cette thèse, on s'intéresse aux tables de positionnement de haute précision. Il s'agit de l'un des éléments essentiels des processus de fabrication de l'industrie du semi-conducteur. On aborde plus précisément les deux problèmes suivants: la conception d'un *algorithme d'initialisation* pour les moteurs synchrones sans balai, et la réalisation de correcteurs capables de *rejeter les perturbations spécifiques de ces systèmes*.

Pour les moteurs synchrones, l'initialisation consiste à estimer la phase initiale du champ magnétique. On considère que seules des mesures de déplacement sont disponibles, les mesures de courant n'étant pas accessibles. On suppose par ailleurs que les frottements, la charge ainsi que les paramètres du moteur, tel que son gain, ne sont pas connus. Compte tenu des frottements, la modélisation du système fait intervenir une équation différentielle à *second membre discontinu.* On conçoit des entrées en boucle ouverte adaptées pour obtenir la phase initiale en fonction de l'amplitude des déplacements mesurés pendant l'initialisation. L'estimation est basée sur une *classification complète des orbites périodiques* du modèle à second membre discontinu considéré, quelles que soient les valeurs des inconnues du problème. Afin de faciliter l'implémentation de l'algorithme dans un environnement temps réel, on propose une résolution approchée. On réalise alors une comparaison expérimentale de notre solution à une autre méthode, implémentable dans les mêmes conditions.

On s'intéresse ensuite au rejet des perturbations affectant ces tables de positionnement de haute précision. Il s'avère que ces systèmes présentent des *perturbations périodiques en fonction de la position*, et, que ces perturbations empêchent d'obtenir les niveaux de précision requis en terme de suivi de trajectoires. Malgré la nature non-linéaire de ce problème, on formule des conditions suffisantes à remplir par un *contrôleur linéaire instationnaire* afin de complètement rejeter ces perturbations et ainsi assurer la *convergence asymptotique globale* de l'erreur de suivi vers zéro. Ces conditions de stabilité sont obtenues par une analyse de perturbations régulières tirant partie des propriétés des *polynômes de Bell de second espèce*.

A l'aide d'un *observateur linéaire instationnaire* ne nécessitant que des mesures de position, on conçoit alors une loi de commande remplissant les conditions précédentes. Il est à noter que les équations définissant l'observateur sont obtenues en évaluant les perturbations non pas le long des trajectoires effectives, mais le long des trajectoires de référence. On utilise également le principe du modèle interne. On montre que le réglage des gains de l'observateur peut être effectué par des *optimisations sous contraintes LMI*, lesquelles optimisations n'ont besoin d'être réalisées qu'une seule fois hors ligne. Il n'y a que très peu de calculs à effectuer en ligne, notamment car le formalisme LMI permet d'aboutir à des gains constants. On propose alors plusieurs résultats expérimentaux pour illustrer les performances de notre méthode. On adresse plus particulièrement l'annulation du *cogging*, ainsi que le filtrage d'erreurs de mesures, plus connues sous le nom d'*erreurs d'interpolation*.

Abstract — In this work, our concern is the study of high-precision positioning systems. They are one of the core elements entering the manufacturing processes of the semiconductor industry. We are more specifically interested in two major issues: conceiving an initialization algorithm for brushless synchronous motors and designing a control scheme to reject disturbances peculiar to these systems.

The previously mentioned *initialization procedure* consists in estimating the initial phase of the magnetic field for brushless synchronous motors. Only displacement measurements are available (no current) while friction, load and motor parameters are supposed to be unknown. Because of friction, the system is modeled by a differential equation with a discontinuous right-hand side. Specific open-loop inputs are designed to get the initial phase as a function of the magnitude of the displacements along the corresponding trajectories. The estimation relies on a complete classification of the possible dynamical behaviors of the considered discontinuous right-hand side system with periodic input, whatever values the unknown parameters may take. For the sake of the online implementation, we propose an approximated formula of the initial phase. Some experimental results are given, together with a comparison of our method to an other technique that may be implemented in the same context.

We then move to the problem of rejecting a class of disturbances affecting the considered high-precision positioning tables. These systems turn out to feature *spatially periodic perturbations*, preventing them from achieving the required accuracy in terms of trajectory tracking. Despite the nonlinear nature of this problem, we derive sufficient conditions for a linear time-varying controller to entirely get rid of these disturbances and allow *global asymptotic convergence* of the tracking error to zero. Such stability conditions result from a regular perturbation analysis, carried out with the use of the *Bell polynomials of the second kind*.

We propose a linear time-varying observer-based controller that meets the previously mentioned stability conditions and only relies on position measurements. It is quite noteworthy that the observer equations are obtained by evaluating the spatially periodic perturbations along the desired trajectories, and not along the actual positions. We make use of the *LMI formalism* to cast the observer gains tuning issue into an optimization problem, subject to LMI constraints, carried out offline. Little computation is required online as the observer gains are constant. We then provide several experimental results to exhibit the performances of the proposed method. We namely address the experimental cancellation of *cogging forces*, as well as position measurements errors, known as *interpolation errors*.

Contents

Introduction

The products of the semiconductor industry take a larger and larger part in our everyday life. From the laptop used to typeset this manuscript, to the microchips embedded in cellulars, to the flat screens becoming more and more popular, we are clearly surrounded by this technology. Only a few initiated consumers are aware of what is concealed behind the ever growing megapixels specifications of a brand new digital camera for instance. Roughly speaking, these items are all manufactured in the same way, and, the machines required for this process are by far more hi-tech than any of the consumer electronics articles they produce. Given the growing demand for consumer electronics items with larger memory or more powerful signal processing engines, these machines are expected to achieve more and more stringent specifications. Our concern is to improve the behavior of such high-end machines tools. In some aspects, our contribution may be regarded as a background study whose eventual goal is to fulfill the headlong rush into ever more demanding megapixels, gigaoctets and gigahertz expectations.

These machines are for instance in charge of memory inspecting or wafer engraving. In the latter case, these systems are made up of valuable elements such as pristine glass lenses in charge of focusing a laser beam to engrave patterns on a silicon wafer. The wafer itself is mounted on a motorization device, namely a positioning table, able to perform stringent accuracy positioning with respect to the laser beam, the overall quality of the resulting chips is clearly at stake. To have a complete survey of this high technology machine, note it is located inside a clean room, namely, sealed and free from the least dust particles. This work aims at improving the previously mentioned positioning tables, especially regarding two major technological issues: the initialization and the rejection of a class of disturbances.

A classical initialization procedure, whose most obvious advantage is its simplicity, is achieved with constant electrical currents. In some situations, it generates large oscillations and takes a long time to compete. Shaky motions of this kind may not be suitable for some sensitive elements embedded in these systems. This point motivates the development of a new technique. The initialization algorithm we

propose generates imperceptible displacements, resulting from time-varying electrical currents. According to the experiments carried out on the considered motors, our method takes less time to complete and also offers a better accuracy than the classical procedure. Moreover, the proposed method enhances the functioning of the considered positioning tables, from an energy point of view.

It is also rather classical to drive positioning tables with a PID controller, to have the system tracking a reference trajectory. For technological reasons, existing disturbances are not entirely removed by a PID controller. They may be attenuated by using elements, namely actuators and sensors, of the highest quality. However, on the considered scale, the positioning tables still have a tendency to jerk along. Though minimal for some applications, it may alter the accuracy of the manufacturing processes. To have a good understanding of this phenomenon, and also to circumvent it, we model these perturbations as state-periodic functions acting on both the actuators and the sensors of positioning tables. The resulting modeling turns out to be nonlinear. Thanks to a regular perturbation analysis, we prove that an observer-based controller may be designed via a linear approximation of the previous nonlinear modeling. This control scheme allows the global stability of the tracking errors despite the perturbations and the proposed approximation. Our method turns out to cancel their harmful effects to the positioning of wafers beneath the laser beam. The performances of a least quality motor driven by this algorithm are close to the performances of a high-end motor driven by a PID controller. The even more interesting point is when one drives a high quality motor with this new control scheme, the solution performs upstream specifications, not necessarily required yet.

The previously detailed solutions are constrained to be implemented within the existing hardware architecture, that may not be turned upside down. Not only is this point fulfilled, but, the effectiveness of these algorithms is established via experiments carried out on production line systems. Note the proposed solutions are protected by industrial patents [33, 32] and already marketed or about to get so. Let us insist on the theoretical bases proving the results exposed hereafter and in [34, 35]. In view of an industrial use, it is particularly satisfactory to implement functions featuring theoretical justifications. We have also endeavored to propose convenient ways of tuning these techniques, like, for instance, the LMI optimization tools [10] used to determine some parameters.

This manuscript is organized as follows. In the chapter 1, we first give a detailed description of the systems entering the design of the considered high-precision positioning tables. We more specifically focus on the need for a performing initialization procedure, as well as on a description of the defects peculiar to both the sensors and actuators. It is showed that they generate state-periodic perturbations. The chapter 2 addresses the initial phase estimation problem for brushless synchronous motors. Only displacement measurements are used (no current) and friction, load and motor parameters are assumed unknown. Because of friction, the system is modeled by a differential equation with a discontinuous right-hand side. Open-loop inputs are designed to get the initial phase as a function of the magnitude of

the displacements along the corresponding trajectories. The estimation relies on a complete classification of the possible dynamical behaviors of the considered discontinuous right-hand side system with periodic input, whatever values the unknown parameters may take. We propose an estimation formula of the initial phase. Some experimental results are given, together with a comparison of our method to the preexisting procedure. In the chapter 3, we consider the integration of a linear system affected by state-periodic disturbances. To exhibit the solution of the corresponding nonlinear differential equation, our approach relies on the *Bell polynomials of the second kind*. They allow us to conduct a complete regular perturbation analysis, and, the integration is done via a power series expansion. We also derive sufficient conditions yielding *global asymptotic stability* of these systems. When these conditions are met, the state-periodic perturbations do not affect the evolution of the system. We turn this result into best account in the chapter 4, which addresses the high precision positioning of tables in presence of spatially periodic perturbation forces and measurements errors, namely cogging forces and interpolation errors. Using an internal model representation of these disturbances, an *observer-based controller* only relying on position measurements is derived. The key point is the use of the regular perturbation analysis of the chapter 3 to obtain the observer equations. Our solution guarantees global asymptotic convergence of the tracking errors to zero, although the observer is based on the first order approximation resulting from a regular perturbation analysis. The control scheme we come up with enables extremely accurate trajectory tracking by canceling the harmful effects of cogging forces and interpolation errors. The tuning of the observer gains is cast into some *LMI optimization problems*, allowing to set the desired performances of the system in closed loop. To assess the validity of our approach, experimental results conducted on production line linear brushless motors are presented in the chapter 5. Finally, for the sake of clarity, some points are presented in appendices. Some proofs required to the establish the orbits classification of the chapter 2 are presented in the appendix A. The appendix B defines the Bell polynomials of the second kind, and lists some of their main properties. In the appendix C, a review of the main results on analytical functions is drawn up.

CHAPTER 1

High-Precision Positioning Systems Description

1.1 Introduction

This chapter aims at giving a quick overview of the positioning systems used in the semiconductor industry, such as wafer-steppers for lithography process. These machines are intended to perform repetitive tasks at a high pace as the throughputs of the wafer fabs where they are set up directly rely on them. As illustrated hereafter, these cycles are typically made up of step-and-scan motion phases under stringent accuracy requirements. For instance, a step motion consists in performing a 10mm displacement within 200ms to eventually lie within a precision window 0.1μm wide. During scanning phases, systems are driven at constant speed, namely they have to track a reference trajectory moving as fast as 500mm/s while the considered accuracy specifications are at least as low as 1μm. These considerations may be interpreted through a more common example. According to stepping specifications, a commercial plane leaving Paris and heading for New-York would be required to arrive right in the center of the landing runaway. Now consider two planes (more presumably jet fighters) flying side by side at Mach 2, to have them fulfilling scanning specifications, their relative lateral displacements may not be larger than 1mm.
The framework of this study is the one depicted by the control architecture of figure 1.1. For technological reasons far beyond the scope of our work, the different algorithms proposed hereafter are constrained to be implemented within the so-called *position controller*. As a consequence, throughout all this work, the following assumptions remain true and they widely motivate most of our choices:

(i) We shall only assume relative position measurements available, and, even though technologically present, electrical currents may not be accessed. Optical resolvers, or absolute position sensors, are too expensive and hard to set up, we only consider optical incremental position sensors measuring relative displacements around the initial position.

(ii) Given the inner loop dedicated to current control, we shall hereafter suppose it is tuned in such a way that electrical currents instantaneously reach their desired values.

The different solutions we arrive at in the following may therefore be regarded as thrust or force control schemes for the systems depicted on figure 1.1 (by implicitly assuming currents to directly generate thrust). Let's now give a brief survey of the systems used in the design of high-precision positioning tables.

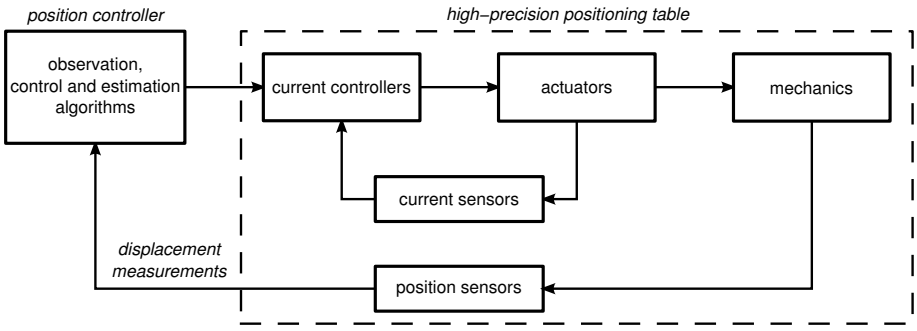

Figure 1.1: General context of the study.

1.2 Modeling of the systems used for high-precision positioning

1.2.1 Interpolation errors

Sticking to the assumptions mentioned in the introduction, a one-dimensional position sensor mounted on a motor (see figures 1.2 or 1.3 for instance) yields measurements of its displacements, hereafter referred to as d, around its initial position ξ_0, namely the position of the motor when first turned on. Obviously, if ξ is the actual position of the motor, the following relation holds:

$$\xi = \xi_0 + d. \tag{1.1}$$

Let's assume an estimate of ξ_0 is available and noted $\widehat{\xi_0}$[1].

Denoting by y the displacement measurements, the following relation holds:

$$y = d + w(\xi, t), \tag{1.2}$$

with w a periodic function of the absolute position ξ (as well as of the displacement itself) which is slowly time-varying. The function w models a phenomenon known as the interpolation error, which may be explained as follows by first giving a brief description of this sensor. Practically speaking, an optical scale is mounted on the fixed part of the motor. This scale features patterns equally spaced along a grating of period P' in the ξ-direction. On the moving part of the motor, an optical probe is in charge of counting the number of previous patterns and interpolate within a period P'. Its embedded electrical circuits generate the two following signals:

$$y_1 = a_1 \cos\left(\frac{2\pi}{P'}\xi\right) + b_1 \quad \text{and} \quad y_2 = a_2 \cos\left(\frac{2\pi}{P'}\xi\right) + b_2. \tag{1.3}$$

[1] Deriving such a value is addressed in the chapter 2.

First, it is rather obvious that, at most, this sensor is able to measure ξ modulo P'. Since the number of periods P' may be counted during a travel, the displacements recorded since the machine is on are obtained. The most basic way to process data resulting from (1.3) consists in computing the following value:

$$\eta = \frac{P'}{2\pi}\text{atan}\left(\frac{a_1\left(y_2 - b_2\right)}{a_2\left(y_1 - a_1\right)}\right).$$

However, the magnitudes (a_1 and a_2) and biases (b_1 and b_2) are likely to be slowly position dependent and time-varying. With no additional information, or corrupted values of a_1, a_2, b_1 and b_2, the equation (1.2) is thus derived from:

$$\eta = \xi + w(\xi, t) \mod P'.$$

Remark 1.1 *w is mainly made up of harmonic components of periods P' and $\frac{P'}{2}$ whose magnitudes are usually a few dozens nanometers. Moreover, P' is only a couple microns large, usually $4\mu m$, $10\mu m$ or $20\mu m$.*

1.2.2 Permanent magnet linear motors

When such stringent accuracy requirements are at stake, direct drive solutions are chosen to actuate these machines. They are capable of providing sufficient precision levels and needed smoothness of motion by getting rid of undesirable phenomena such as hysteresis, backlash or mechanical play. In the following, we are more specifically concerned with the use of brushless synchronous motors. They are preferred to other actuators such as DC motors, for, among other things, their longer life time, improved cleanliness of operation and better resistance to wear and tear. Note that we mainly focus on the use of linear motors even though our results may easily extend to rotary motors.

There are two kinds of permanent magnets linear motors, namely ironless (see figure 1.3 and picture 1.5) and ironcore motors (see figure 1.2 and picture 1.4). While ironless motors feature two magnetic tracks, made up of permanent magnets, ironcore motors trap and guide the magnetic field generated by only one track in the vicinity of the rotor windings. This cost-effective design spares the use of expensive and eventually superfluous rare earths magnets and yields more powerful motors. However, as we shall see later this design generates perturbation forces called cogging that significantly affects their performances, while, ironless motors, though much more expensive, turn out to be significantly less affected by cogging.

1.2.3 Thrust expression

Whatever motors we consider, the expressions of the force directly generated by the electrical currents turn out to be the same. The modeling proposed hereafter, though pertaining to two-phase motors, may extend to those with three-phase windings.

Referring to the figures 1.2 and 1.3, a track made up of permanent magnets creates a magnetic field assumed to be sinusoidal with respect to the position. Respectively note B_0 and P the magnitude and

spatial period of the magnetic field, and let l be the length of the active windings so that the electrical phase #1 creates a force F_1:

$$F_1 = i_1 l B_0 \sin\left(\frac{2\pi}{P}\xi\right) + (-i_1) l B_0 \sin\left(\frac{2\pi}{P}(\xi - \frac{P}{2})\right) = K i_1 \sin\left(\frac{2\pi}{P}\left(d + \xi_0\right)\right), \tag{1.4}$$

with $K = 2lB_0$ the motor gain, i_1 the electrical current in phase #1, d the displacements around the initial position ξ_0 as given by the definition (1.1). By calculations similar to (1.4), the force created by the second electrical phase is derived:

$$F_2 = K i_2 \cos\left(\frac{2\pi}{P}\left(d + \xi_0\right)\right), \tag{1.5}$$

with i_2 the electrical current value in phase #2.

Thanks to the current controller, the currents are actually given by:

$$i_1 = i_1^* + \delta i_1 \quad \text{and} \quad i_2 = i_2^* + \delta i_2, \tag{1.6}$$

where i_1^* and i_2^* are commands and δi_1 and δi_2 model time-varying currents offsets.

The field-oriented method consists in driving the currents according to:

$$i_1^* = I(t) \sin\left(\frac{2\pi}{P}\left(d + \widehat{\xi}_0\right)\right) \quad \text{and} \quad i_2^* = I(t) \cos\left(\frac{2\pi}{P}\left(d + \widehat{\xi}_0\right)\right), \tag{1.7}$$

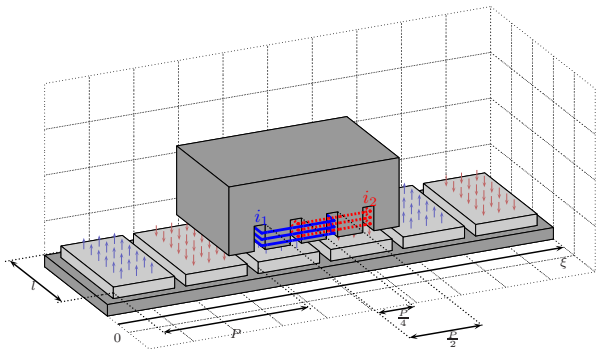

Figure 1.2: Schematic view of a two-phase ironcore motor.

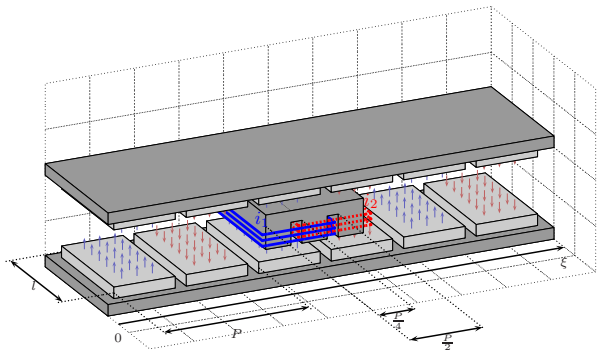

Figure 1.3: Schematic view of a two-phase ironless motor.

Figure 1.4: Picture of the considered two-phase ironcore motor.

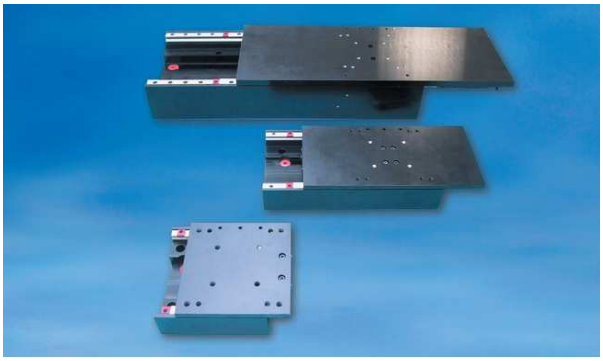

Figure 1.5: Picture of the considered two-phase ironless motor.

where I is the only input to the current controller and $\widehat{\xi}_0 + d$ matches (1.1) with the use of an available estimate of the initial position. Combining the equation (1.7) together with (1.4) and (1.5) yields the expression of the global thrust F_e caused by the currents:

$$F_e = F_1 + F_2 = K\cos(\varphi_0 - \widehat{\varphi}_0)\, I + K\sin\left(\frac{2\pi}{P}\xi\right)\delta i_1 + K\cos\left(\frac{2\pi}{P}\xi\right)\delta i_2, \tag{1.8}$$

where φ_0, called the initial phase of the magnetic field seen by the rotor (*initial phase* in short), and $\widehat{\varphi}_0$ an estimated value of φ_0 are given by:

$$\varphi_0 = \frac{2\pi}{P}\xi_0 \quad \text{and} \quad \widehat{\varphi}_0 = \frac{2\pi}{P}\widehat{\xi}_0. \tag{1.9}$$

Remark 1.2 *Let's now be more concrete in highlighting the need for a precise initial phase determination. The controllable thrust created by the windings is expressed as:*

$$K\cos(\varphi_0 - \widehat{\varphi}_0)\, I,$$

and, thus, $\widehat{\varphi}_0$ is different from φ_0, the actual thrust is less than the expected one, KI. This may affect both the stability and the optimal use of the motors from an energy point . For a given reference current I, as soon as the estimation error $\varphi_0 - \widehat{\varphi}_0$ is non-zero, the motor does not deliver the maximal accessible thrust. To reach a desired power, the user may then have to require larger currents. The term $\cos(\varphi_0 - \widehat{\varphi}_0)$ is called the efficiency of the motor. Once the estimation is carried out, the motor is intended to be controlled in closed loop from the position measurements. It is then rather sensible to assume $\cos(\varphi_0 - \widehat{\varphi}_0) \approx 1$. If the estimation error actually turns out to be greater than $\frac{\pi}{2}$, applying a negative feedback will jeopardize the overall stability of the system.

Remark 1.3 *For the experiments conducted hereafter, the magnetic pitch of the ironless motor is $P = 42mm$, while for the ironcore motor $P = 24mm$.*

1.2.4 Cogging forces

Cogging forces are due to the interaction of the magnetic field with the ferromagnetic material of the rotor. Allowing for the periodic layouts of both the magnets and slots where rotor windings are located, cogging forces are shown to be spatially periodic perturbations, see [53, 54, 55]. If we denote by $F_c(\xi)$ the cogging forces, supposed to be periodic with respect to the position ξ, the global thrust F of the motor is then given by $F = F_e + F_c$ which may be rewritten in:

$$F = K_m\cos(\varphi_0 - \widehat{\varphi}_0)\, I + \Gamma(\xi, t), \tag{1.10}$$

where $\Gamma(\xi, t) = F_c(\xi) + \delta i_1 \sin\left(\frac{2\pi}{P}\xi\right) + \delta i_2 \cos\left(\frac{2\pi}{P}\xi\right)$ is periodic with respect to ξ and slowly time-varying. Roughly speaking, under the effects of both cogging and currents offsets, the considered motors have a tendency to stabilize at specific positions so as to minimize magnetic energy.

Remark 1.4 *The magnitude of the cogging force directly relies on the amount of ferromagnetic material used to build the rotor. As illustrated on the figure 1.2, to trap the magnetic field, ironcore motors require a lot of this material. This generates cogging forces much larger than witnessed for ironless motors. Actually, the motors of the figure 1.3 are only affected by currents offsets and to a much more limited extent by cogging.*

Remark 1.5 *Some studies emphasize the role of symmetry breakings in the appearance of cogging forces. The finite length of the rotor as well as slots (see figure 1.2), where windings are embedded, are some of the design parameters inducing cogging forces. Each of them yields position periodic forces with a specific spatial period, which, in the case of the finite length of the rotor turns out to be* $\frac{P}{2}$*. Since* P *is usually a few dozens millimeters large, cogging forces are slowly varying with respect to the position but may have quite large magnitudes.*

1.2.5 Mechanical description

We now move on to the mechanical modeling of the considered positioning devices. The equations presented hereafter are greatly inspired by [7, 6]. Despite their apparent simplicity, the convincing experimental results presented in the chapter 5 are entirely based on these modelings. For some applications, it may be necessary to allow for high frequency mechanical modes. For the considered experimental testbed, interpolation errors and cogging forces turned out to be the most limiting disturbances, as a consequence, these are the only disturbances taken into account. However, especially regarding the cancellation of spatially periodic perturbations, the chapters 3 and 4 are presented in a very general way, so that other modeling featuring additional mechanical defects may fall under the scope of the presented work.

Fixed base

Denote by m the moving mass attached to the motor. From the expression of the forces created by the motor (see (1.10)), applying the well-known fundamental principle of mechanics yields the following system with control I and measurement y:

$$\begin{aligned} \ddot{\xi} &= u + d(\xi,t) - \frac{\mu}{m}\dot{\xi} - \frac{f}{m}\text{sign}\left(\dot{\xi}\right) \\ u &= \frac{K}{m}\cos\left(\varphi_0 - \widehat{\varphi}_0\right) I \\ y &= \xi + w(\xi,t). \end{aligned} \tag{1.11}$$

It is moreover assumed that the motor is attached to a fixed frame and:

- μ and f respectively model viscous and dry frictions,
- given the equation (1.10), $d(\xi,t) = \Gamma(\xi,t)/m$.

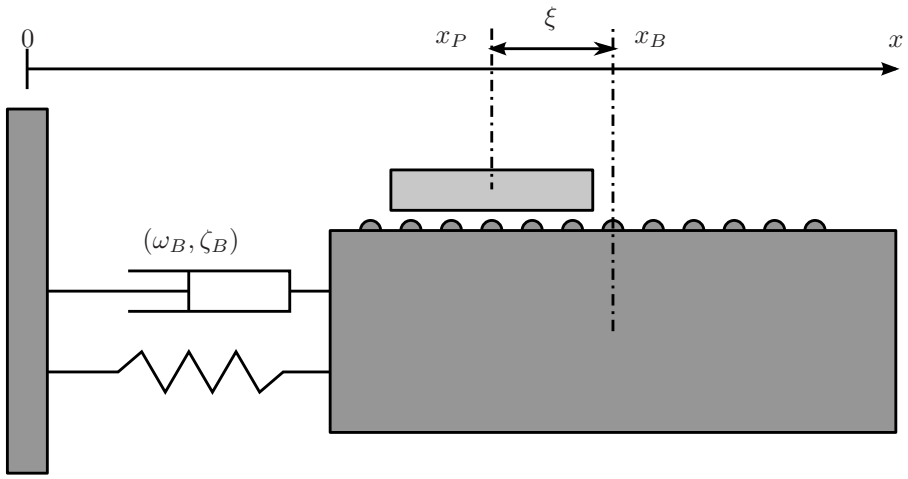

Figure 1.6: Linear motor mounter on a moving base.

Moving base

The systems to be considered now are represented on the figure 1.6. The motor is mounted on a moving base of mass M, whose movements with respect to a fixed frame are modeled by a second order linear system with pulsation ω_B and damping ratio ζ_B. The thrust given by (1.10) both acts on the moving part of the motor $(+F)$ and the moving base $(-F)$. If we use the previous notations, together with $\xi = x_P - x_B$, the following equations model the system depicted on figure 1.6:

$$\begin{aligned}
\begin{pmatrix} \dot{\xi} \\ \ddot{\xi} \\ \dot{x}_B \\ \ddot{x}_B \end{pmatrix} &= \begin{pmatrix} 0 & 1 & 0 & 0 \\ 0 & -\frac{\mu}{m} & \omega_B^2 & 2\zeta_B\omega_B \\ 0 & 0 & 0 & 1 \\ 0 & 0 & -\omega_B^2 & -2\zeta_B\omega_B \end{pmatrix} \begin{pmatrix} \xi \\ \dot{\xi} \\ x_B \\ \dot{x}_B \end{pmatrix} + \begin{pmatrix} 0 \\ \frac{m+M}{mM} \\ 0 \\ \frac{-1}{M} \end{pmatrix} \left(u + d(\xi, t) - \frac{f}{m}\text{sign}\left(\dot{\xi}\right) \right) \\
u &= \frac{K}{m}\cos\Big(\varphi_0 - \widehat{\varphi}_0\Big) I \\
y &= \xi + w(\xi, t).
\end{aligned} \tag{1.12}$$

The optical scale and the probe are respectively attached to the moving base and the rotor of the motor. As a consequence, the available measurements y are the relative displacements of the motor above the moving base.

Remark 1.6 *Some representative values for the previous system are the following:*

$$m = 10kg, \quad M = 1000kg, \quad \zeta_B = 0.2, \quad \omega_B = 2\pi \times 5 rads^{-1}.$$

CHAPTER 2

Brushless Synchronous Motors Initialization

2.1 Introduction

We are concerned with getting the electrical currents in phase with the position of the motor coils inside the magnetic field while sticking to the framework presented in the chapter 1 (see the figure 1.1). For DC motors (with brushes), current commutations, as well as initialization, are performed mechanically, while, for brushless motors (without mechanical contact), additional measurements and an algorithm are required for the currents and the magnetic field to be in phase. This is exactly the purpose of the so-called initialization procedure without which the electrical currents may not be driven according to the equation (1.7). Moreover, as underlined with the remark 1.2, this initialization has to performed very accurately. The method proposed hereafter uses only displacement measurements to determine the initial rotor position (modulo the magnetic pitch) for brushless synchronous motors.

When it comes to reducing the number of sensors for economical reasons, current sensors are usually preferred to position encoders. Several papers address sensorless control of synchronous motors, namely the determination of the initial rotor position from current measurements. Some existing techniques consist in using an observer to estimate the back-electromotive force induced in the coils, see [18] and [30] for example. Other approaches determine the motor windings inductance by injecting either specific carrier-frequency signals ([39], [43] and [37]) or no signal at all ([27] and [38]). Both these techniques rely on current measurements to determine an electrical variable in phase with the magnetic field.

As described in the chapter 1, for applications featuring very demanding positioning precision, incremental position sensors are prevailing, they only provide relative displacements around the initial position. According to the general framework set by the figure 1.1, we propose a method that provides an autonomous current controller (whose current measurements are not made available to the initialization algorithm) with specific inputs computed offline and simply get the corresponding displacement measurements back

to estimate the initial rotor position. This estimation scheme spares the use of additional and eventually unnecessary Hall effect sensors.

An existing solution, falling under the scope of this context, consists in maintaining the electrical current to a constant value in an electrical phase, and wait for the mechanical equilibrium. The corresponding position shift is then used to compute an estimate of the initial phase. Unfortunately, before stabilizing, erratic oscillations around the equilibrium position are witnessed. These movements are as large as the magnetic pitch (typically a couple of millimeters according to the remark 1.3) and cannot be avoided. This behavior might not be suitable for the aforementioned high precision applications. From now on, this method is referred to as the classical method.

The method to be presented can be tuned to generate arbitrarily small magnitude displacements (a couple of microns). According to the framework 1.1, neither magnetic field nor currents have to be fed to the algorithm and the motor parameters are unknown (gain, load and friction). In these conditions, our method features an accurate initial phase estimation with little computation, which eases real-time implementation.

In the following, we shall derive the relation between the initial phase, the other unknown parameters and the magnitude of the displacements when the system is driven by a periodic and open-loop input. This analysis entirely relies on an exhaustive classification of the periodic orbits of the considered motors under forced oscillations (section 2). It is more precisely shown how the friction, modeled by a discontinuous function of the speed (which gives rise to a discontinuous right-hand side system in the sense of Filippov, see [22]), affects the trajectories followed by the system. The measured displacements are then compared with those predicted by the classification, and, thanks to an approximation, the initial position is obtained (section 3). In section 4, experimental results are provided to consolidate the different assumptions and show that our initialization procedure outperforms the so-called classical method.

2.2 Periodic orbits and dry friction

Prior to addressing the estimation problem pointed out in the previous introduction, a much more theoretical study is required. Throughout this section, we are concerned with integrating a parameter-dependent system featuring a discontinuous right-hand side. The main difficulty arises from the possible sliding motion on the discontinuity surface. As illustrated in the next section, when a brushless motor is driven by a periodic input, by using appropriate changes of coordinates, this study is of prime interest to relate the magnitude of the measured displacements to the magnetic field phase when its load and gain, as well as friction are unknown.

2.2.1 Periodic orbits classification

We are concerned with the study of the following system:

$$y'' = u - \lambda \text{sign}\,(y')\,, \tag{2.1}$$

where u is the command, λ a positive scalar, and, this system is furthermore assumed to be initially at rest.

Let y_0 and y_1 be two scalars, we define the function y_r by:

$$\forall \tau,\ 0 \leq \tau \leq 1, \quad y_r(\tau) = y_0 + (y_1 - y_0)\left(6\tau^5 - 15\tau^4 + 10\tau^3\right). \tag{2.2}$$

Let u_0 be given by:

$$\forall \tau,\ 0 \leq \tau \leq 1, \quad u_0(\tau) = y_r''(\tau) \Big/ y''_{\max} \quad \text{and} \quad y''_{\max} = \max_{0 \leq \tau \leq 1} |y_r''(\tau)|. \tag{2.3}$$

The command u is built by intervals of length 1 according to:

$$\forall k \geq 0, \quad I_k = [k,\ k+1], \quad \forall \tau \in I_k, \quad u(\tau) = (-1)^k\, u_0(\tau - k). \tag{2.4}$$

This part aims at integrating the equation (2.1) driven by the command u for any $\lambda > 0$. Since this system features a discontinuous right-hand side, one has to allow for two kinds of behaviors, according to [22]:

- whenever $y' < 0$ or $y' > 0$, the sign function is constant,
- if $y' = 0$, the system slides on the discontinuity surface $y' = 0$ as long as $|u(\tau)| \leq \lambda$.

The command is bounded by 1. If $\lambda \geq 1$, the system remains indefinitely at rest. The following theorem completely classifies the periodic orbits of period 2 for any λ such that $0 \leq \lambda \leq 1$.

Theorem 2.1

For any λ between 0 and 1, the system (2.1)*, initially at rest and driven by the command u defined by the equation* (2.4)*, features a unique attractive periodic orbit of period 2. There exist two scalars λ_1 and λ_2 with $0 < \lambda_1 \leq \lambda_2 \leq 1$, depending only on the expression of u_0 given by* (2.3)*. They define three and only three possible behaviors:*

(i) $0 \leq \lambda \leq \lambda_1$: The system asymptotically reaches an orbit along which no sliding motion on $y' = 0$ occurs (see simulation results on figure 2.1).

(ii) $\lambda_1 < \lambda \leq \lambda_2$: Within a period, the system reaches a periodic orbit along which two sliding motion phases occur (see simulation results on figure 2.2).

(iii) $\lambda_2 < \lambda \leq 1$: Within a period, the system reaches a periodic orbit along which four sliding motion phases occur (see simulation results on figure 2.3).

The proof of this theorem requires several definitions and properties to be given. Each of the cases enumerated in the theorem are then proved for the command u based on the polynomial function y_r. However, our findings are presented in a broad context, and, the proposed approach is likely to cope with any other elementary function y_r.

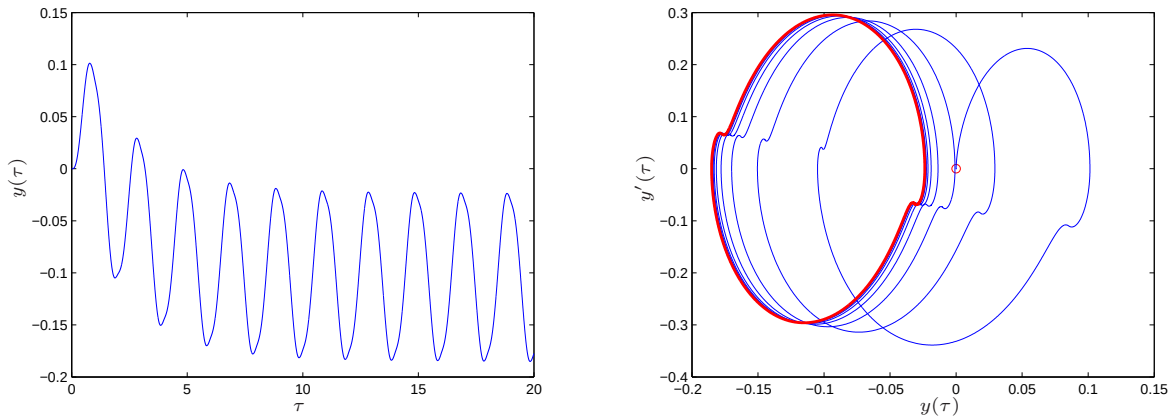

Figure 2.1: Trajectories versus time and in the state-space domain for the system (2.1) with $0 \leq \lambda \leq \lambda_1$.

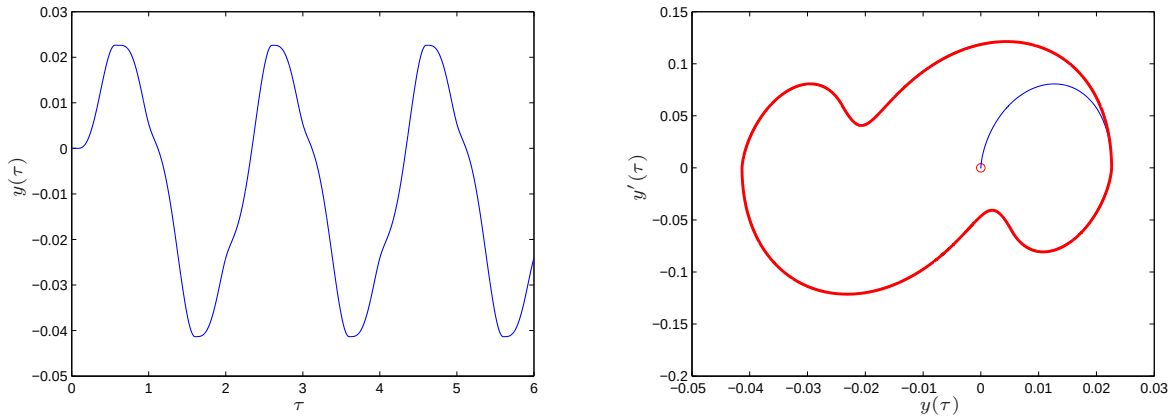

Figure 2.2: Trajectories versus time and in the state-space domain for the system (2.1) with $\lambda_2 \leq \lambda \leq \lambda_1$.

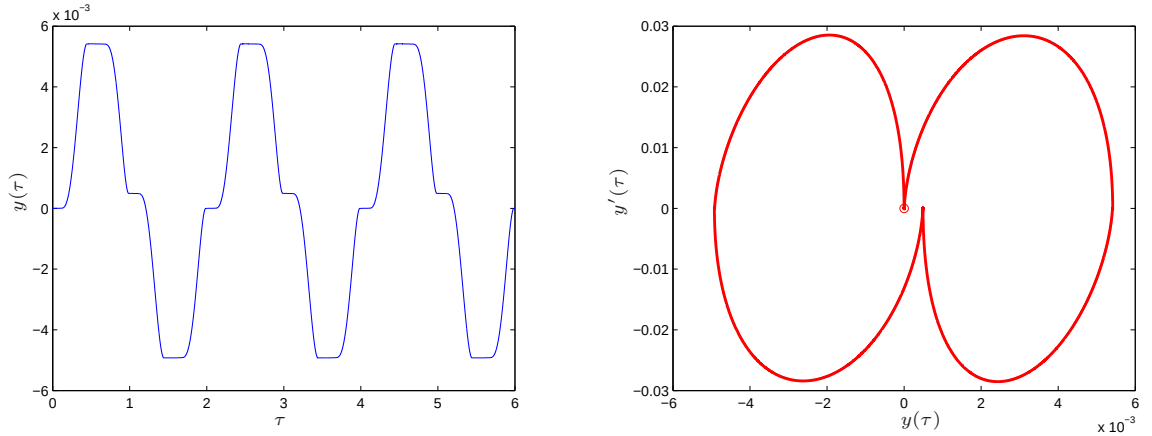

Figure 2.3: Trajectories versus time and in the state-space domain for the system (2.1) with $\lambda_2 \leq \lambda \leq 1$.

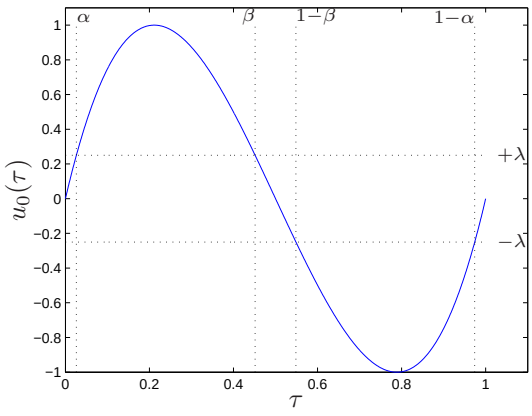

Figure 2.4: Plot of u and the roots α, β.

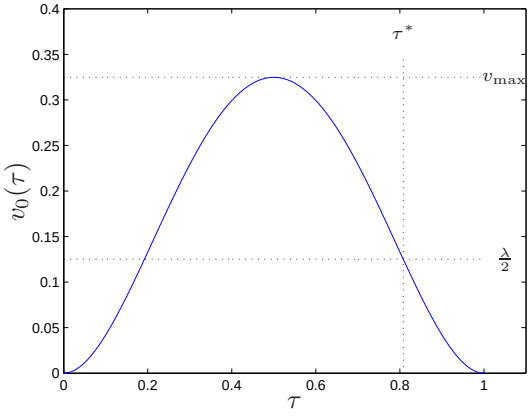

Figure 2.5: Plot of v_0 and τ^*.

2.2.2 Preliminaries

Let first give some definitions of crucial interest for the following.

Definition 2.1 *As illustrated on the figure 2.4, for any λ lying between 0 and 1, let α and β be the roots located in $[0,\ 1/2]$ of the equation $u_0(\tau) = \lambda$.*

Remark 2.1 *Since u_0 is antisymmetric with respect to $1/2$, the following relation holds:*

$$u_0(1-\alpha) = u_0(1-\beta) = -\lambda.$$

Definition 2.2 *We define v_0 by integrating u_0, more precisely $v_0(t) = \int_0^t u_0(t')dt'$. The function v_0 is plotted on the figure 2.5. It can be seen that v_0 is symmetric with respect to $1/2$, increasing on $[0, 1/2]$ and then decreasing on $[1/2, 1]$. Let $v_{\max} = v_0(1/2)$ be its maximal value.*

Definition 2.3 *Let f_λ, g_λ and h_λ be the following functions:*

$$\forall \tau, 0 \leq \tau \leq 1, \quad f_\lambda(\tau) = v_0(\tau) - \lambda\tau, \quad g_\lambda(\tau) = v_0(\tau) + \lambda\tau, \quad h_\lambda(\tau) = -f_\lambda(1-\tau) = -v_0(\tau) - \lambda\tau + \lambda. \quad (2.5)$$

Remark 2.2 *We compute the derivatives of these functions with respect to τ:*

$$f'_\lambda(\tau) = u_0(\tau) - \lambda, \quad g'_\lambda(\tau) = u_0(\tau) + \lambda, \quad h'_\lambda(\tau) = -u_0(\tau) - \lambda.$$

According to the definitions of α and β together with the figure 2.4, the variations of these functions are given by the figure 2.6.

Remark 2.3 *For a different function y_r, the same variations as those of the figure 2.6 would be derived provided u_0 were still antisymmetric with respect to $1/2$ and there were only two roots α and β to the equation $u_0(\tau) = \lambda$ on $[0, 1/2]$.*

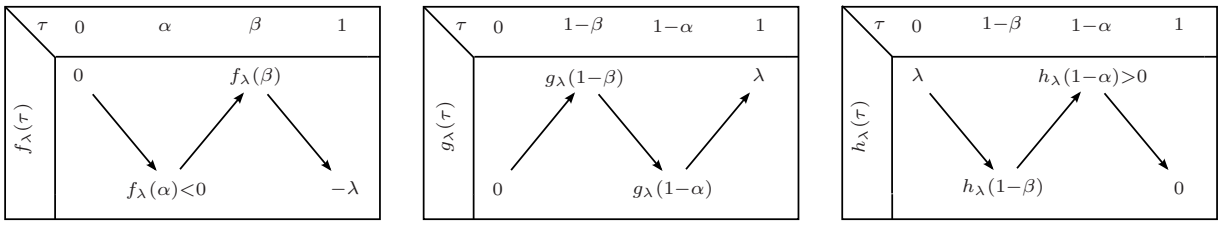

Figure 2.6: Variations of the functions f_λ, g_λ and h_λ.

Definition 2.4 *If $\lambda \leq 2v_{\max}$, τ^* is defined as the unique root lying between $1/2$ and 1 of the equation $f_\lambda(\tau^*) = h_\lambda(\tau^*)$. Actually, τ^* satisfies the relation:*

$$\frac{1}{2} \leq \tau^* \leq 1, \quad v_0(\tau^*) = \frac{\lambda}{2}. \tag{2.6}$$

Remark 2.4 *Note that:*

$$h_\lambda(\tau^*) = \lambda \left(\frac{1}{2} - \tau^* \right) \leq 0.$$

Since h_λ is positive between $1-\alpha$ and 1 (see figure 2.6), τ^* may not be greater than $1-\alpha$. It results that τ^* is a decreasing function of λ (see figure 2.5) located between $1/2$ and $1-\alpha$.

We now set out two properties whose respective proofs are given by the figures 2.7 and 2.8. These plots are specific to the polynomial function y_r in the equation (2.2), however, the same curves could be obtained for any other function y_r.

Property 1 *There exists a scalar $\lambda_1 > 0$ such that if $0 \leq \lambda \leq \lambda_1$:*

$$1 - \beta \leq \tau^* \leq 1 - \alpha,$$

while, if $\lambda_1 < \lambda \leq 2v_{\max}$:

$$\frac{1}{2} \leq \tau^* < 1 - \beta.$$

For the function u_0 defined by (2.3), $\lambda_1 = 0.58$.

Property 2 *There exists a scalar $\lambda_2 > 0$ such that if $0 \leq \lambda \leq \lambda_2$:*

$$f_\lambda(\alpha) + f_\lambda(\beta) \geq 0$$

while if $\lambda_2 < \lambda \leq 1$:

$$f_\lambda(\alpha) + f_\lambda(\beta) < 0.$$

For the function u_0 defined by (2.3), $\lambda_2 = 0.71$.

In order to prove the theorem 2.1, we shall deal with the following issues:

- studying τ_0 solving the equation $f_\lambda(\tau_0) = f_\lambda(\alpha)$,
- studying the mapping from x to y according to $g_\lambda(y) = g_\lambda(x)$,

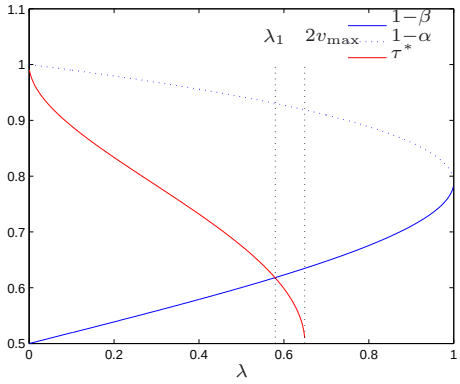

Figure 2.7: Existence of λ_1 introduced in the property 1.

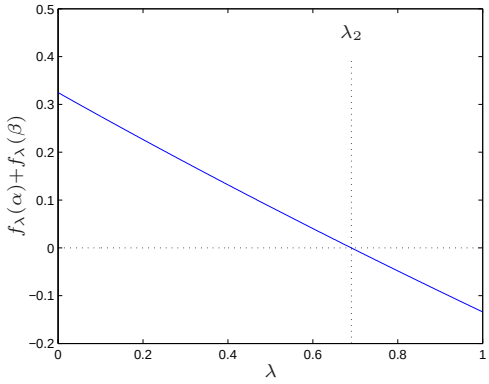

Figure 2.8: Existence of λ_2 introduced in the property 2.

- studying the mapping from x to y according to $f_\lambda(y) = h_\lambda(x)$.

These points are discussed hereafter in several properties. The properties 1 and 2 entirely rely on the expression of y_r (equation (2.2)) to get the plots of the figures 2.7 and 2.8. From now, we give results as general as possible in that they do not necessarily depend upon the function y_r. In the end, the approach we propose hereafter to integrate (2.1) may easily be carried out for any other y_r. For simplicity's sake, the sometimes tedious proofs of these properties are reported in the appendix A.

Property 3 *For all λ such that $\lambda \geq \lambda_1$, if $\tau_0 > \alpha$ solves the equation $f_\lambda(\tau_0) = f_\lambda(\alpha)$, then τ_0 belongs to the interval $[\beta, 1-\beta]$.*

Property 4 *For any λ such that $\lambda \leq \lambda_1$, if the relation $f_\lambda(\alpha) \geq f_\lambda(\tau^*)$ holds, one may build an interval I_λ satisfying the properties:*

(i) *I_λ is included in $[1-\beta, 1-\alpha]$,*

(ii) *τ^* (given by the equation (2.6)) belongs to I_λ,*

(iii) *for any $x \in I_\lambda$, the equation $f_\lambda(y) = h_\lambda(x)$ admits a unique root y in the interval $[0,1]$, y belongs to I_λ.*

Property 5 *For any λ such that $\lambda \leq \lambda_1$, we consider the intervals I_λ of the property 4 and we define the series u_n by:*

- $u_0 \in I_\lambda$,
- $\forall n \geq 0, \quad f_\lambda(u_{n+1}) = h_\lambda(u_n)$.

For all $n \geq 0$, $u_n \in I_\lambda$ and the numerical series u_n converges to τ^*, the root of the equation (2.6).

Property 6 *For any λ between λ_1 and λ_2, the equation $f_\lambda(y) = h_\lambda(1-\beta)$ has only one root, denoted by y, in the interval $[0,1]$, moreover y belongs to $[1-\beta, \beta]$.*

Property 7 *For any λ such that $\lambda \leq \lambda_1$, consider the intervals I_λ defined by the property 4, for all $x \in I_\lambda$, the equation $g_\lambda(y) = g_\lambda(x)$ has no root y in $[x, 1]$.*

Property 8 *For any λ such that $\lambda \leq \lambda_2$, the equation $g_\lambda(y) = g_\lambda(1-\beta)$ has no root y in $[1-\beta, 1]$.*

Property 9 *For any $\lambda \geq \lambda_2$,*

- *If $h_\lambda(1-\beta) \leq 0$, the equation $f_\lambda(y) = h_\lambda(1-\beta)$ has a unique root y in $[0, \alpha]$ while the equation $g_\lambda(z) = g_\lambda(1-\beta)$ has no root z in $[1-\beta, 1]$.*
- *If $h_\lambda(1-\beta) \geq 0$, the equation $g_\lambda(z) = g_\lambda(1-\beta)$ has a unique root z in $[1-\beta, 1]$ while $f_\lambda(y) = h_\lambda(1-\beta)$ has no root y in $[0, \alpha]$.*

2.2.3 Orbits of the first kind

On the figure 2.9 we can see that, for $\lambda \leq \lambda_1$, $f_\lambda(\alpha)$ is greater than $> f_\lambda(\tau^*)$. For the specific function y_r, we may then make use of the intervals I_λ defined by the property 4. We shall moreover be interested in the series τ_n and τ'_n that we define on each intervals I_n (given by (2.4)) as follows:

- the speed y' of the system (2.1) vanishes in $\tau = nT + \tau_n$,
- the system (2.1) slides on the discontinuity surface $y' = 0$ from $nT + \tau_n$ to $nT + \tau'_n$.

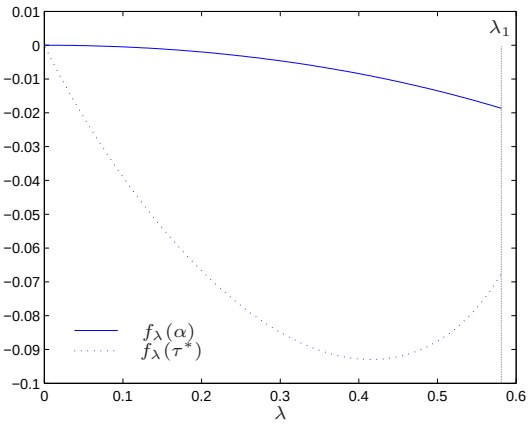

Figure 2.9: Plots of $f_\lambda(\alpha)$ and $f_\lambda(\tau^*)$.

The proof of the lemma 2.1 is also the proof of the point (i) of the theorem 2.1.

Lemma 2.1 *For any λ such that $\lambda \leq \lambda_1$, if the system (2.1), initially at rest, is driven by u (given by (2.4)), for all $n \geq 1$, $\tau'_n = \tau_n$ and τ_n converges to τ^* defined by (2.6).*

PROOF:

According to the plot of the figure 2.4 and the definitions of α and β, the system leaves the discontinuity surface in $\tau = \alpha$. Until the next cancellation of the speed supposed to happen in $\tau = \tau_0$, it operates

with positive velocity. As a consequence:

$$y'(\tau_0) - y'(\alpha) = 0 = \int_{\alpha}^{\tau_0} (u_0(t') - \lambda)\, dt' = f_\lambda(\tau_0) - f_\lambda(\alpha). \tag{2.7}$$

According to the property 3, two situations may occur:

- τ_0 belongs to $[\beta, 1-\beta]$. In this case, when the velocity vanishes, the input is not large enough to leave the discontinuity surface. Referring to the figure 2.4, a sliding motion phase happens until $\tau_0' = 1-\beta$ where u equals $-\lambda$.

- τ_0 belongs to $[1-\beta, 1-\alpha]$ where the command u is larger than friction λ as depicted on the figure 2.4. The system simply goes through the discontinuity surface and $\tau_0' = \tau_0$.

The velocity y' takes negative values until the next velocity cancellation, which may occur either between τ_0' and 1 or for τ greater than 1. Consider the first case, we are looking for x, with $\tau_0' < x < 1$, such that:

$$y'(x) - y'(\tau_0') = 0 = \int_{\tau_0}^{x} (u_0(t') + \lambda)\, dt' = g_\lambda(x) - g_\lambda(\tau_0').$$

Using the property 7, since $\tau_0' \in I_\lambda$, the previous equation has no root in $[\tau_0', 1]$. The next time y' vanishes necessarily happens for τ greater than 1. Suppose this is the case in $1+\tau_1$ with τ_1 satisfying the following relation:

$$\begin{aligned} y'(1+\tau_1) - y'(\tau_0') &= \int_{\tau_0'}^{1+\tau_1} u(t')dt' + \lambda(1+\tau_1-\tau_0') \\ &= \int_{\tau_0'}^{1} u_0(t')dt' + \int_0^{\tau} (-u_0(t'))\, dt' + \lambda(1+\tau_1-\tau_0') \\ &= h_\lambda(\tau_0') - f_\lambda(\tau_1) = 0. \end{aligned} \tag{2.8}$$

According to the property 4, there is a unique root τ_1 fulfilling the equation (2.8), and τ_1 belongs to I_λ. Since I_λ is included in $[1-\beta, 1-\alpha]$, where $|u| \geq \lambda$, we have $\tau_1' = \tau_1$.
We shall now prove the following assumption by induction:

$(\mathcal{H}_n) \quad \tau_{n-1}' \in I_\lambda, \quad f_\lambda(\tau_n) = h_\lambda(\tau_{n-1}')$

We have already proved that $\mathcal{H}_1$ is valid. Suppose now that $n = 2p$ and $\mathcal{H}_{2p}$ is fulfilled. According to the definition of the intervals I_λ (see property 4), if $\tau_{2p} \in I_\lambda \subset [1-\beta, 1-\alpha]$, the system simply crosses the discontinuity surface in $2p+\tau_{2p}$ and thus $\tau_{2p}' = \tau_{2p}$. The command u is built in such a way that the velocity becomes negative in $2p+\tau_{2p}'$. As previously discussed to derive τ_1, the velocity may either vanish between $2p+\tau_{2p}'$ and $2p+1$ or beyond $2p+1$. Consider the first case, we are looking for

τ between τ_{2p} and 1 solution of $y'(2p+\tau)=0$, τ is given by:

$$\begin{aligned} y'(2p+\tau)-y'(2p+\tau_{2p}) &= \int_{2p+\tau_{2p}}^{2p+\tau}(u(t')+\lambda)\,dt' \\ &= \int_{\tau_{2p}}^{\tau}(-1)^{2p}u_0(t')dt'+\lambda\,(\tau-\tau_{2p}) \\ &= g_\lambda(\tau)-g_\lambda(\tau_{2p})=0. \end{aligned}$$

We use the property 7 to conclude that, since $\tau_{2p}\in I_\lambda$, there is no root to the previous equation between τ'_{2p} and 1. The next time the velocity equals zero happens in $2p+1+\tau_{2p+1}$ such that

$$\begin{aligned} y'\left(2p+1+\tau_{2p+1}\right)-y'\left(2p+\tau_{2p}\right) &= \int_{\tau_{2p}}^{1}\left((-1)^{2p}u_0(t')+\lambda\right)dt'+\int_0^{\tau_{2p+1}}\left((-1)^{2p+1}u_0(t')+\lambda\right)dt' \\ &= h_\lambda(\tau_{2p})-f_\lambda(\tau_{2p+1})=0. \end{aligned} \tag{2.9}$$

This proves the assumption $(\mathcal{H}_{2p+1})$. The same reasoning would apply for $n=2p+1$, except one would replace λ by λ and u_0 by $-u_0$ whenever this quantity would be used. According to the property 5, since $\tau'_1=\tau_1\in I_\lambda$:

$$\forall n\geq 1,\quad \tau'_n=\tau_n,\quad \tau_n\to\tau^*. \tag{2.10}$$

2.2.4 Orbits of the second kind

The series τ_n and τ'_n still have the same meanings. The following lemma may be seen as the proof of the point (ii) of the theorem 2.1.

Lemma 2.2 *For any λ between λ_1 and λ_2, if the system (2.1) is initially at rest and driven by the command u of the equation (2.4), for all $n\geq 1$, $\tau'_n=1-\beta$ and $\tau_n=\tau$ the unique root on $[0,1]$ of the equation $f_\lambda(\tau)=h_\lambda(1-\beta)$.*

Proof:

The property 3 ensures that τ_0 belongs to the interval where u is smaller than friction λ. This implies that sliding occurs until $\tau'_0=1-\beta$. Let's now find out whether the next speed cancellation happens before or after 1. In the first case, this amounts to exhibiting τ between $1-\beta$ and 1 such that $g_\lambda(\tau)=g_\lambda(1-\beta)$. The previous equation does not have any roots of this kind as suggested by the property 8. Our task consists then in finding τ_1 such that $y'(1+\tau_1)=0$, this boils down to solving the following equation:

$$y'(1+\tau_1)-y'(\tau'_0)=\int_{\tau'_0}^{1}(u_0(t')+\lambda)\,dt'+\int_0^{\tau_1}(-u_0(t')+\lambda)\,dt'=f_\lambda(\tau_1)-h_\lambda(1-\beta)=0.$$

The unique root τ_1 belongs to $[\beta,1-\beta]$ as provided by the property 6. The system slides on the discontinuity surface until $1+\tau'_1$, namely as long as $|u|$ is smaller than λ. We basically have $\tau'_1=1-\beta$ and the situation is similar to the situation in $\tau'_0=1-\beta$, apart from the fact that $u(1+\tau'_1)=-u(\tau'_0)$.

It is then obvious that:

$$0 \leq \tau \leq 1 \,/\, f_\lambda(\tau) = h_\lambda(1-\beta), \quad \tau_n = \tau, \quad \tau'_n = 1-\beta, \quad \forall n \geq 0. \tag{2.11}$$

2.2.5 Orbits of the third kind

The series τ_n and τ'_n still bear the same meanings. Consider furthermore ε_n and ε'_n defined by:

- the velocity of the system (2.1) is non zero from $n+\tau'_n$ to $(n+1)+\varepsilon_n$ and from $(n+1)+\varepsilon'_{n+1}$ to $(n+1)+\tau_{n+1}$,
- sliding on the discontinuity surface occurs between $(n+1)+\varepsilon_n$ and $(n+1)+\varepsilon'_{n+1}$.

As illustrated hereafter, ε_n may sometimes take negative values while ε'_n is always greater than zero. The following lemma may be regarded as the proof of the point (iii) of the theorem 2.1.

Lemma 2.3 *For any λ such that $\lambda \geq \lambda_2$, if the system is initially at rest and driven by the command u defined by the equation (2.4), for all $n \geq 0$, $\varepsilon'_n = \alpha$, $\tau'_n = 1-\beta$, $\tau_n = \tau_0$ defined in the property 3 and ε_n is derived from the unique root resulting from the property 9.*

PROOF:

In view of the property 3, τ_0 belongs to $[\beta, 1-\beta]$ and $\tau'_0 = 1-\beta$. We split this study according to the two cases of the property 9:

- $h_\lambda(1-\beta) \leq 0$: Let τ be the next time the speed vanishes. If τ belonged to the interval $[1-\beta, 1]$, the equation $g_\lambda(x) = g_\lambda(1-\beta)$ would have a root in that interval. From the property 9, we know that may not occur. Necessarily $x \geq 1$, and we rewrite it into $1+\varepsilon_0$ with ε_0 solving $f_\lambda(\varepsilon_0) = g_\lambda(1-\beta)$. The smallest ε_0 satisfying this equation belongs to $[0, \alpha]$ and is also unique according to the property 9. The system may not leave the discontinuity surface before the command becomes larger than friction. Basically, it happens in $1+\alpha$ and thus $\varepsilon'_1 = \alpha$. The steady state is thus reached before $\tau = 2$ and four sliding motion phases occur along the orbit:

$$0 \leq \varepsilon \leq \alpha \,/\, f_\lambda(\varepsilon) = h_\lambda(1-\beta), \quad \tau_n = \tau_0, \quad \tau'_n = 1-\beta, \quad \varepsilon'_n = \alpha, \quad \varepsilon_n = \varepsilon, \quad \forall n \geq 0. \tag{2.12}$$

- $h_\lambda(1-\beta) \geq 0$: The next speed cancellation occurs before 1. Actually, as suggested by the property 9, the equation $g_\lambda(1-\beta) = g_\lambda(\varepsilon)$ may be solved for ε between $1-\alpha$ and 1, while $f_\lambda(\varepsilon) = h_\lambda(1-\beta)$ may no longer be solved on $[0, \alpha]$. The system remains at rest until $1+\alpha$. As previously, the steady state is reached within one period and four sliding motion phases happen along the orbit. Moreover, one defines:

$$1-\alpha \leq \varepsilon \leq 1 \,/\, g_\lambda(\varepsilon) = g_\lambda(1-\beta), \quad \tau_n = \tau_0, \quad \tau'_n = 1-\beta, \quad \varepsilon'_n = \alpha, \quad \varepsilon_n = \varepsilon - 1, \quad \forall n \geq 0. \tag{2.13}$$

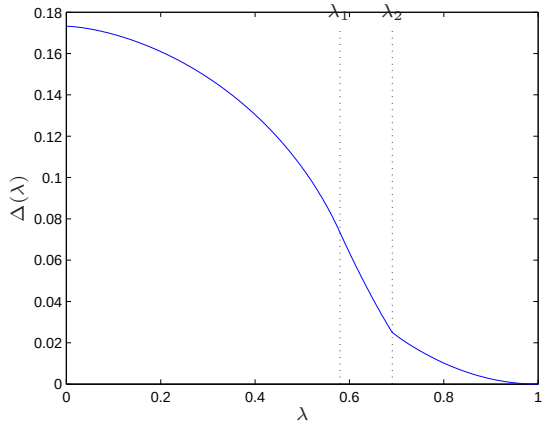

Figure 2.10: Magnitude of the displacements in steady state.

2.2.6 Integration despite dry friction

For any λ, the system reaches a periodic orbit. One may then integrate (2.1) twice to derive the maximal magnitude of the displacements in steady state. Let $\Delta(\lambda)$ represent this quantity. For any λ, in steady state, the velocity is less than zero before $2p+1+\tau_{2p+1}$, equals zero in $2p+1+\tau_{2p+1}$, remains constant at zero until $2p+1+\tau'_{2p+1}$, and then, at least locally, becomes negative beyond $2p+1+\tau'_{2p+1}$. The position thus reaches a local minimum in $2p+1+\tau'_{2p+1}$. Using some rather similar considerations, one may show that the position is locally maximal in $2p+2+\tau_{2p+2}$.

$$\Delta(\lambda) = \lim_{n\to\infty} \left| y(n+1+\tau_{n+1}) - y(n+\tau'_n) \right| = \lim_{p\to\infty} \Big(y(2p+2+\tau_{2p+2}) - y(2p+1+\tau'_{2p+1}) \Big). \quad (2.14)$$

Note that for $\lambda \geq \lambda_2$, even if the velocity may equal zero between $2p+2+\varepsilon_{2p+1}$ and $2p+2+\varepsilon'_{2p+2}$, its sign does not change. This is only an inflexion point, and the relation (2.14) is well valid for $\lambda \geq \lambda_2$. In steady state, if we use the equations (2.10) for $\lambda \leq \lambda_1$, (2.11) for $\lambda_1 \leq \lambda \leq \lambda_2$ and the equations (2.12) and (2.13) for $\lambda_2 \leq \lambda \leq 1$, integrating (2.1) twice is easily conducted and the function $\Delta(\lambda)$ of the equation (2.14) is plotted on the figure 2.10.

2.3 Estimation procedure

2.3.1 Brushless synchronous motors in steady state

From now on and until the end of this chapter, we consider that the mechanical behavior of the considered motors is given by the very simplified modeling:

$$\ddot{\xi} = \frac{K}{m}\cos(\varphi_0 - \varphi)\, I(t) - \frac{f}{m}\text{sign}\left(\dot{\xi}\right), \quad (2.15)$$

that we have come up with according to the elements reported in the remark 2.5. The notations remain the same as in the chapter 1, and, moreover I and φ may be set to any desired values. This chapter is

intended to estimating φ_0 from the only measurements of the displacements $d = \xi - \xi_0$ around the initial position.

In view of the equation (2.2), y_0 and $y_1 > y_0$ are two scalars, and we also consider a length of time $T > 0$ so that the function $I(t)$ is defined as follows:

$$\forall k \geq 0, \quad \forall t,\, kT \leq t \leq (k+1)T, \quad I(t) = (-1)^k\, y_r\left(\frac{t-kT}{T}\right) \widehat{m}/\widehat{K}, \tag{2.16}$$

where $\widehat{m}$ and $\widehat{K}$ are rough estimated values of respectively the mass and the gain of the motor. Let η be the following rate $\eta = K\widehat{m}/\left(\widehat{K}m\right)$, measuring to what extent $\widehat{m}$ and $\widehat{K}$ are corrupted. The value of η is thus supposed unknown.

Let δ be the magnitude of the displacements in steady state when the command given by the equation (2.16) is applied to the motor (2.15). The following quantities will also be used in the following:

$$\ddot{\xi}_{\max} = y''_{\max}/T^2, \quad \mu = m\eta\,|\cos(\varphi_0 - \varphi)|\,\ddot{\xi}_{\max}/f, \quad \varepsilon = \operatorname{sign}(\cos(\varphi_0 - \varphi)). \tag{2.17}$$

The theorem to be proved hereafter states that, under the effect of the $2T$-periodic function $I(t)$, the motor reaches a periodic orbit of period $2T$ and the expression of the displacements in steady state is derived.

Theorem 2.2

The system (2.15) *driven by the command given by the equation* (2.16) *reaches a* $2T$*-periodic orbit along which the magnitude of the displacements is given by:*

$$\delta = \varepsilon\eta\cos(\varphi_0 - \varphi)\, y''_{\max}\Delta\left(\frac{1}{\mu}\right), \tag{2.18}$$

with Δ *plotted on the figure 2.10.*

PROOF:

Let τ be the reduced time $\tau = t/T$. The equation (2.15) may be written with respect to τ. Recalling the definition of the interval I_{2p} by the equation (2.4), if τ belongs to this interval, one has:

$$d'' = \eta\cos(\varphi_0 - \varphi)\, y''_r - \frac{fT^2}{m}\operatorname{sign}(d'),$$

where d' and d'' stand for the first and second derivative of $d(\tau T)$ with respect to τ. We now divide both sides of the previous equation by $\eta\,|\cos(\varphi_0 - \varphi)|\, y''_{\max}$ and use the notations (2.17) at the same time. The equation (2.15) is rewritten in:

$$y'' = u - \mu^{-1}\operatorname{sign}(y'), \tag{2.19}$$

where u defined by the equation (2.4) and $y = \dfrac{d}{\eta\,|\cos(\varphi_0 - \widehat{\varphi}_0)|\, y''_{\max}}$. The theorem 2.1 classifies the

periodic orbits of the system (2.19). The magnitude of y in steady state equals $\Delta(1/\mu)$, represented on the figure 2.10. Writing the system (2.19) back with time t, we arrive at the conclusion that the commands (2.16) creates oscillations of period $2T$. With δ the magnitude of the displacements $d = \eta \left|\cos(\varphi_0 - \widehat{\varphi}_0)\right| y''_{\max}$ in steady state. The following holds:

$$\delta = \eta \left|\cos\left(\varphi_0 - \varphi\right)\right| y''_{\max} \Delta\left(\frac{1}{\mu}\right) = \varepsilon\eta \cos\left(\varphi_0 - \varphi\right) y''_{\max} \Delta\left(\frac{1}{\mu}\right).$$

Remark 2.5 *In the chapter 1, to compute the thrust generated by the electrical currents (see* (1.8)*), we assumed an estimate* $\widehat{\varphi}_0$ *of the initial phase* φ_0 *was available (as defined by the equation* (1.9)*). With such a prerequisite, the electrical currents were driven according to the equation* (1.7)*. This chapter is dedicated to obtaining such an estimate with the only knowledge of the displacements* d *(defined by the equation* (1.1)*). We may for instance feed the currents controllers with the following references:*

$$i_1^* = I(t) \sin\left(\frac{2\pi}{P} d + \varphi\right) \quad \textit{and} \quad i_2^* = I(t) \cos\left(\frac{2\pi}{P} d + \varphi\right). \tag{2.20}$$

Instead of the equation (1.8)*, we arrive at the following expression of the thrust:*

$$F_e = K \cos\left(\varphi_0 - \varphi\right) I, \tag{2.21}$$

where the currents offsets δi_1 *and* δi_2 *(see equation* (1.6)*) are neglected. Let's now use this expression together with the mechanical description* (1.11) *of a motor mounted on a fixed frame where cogging forces, as well as interpolation errors are also neglected. We arrive at the very simple modeling* (2.15) *used throughout this chapter.*

Remark 2.6 *Let* $\Gamma(\mu)$ *be the following function:*

$$\Gamma(\mu) = y''_{\max} \Delta(1/\mu) / \left(y_1 - y_0\right), \tag{2.22}$$

whose representation is given by the figure 2.11. Γ *takes values between 0 and 1 and only depends on the polynomial part of the equation* (2.2) *defining* y_r*. From now on, we only consider the following expression of* δ*:*

$$\delta = \varepsilon\eta \cos\left(\varphi_0 - \varphi\right) \left(y_1 - y_0\right) \Gamma\left(\mu\right). \tag{2.23}$$

Remark 2.7 *Observer that* δ *can be measured and* ε *also, it is related to the direction in which the system* (2.15) *initially leaves the discontinuity surface. By an appropriate choice of* φ*, our open goal now consists in extracting* φ_0 *from the relation* (2.23) *in spite of the lack of knowledge on the motor's gain, mass (parameter* η*) and friction (*f*). During the estimation procedure, the displacements magnitude is controlled by tuning* y_1 *and* y_0 *so that the motor remains close to its initial position.*

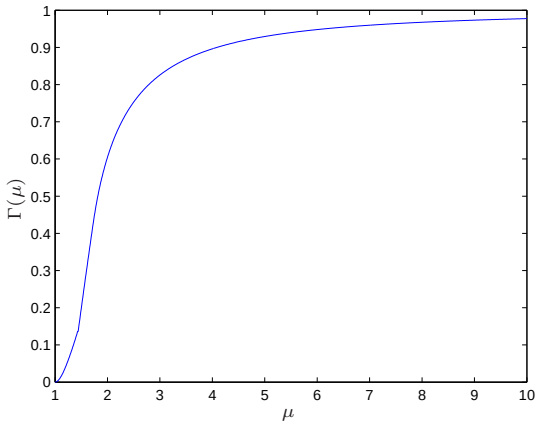

Figure 2.11: Plot of the function $\Gamma(\mu)$.

2.3.2 Estimation formula

We consider a set of N real numbers φ_i, and, for each of them, we measure δ_i when applying the command (2.16):

$$\forall i\,, 1 \leq i \leq N, \quad \delta_i = \eta \varepsilon_i \cos(\varphi_0 - \varphi_i)\,(y_1 - y_0)\,\Gamma(\mu_i), \tag{2.24}$$

where we furthermore note:

$$\mu_0 = m\eta \ddot{\xi}_{\max}/f, \quad \forall i,\ 1 \leq i \leq N, \quad \varepsilon_i = \operatorname{sign}\left(\cos(\varphi_0 - \varphi_i)\right) \ \text{ and } \ \mu_i = \varepsilon_i \mu_0 \cos(\varphi_0 - \varphi_i). \tag{2.25}$$

According to the previous notations, picking up i and j between 1 and N with $i \neq j$, the following relation holds:

$$\delta_i\, \mu_j\, \Gamma\left(\mu_j\right) = \delta_j\, \mu_i\, \Gamma\left(\mu_i\right).$$

We define $J_{ij}\left(\mu_0\,, \varphi_0\right)$ by:

$$J_{ij}\left(\varphi_0\,, \mu_0\right) = \Big(\delta_i\, \mu_j\, \Delta(\mu_j) - \delta_j\, \mu_i\, \Delta(\mu_i)\Big)^2. \tag{2.26}$$

Keep in mind that μ_i depends on both φ_0 and μ_0 as suggested by (2.25).

Estimating the initial phase eventually amounts to solving the following optimization problem:

$$(\widehat{\varphi}_0\,, \widehat{\mu}_0) = \arg \min_{\substack{\varphi_0 \in \mathbb{R} \\ \mu_0 \in \mathbb{R}^+}} \left(\sum_{\substack{i\,,j \\ j>i}} J_{ij}\left(\varphi_0\,, \mu_0\right) \right) \tag{2.27}$$

2.3.3 Approximated solution

Solving the problem (2.27) may be undertaken by numerical iterative methods. We suggest to approximate the original problem by another optimization problem whose resolution is rather straightforward. This approach is best suited for the online implementation as it lightens the computation burden. The relevancy of the approximation will be illustrated by experimental results.

We shall derive an optimization problem close to (2.27) but whose resolution may be conducted analytically rather than numerically. To this end, the function $\mu\Gamma(\mu)$ is linearized in the vicinity of 1 by assuming there exists a scalar $\gamma > 0$ such that:

$$\forall \mu \geq 1, \quad \mu\Gamma(\mu) \approx \gamma(\mu - 1). \tag{2.28}$$

The previous approximation is illustrated on the figure 2.12 and is only valid for $\mu \geq 1$. The linearization (2.28) may now be used to approximate $J_{ij}\,(\varphi_0\,\mu_0)$, previously defined by (2.26), into $J^*_{ij}\,(\varphi_0\,\mu_0)$:

$$J^*_{ij}\,(\varphi_0\,\mu_0) = \gamma^2\,(\delta_i\;(\mu_j - 1) - \delta_j\;(\mu_i - 1))^2 = \gamma^2\left(\begin{pmatrix}\mu_i & \mu_j\end{pmatrix} A_{ij} \begin{pmatrix}\mu_i \\ \mu_j\end{pmatrix} + b^T_{ij}\begin{pmatrix}\mu_i \\ \mu_j\end{pmatrix} + c^2_{ij}\right), \tag{2.29}$$

where the notations are the following, for all i and j satisfying $i \neq j$:

$$A_{ij} = \begin{pmatrix}\delta_j^2 & -\delta_i\delta_j \\ -\delta_i\delta_j & \delta_i^2\end{pmatrix}, \quad b^T_{ij} = -2\,(\delta_i - \delta_j)\begin{pmatrix}-\delta_j & \delta_i\end{pmatrix}, \quad c_{ij} = (\delta_i - \delta_j)^2. \tag{2.30}$$

The index to minimize in (2.27) may also be approximated by $J^*(\varphi_0, \mu_0)$, a quadratic form in the vector $\overline{\mu} = \begin{pmatrix}\mu_1 & \dots & \mu_N\end{pmatrix}^T$:

$$J^*(\varphi_0, \mu_0) = \gamma^2\left(\overline{\mu}^T A \overline{\mu} + b^T\overline{\mu} + c\right). \tag{2.31}$$

A is a square matrix of size N, b is an N-dimensional column vector and c a scalar. We denote by $A(i,j)$ the elements of the matrix A, $b(i)$ those of b, they are given by:

$$\begin{aligned}
&\bullet\ \forall\,(i,j)\,,\ A(i,i) = \sum_{j\neq i}\delta_j^2 \quad \text{and} \quad A(i,j) = A(j,i) = -\delta_i\delta_j,\ \text{for } j > i,\\
&\bullet\ \forall i,\ b(i) = 2\sum_{j\neq i}(\delta_j\;(\delta_i - \delta_j))\,,\\
&\bullet\ c = \sum_{i,j} c_{ij}.
\end{aligned} \tag{2.32}$$

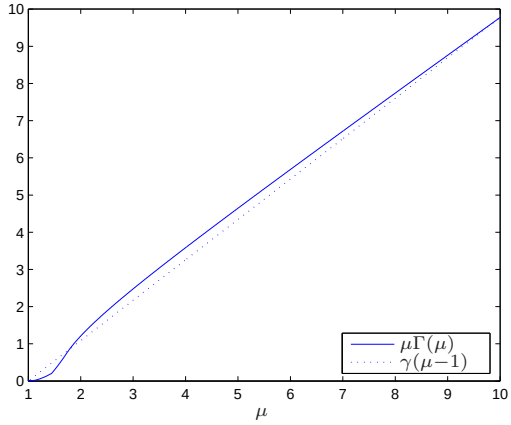

Figure 2.12: Plot of the function $\mu\Gamma(\mu)$ and its approximation $\gamma\,(\mu - 1)$.

Observe that the constant γ does not play any role on the minimization of J^*. To turn to best account that J^* is quadratic in $\overline{\mu}$, the μ_i's are now expressed in cartesian coordinates:

$$\mu_i = \mu_0 \begin{pmatrix} \varepsilon_i \cos(\varphi_i) & \varepsilon_i \sin(\varphi_i) \end{pmatrix} \begin{pmatrix} \cos(\varphi_0) \\ \sin(\varphi_0) \end{pmatrix}.$$

Let $\theta \in \mathbb{R}^2$ and $M \in \mathbb{R}^{N\times 2}$ be defined as:

$$\theta = \mu_0 \begin{pmatrix} \cos(\varphi_0) \\ \sin(\varphi_0) \end{pmatrix} \quad \text{and} \quad M = \begin{pmatrix} \varepsilon_1 \cos(\varphi_1) & \varepsilon_1 \sin(\varphi_1) \\ \vdots & \vdots \\ \varepsilon_N \cos(\varphi_N) & \varepsilon_N \sin(\varphi_N) \end{pmatrix},$$

so that relation $\overline{\mu} = M\theta$ holds and $\overline{\mu}$ is linear in the new optimization variable θ. Note that φ_0 is the phase of θ and μ_0 its norm. According to the previous change of coordinates, the original function to minimize, J, admits the following approximation $\widetilde{J}(\theta) = J^*\left(\varphi_0(\theta), \mu_0(\theta)\right)$ explicitly given by::

$$\widetilde{J}(\theta) = \theta^T M^T A M \theta + b^T M \theta + c.$$

Since the linearization (2.28) is only valid for $\mu \geq 1$, the minimization of the quadratic form $\widetilde{J}(\theta)$ has to be carried out while simultaneously fulfilling the N constraints:

$$\forall i,\ 1 \leq i \leq N, \quad \varepsilon_i \big(\cos(\varphi_i)\ \sin(\varphi_i)\big)\theta \geq 1.$$

Let $\widehat{\theta}$ be the solution of the optimization problem:

$$\left| \begin{array}{l} \widehat{\theta} = \arg\min\limits_{\theta\in\mathbb{R}^2} \widetilde{J}(\theta) \\ \text{subject to:} \\ \forall i, 1 \leq i \leq N, \quad \varepsilon_i \begin{pmatrix} \cos(\varphi_i) & \sin(\varphi_i) \end{pmatrix} \theta \geq 1 \end{array} \right. \tag{2.33}$$

$\widehat{\theta}$ is obtained by writing the optimality conditions of Kuhn and Tucker, see [17]. The phase of the vector $\widehat{\theta}$ is the much-sought after $\widehat{\varphi}_0$.

2.4 Experimental results

2.4.1 Classical method

We want to compare the previously presented method to the so-called classical method briefly exposed hereafter. The context depicted by the figure 1.1 is still considered, namely the electrical currents are controlled and only displacements around the initial position are measured. The currents are now driven as follows:

$$i_1^* = \frac{\widehat{m}}{\widehat{K}} \ddot{\xi}_0 \quad \text{and} \quad i_2^* = 0, \tag{2.34}$$

where $\ddot{\xi}_0$, constant and homogeneous to an acceleration, is set to any desired value while $\widehat{m}$ and $\widehat{K}$ are still *a priori* estimates of the motor's mass and gain. Rather than (2.15), the evolution of the system is now given by:

$$\ddot{\xi} = \eta \sin\left(\frac{2\pi}{P}\, d + \varphi_0\right) \ddot{\xi}_0 - \frac{f}{m} \operatorname{sign}(\dot{\xi}), \tag{2.35}$$

with η still bearing the same meaning as previously. In a way similar to (2.17), we define the parameter μ' by:

$$\mu' = m\eta\ddot{\xi}_0/f. \tag{2.36}$$

As we shall show in the following, the effectiveness of this classical method may be determined from the only value μ'.

The system (2.35) features damped oscillations approximately as large as the magnetic pitch P (several millimeters as given by the remark 1.3) and, it eventually stabilizes under the effect of the friction. Note d_∞ the displacement from the initial position $x_0 = \dfrac{P}{2\pi}\varphi_0$ to the position at rest. Once the equilibrium is reached, the magnitude of the friction is necessarily larger than the command:

$$\sin\left(\frac{2\pi}{P}\,d + \varphi_0\right) \leq \frac{1}{\mu'}.$$

The corresponding set of possible values φ_0 is thus given by:

$$-\frac{2\pi}{P}d_\infty + k\pi - \arcsin\left(\frac{1}{\mu}\right) \quad \leq \quad \varphi_0 \quad \leq \quad -\frac{2\pi}{P}d_\infty + k\pi + \arcsin\left(\frac{1}{\mu}\right).$$

The equilibrium positions in the vicinity of points where the magnetic phase if $(2p+1)\pi$ are stable, while those where the magnetic phase is close to $2p\pi$ are unstable. If the system (2.35) is at rest, φ_0 (module 2π) lies within an interval centered at $\pi - \dfrac{2\pi d_\infty}{P}$ whose width equals $2\arcsin\left(\dfrac{1}{\mu'}\right)$. Since μ' is unknown, the so-called classical method consists in estimating φ_0 according to:

$$\widehat{\varphi}_0 \approx \pi - \frac{2\,\pi}{P}\,d_\infty \mod 2\,\pi. \tag{2.37}$$

Actually, the smaller μ', the larger the error on the estimate. The classical method is getting quite biased if friction gets too large with respect to the magnitude of the command, namely $\ddot{\xi}_0$. This may be interpreted as the command (given by (2.34)), or this method more exactly, being not adapted to friction.

2.4.2 Results

We now illustrate the results of our method in comparison with the classical method. To this end, let's consider two brushless linear motors. The first of them is an ironless motor featuring high quality ball-bearings, while the second is an ironcore motor known to present more important friction, even if, in practice, this information is not used by the estimation algorithms. According to the previous notations, for the first of them we note η_1, m_1, f_1 and for the latter η_2, m_2 and f_2.

The experiments presented hereafter are carried out while ensuring $\mu_0 = \mu'$, which implies $\ddot{\xi}_0 = \ddot{\xi}_{max}$. We are concerned with the average estimation error $\widehat{\varphi}_0 - \varphi_0$ when the initial phase φ_0 is varied between 0 and 2π. The actual value of the initial phase is derived from complementary back-emf measurements that are not presented here.

We consider the first motor to experimentally check out that the precision of the classical method worsens as $\mu' = \eta_1 m_1 \ddot{\xi}_0/f_1$ decreases, while our solution does not depend upon $\mu_0 = \eta_1 m_1 \ddot{\xi}_{\max}/f_1$. To this end,

we consider the following two experimental setups. First, $\ddot{\xi}_0 = \ddot{\xi}_{max} = 1000\text{mm/s}^2$ with the average estimation error plotted on figure 2.13(a) and then $\ddot{\xi}_0 = \ddot{\xi}_{max} = 500\text{mm/s}^2$ with the same data plotted on the figure 2.13(b). For this motor, our procedure yields an angular precision better than 10°, giving an efficiency, such as defined in the remark 1.2, greater than 98%. For higher values of $\ddot{\xi}_0$ and $\ddot{\xi}_{max}$, the classical method yields almost the same performances, though less accurate. However, keep in mind that erratic and large magnitude (closely related to the magnetic picth P, namely several millimeters) displacements are generated while our method is tuned to cause very small deviations (a couple micrometers) around the initial position by an appropriate choice of T, y_0 and y_1 in the equation (2.16). As expected, when μ' decreases (see figure 2.13(b)), the classical method exhibits an only 30° precision and a corresponding efficiency of 87% while our method still offers the same 98% efficiency. For the motor with little friction (figures 2.13(a) and 2.13(b)), the precision of our method does not depend on the unknown motor parameters (μ_0) and guarantees a substantially better energetic efficiency.

Let's now move on to the second motor which features much friction, therefore the reference acceleration has to be larger and is set to $\ddot{\xi}_{\max} = \ddot{\xi}_0 = 4000\text{mm/s}^2$. The average estimation error is given for both methods on the figure 2.13(c). Our method turns out to be very robust to dry friction since the angular precision remains close to 10° while the classical method does not perform that well.

As illustrated by these experimental results carried out on production line motors, our method turns out to be independent of friction and a lack of knowledge on both the gain and the mass of the motor. Whatever values these parameters may take, for the considered motor, our method outperforms the so-called classical method and permanently achieves a 10° precision in estimating the initial magnetic phase.

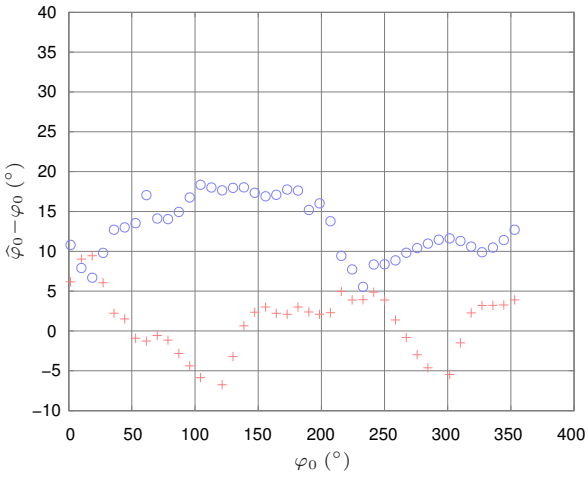

(a) Ironless motor, $\ddot{\xi}_0 = \ddot{\xi}_{\max} = 1000\text{mm/s}^2$.

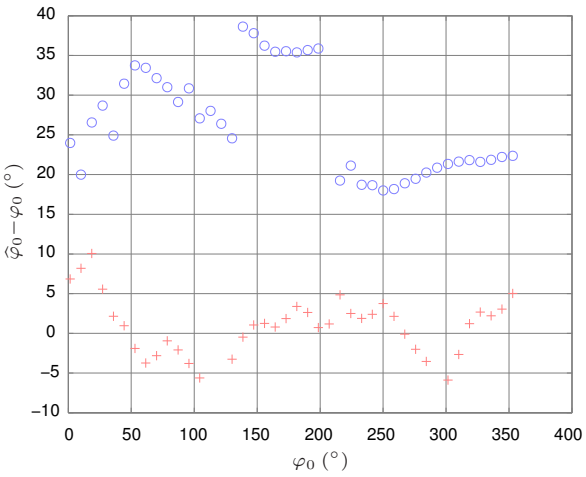

(b) Ironless motor, $\ddot{\xi}_0 = \ddot{\xi}_{\max} = 500\text{mm/s}^2$.

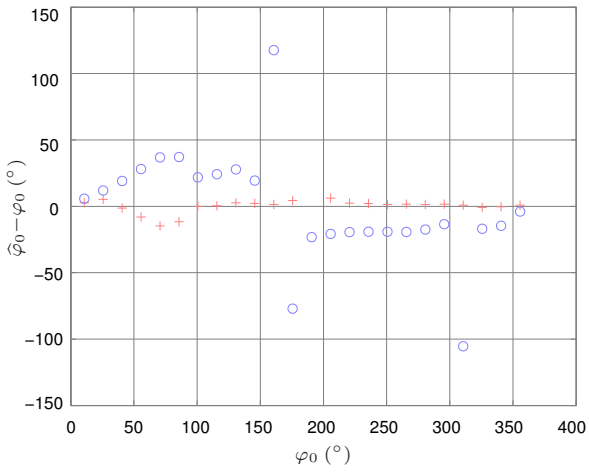

(c) Ironcore motor, $\ddot{\xi}_{\max} = \ddot{\xi}_0 = 4000\text{mm/s}^2$.

Figure 2.13: Average estimation error $\widehat{\varphi}_0 - \varphi_0$ for different values of φ_0. Our method (+) versus classical methods (∘).

CHAPTER 3

State-periodic Disturbances and Regular Perturbations

3.1 Introduction

3.1.1 Presentation

The different modelings provided by the chapter 1 underline the prevalence of perturbing phenomena periodic with the position of the motors. On the top of cogging and interpolation errors, one may also consider the perturbations caused by ball bearings or eccentricity for rotative systems. They also turn out to be spatially periodic.

We are now exclusively interested in the more general case of state-periodic perturbations. They may for instance arise in the analysis of the positioning systems used in the semi-conductor industry. These machines usually result from a complex mechanical assembling of several motors. Through existing couplings, the position-periodic perturbations pertaining to a given motor are likely to affect the evolution of the other motors. In the end, the whole system features state-periodic perturbations.

These state-periodic phenomena clearly affect the performances of the considered systems, especially when high precision trajectory tracking matters. In the following, we assume one may derive the equations of the systems around the reference trajectories, and, our goal is twofold:

1. understanding to what extent and in which way the system deviates from the desired trajectories,
2. deriving conditions under which the system reaches the origin despite state-periodic perturbations.

To answer these questions, we carry out the integration of the differential equation modeling the considered systems. We first make use of the Cauchy-Lipschitz theorem [15] to implicitly get the solutions. Even if the differential equation cannot be straightforwardly solved, it may still be established that, under some rather mild assumptions, the system only slightly deviates from its desired trajectory. This point is discussed by exhibiting a small magnitude parameter in the considered differential equation.

Hoping for the solution in closed form is unrealistic given the non-linear nature of the equations. The previously mentioned small parameter makes lean toward a regular perturbation analysis of these equations, see for instance [3]. This technique is very informative and widely used in technical domains such as fluid mechanics [52] or non linear oscillating systems [23]. The resulting expansion is usually truncated, either because it is diverging or because the first order terms yield enough information.

An approximated solution does not match our needs. An infinite expansion may not be spared to derive stability conditions. This is definitely unsatisfactory to conclude toward the convergence to zero concerning only the first terms of the expansion. To our knowledge, Cauchy was the first to express the solutions of a differential equation as a power series of a parameter. He stated that, if the right-hand side is analytical in that parameter, so are the solutions. Both Poincaré and Lyapunov fruitfully turn to best account this property in their respective studies on the stability of periodic orbits (in [41, 42]) and equilibrium points (in [29]).

We apply the so-called Cauchy's method to systems featuring state-periodic perturbations. Our main contribution is the use of the *Bell polynomials of the second kind* (see [50, 16]) that enable to explicit the terms of the resulting power series expansion. These polynomials are not widespread in the control community, but they turn out of material interest to generalize the chain rules to higher orders. They also offer nice properties, especially regarding homogeneity, which allow to compute the radius of convergence of the expansion as well as the magnitudes of the successive approximations. What emerges from all these considerations is that only the very first terms of the expansion have noticeable effects on the errors generated around the origin.

Concerning the stability of the origin, we still take advantage of the properties of the Bell polynomials. We eventually come up to the conclusion that the origin is *globally asymptotically stable* provided the first term of the expansion converges to zero. Once more, the proof of this result is entirely based on the nature of the Bell polynomials. Also observe that, in the same situation, the first Lyapunov method only guarantees *local* stability of the origin.

Finally, we shall illustrate that expanding the whole state may sometimes be too conservative. Namely, the convergence of the resulting expansion is guaranteed for slowly-varying and small-magnitude perturbations. We shall see that it is possible to cope with a broader class of perturbations by only expanding a subset of the state. The $\mathcal{L}_1$-norm of the transfer from the perturbations to those components is used to perform such a regular perturbation analysis.

3.1.2 Example

Consider the following equation:

$$\ddot{\xi} = -\frac{\mu}{m}\dot{\xi} + u + \lambda \sin(\omega\xi), \tag{3.1}$$

which falls under the scope of the equation (1.11) modeling the behavior of a motor mounted on fixed frame, except dry friction is omitted for the purpose of this chapter. Suppose the command u is designed

in order to get the position ξ tracking the reference trajectory ξ^*, but, assume both friction and periodic perturbation unknown, the command does not allow for them and is actually given by the following PD controller featuring a feedforward acceleration term:

$$u = \ddot{\xi}^* - \omega_0^2 \left(\xi - \xi^*\right) - 2\zeta_0\omega_0 \left(\dot{\xi} - \dot{\xi}^*\right).$$

Define $e = \xi - \xi^*$, the closed loop system is given by:

$$\ddot{e} = -\omega_0^2 e - \left(2\zeta_0\omega_0 + \frac{\mu}{m}\right)\dot{e} + \lambda \sin\left(\omega e + \omega\xi^*\right) - \frac{\mu}{m}\dot{\xi}^*. \tag{3.2}$$

Let's point out some remarkable facts:

- Without perturbations (friction and position periodic function), the tracking error is actually given by:

  $$\ddot{e} = -2\zeta_0\omega_0\dot{e} - \omega_0^2 e.$$

  So, it asymptotically reaches zero thanks to the previous control law u.

- Provided it is possible to tune the previous controller to yield large enough ω_0, the tracking error gets only slightly altered by the perturbations even if λ and μ take large values.

- If for some technological reasons, it is not possible to have a large ω_0, the state is subjected to small deviations around the origin only if λ and μ are not too large with respect to ω_0.

For this example, $\dfrac{1}{\omega_0}$ represents the $\mathcal{L}_2$ input-output gain between the perturbations and the tracking error. In the end, if both $\dfrac{\lambda}{\omega_0}$ and $\dfrac{\mu}{\omega_0}$ are small enough, the system remains close to the nominal behavior imposed by the command u. The goal of this chapter is to extend this discussion to much more general systems perturbed by state-periodic functions. We shall see that the $\mathcal{L}_1$-norm is better suited to this work.

3.1.3 Modeling

This study is dedicated to systems depicted on figure 3.1 and defined as follows:

Definition 3.1 *Consider the following dynamical system:*

$$\dot{x} = A(t)x + \Lambda(x,t) = A(t)x + \sum_{i=1}^{N} \lambda_i b_i(t) \sin\big(\omega_i c_i(t)x + \varphi_i^*(t)\big) + \lambda_0 b_0(t), \tag{3.3}$$

according to the notations:

- *let $x \in \mathbb{R}^n$ be the state vector, fulfilling the initial conditions $x(0) = x_0$ at $t = 0$,*
- *let $A(t) : \mathbb{R}_+ \to \mathbb{R}^{n\times n}$ be a square matrix assumed both bounded and continuous with respect to time t so that the following may be defined:*

  $$A^\star = \sup_{t\in\mathbb{R}_+} \|A(t)\|.$$

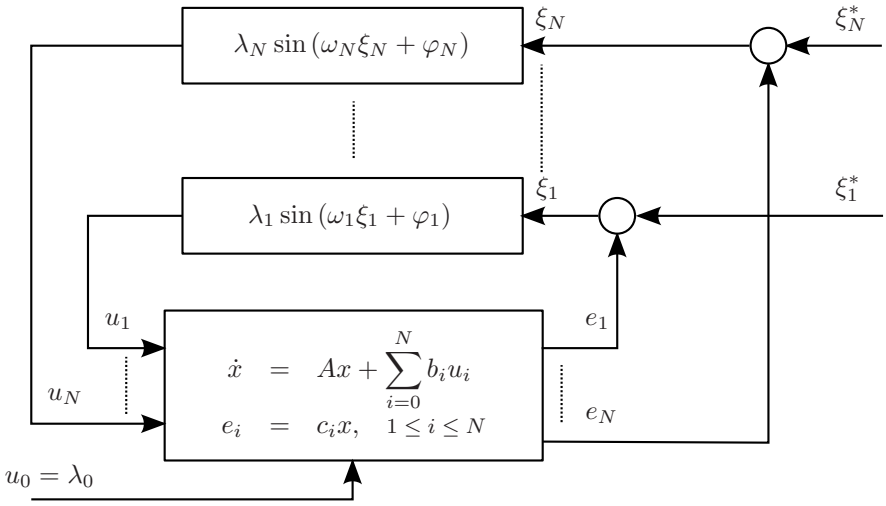

Figure 3.1: State-periodic perturbations.

Moreover, if $\Phi(t,t') : \mathbb{R}_+ \times \mathbb{R}_+ \to \mathbb{R}^{n\times n}$ *is the transition matrix associated with* $A(t)$*, it is assumed that there exist* $K > 0$ *and* $\alpha > 0$ *such that:*

$$\forall t \geq 0, \quad \forall t' \geq 0, \quad \|\Phi(t,t')\| \leq K e^{-\alpha(t-t')}.$$

- *let* $\Lambda(x,t) : \mathbb{R}^n \times \mathbb{R}_+ \to \mathbb{R}^{n\times 1}$ *be a periodic function of the state* x *and* $N \in \mathbb{N}_+$ *the number of elementary harmonic components (supposed to be finite) such that, for all* i*,* $1 \leq i \leq N$*:*
  - $\lambda_i \in \mathbb{R}_+$ *and* $\omega_i \in \mathbb{R}_+$ *are respectively the magnitude and the spatial pulsation of the* i*-th component (*λ_0 *is a scalar), we furthermore assume* $\omega_i = \dfrac{2\pi}{P_i}$*, with* P_i *the state period associated to* ω_i*,*
  - $\varphi_i^*(t) : \mathbb{R}_+ \to \mathbb{R}$ *is a differentiable and bounded function of time whose derivative is also bounded,*
  - $b_i(t) : \mathbb{R}_+ \to \mathbb{R}^{n\times 1}$ *and* $c_i(t) : \mathbb{R}_+ \to \mathbb{R}^{1\times n}$ *are vectors whose entries are continuous and bounded functions of time so that the following definitions make sense:*

$$b_i^\star = \sup_{t\in\mathbb{R}_+} \|b_i(t)\| \;\; et \;\; c_i^\star = \sup_{t\in\mathbb{R}_+} \|c_i(t)\|.$$

Remark 3.1 *In the introductory example, the equation modeling the closed loop system meets the previous definition. Similarly to this example, some components of the state vector* x *may be viewed as errors between physical variables (the position* ξ *in the example) and their desired trajectories (the function* ξ^**). This also explains the terms* φ_i^* *in equation* (3.3)*, whose expression in the example would be given by* $\omega\xi^*$*.*

Remark 3.2 *The definition sets a framework wide enough to cope with situations definitely more complex than the one considered in the introductory example. Let give some examples:*

- *Consider a scalar function $\Lambda(x,t)$ periodic with respect to only one function of the state x, say the position, the vectors c_i (respectively the b_i) are all the same. The pulsations ω_i are chosen to model a periodic functions with several fundamental spatial periods. That is exactly the way cogging forces, assumed periodic with respect to the position, are modeled.*

- *Move on to an even more complex system made up of two mechanically coupled motors, each of them affected by a force periodic in its own position, and by another force depending on the position of the other motor, as a consequence of the previously mentioned coupling. In such a situation, the c_i are split into two subsets, some of them giving the position of the first motor and the others the position of the second motor. For the same reasons, the b_i may model the input of either the first or the second motor. No matter how complex this case may be, we eventually end up with an equation similar to the definition* (3.3).

Remark 3.3 *The existence of the matrix Φ is due to the fact that A is a continuous function of time, see [11]. We also assume that the system $\dot{x} = A(t)x$ is exponentially stable with decay-rate to zero α. This autonomous system represents the system without state-periodic perturbations. Assuming A models a physical system driven by a controller, it is not too conservative to expect this controller to stabilize the known part of the system (namely the matrix A) while the unknown perturbations actually force its evolution around the origin.*

Remark 3.4 *Whenever possible, the dependencies of the previous functions with respect to time t are not mentioned.*

3.2 Qualitative study

3.2.1 Implicit solution

The solution of the system (3.3) is implicitly given by the following theorem.

Theorem 3.1

Let $x : \mathbb{R}_+ \to \mathbb{R}^n$ be the solution of the differential equation (3.3) *with initial conditions $x(0) = x_0$. Then x solves the following equation:*

$$x(t) = \Phi(t,0)x_0 + \sum_{i=1}^{N} \lambda_i \left(\int_0^t \Phi(t,t')b_i(t') \sin\left(\omega_i c_i(t')x(t') + \varphi_i^*(t')\right) dt' \right) + \lambda_0 \int_0^t \Phi(t,t')b_0(t')dt' \tag{3.4}$$

Proof:

Let's recall that existence and uniqueness of x on $\mathbb{R}_+$ is a consequence of the global Cauchy-Lipschitz

theorem (see [15]. The right-hand side of the equation (3.3) is obviously continuous, and, we shall prove it is uniformly Lipschitz with respect to x and t:

$$\begin{aligned}
&\forall (x,y) \in \mathbb{R}^n \times \mathbb{R}^n,\ \forall t \geq 0,\\
\|A(t)(x-y) + \Lambda(x,t) - \Lambda(y,t)\| &\leq \|A(t)\|\,\|x-y\| + 2\sum_{i=1}^{N} \lambda_i \|b_i(t)\|\,\|\sin\left(\omega_i c_i(t)(x-y)/2\right)\| \\
&\leq \left(A^\star + \sum_{i=1}^{N} \lambda_i \omega_i b_i^\star c_i^\star\right)\|x-y\|,
\end{aligned}$$

The first inequality is derived from:

$$\sin(a) - \sin(b) = 2\sin\left(\frac{a-b}{2}\right)\cos\left(\frac{a+b}{2}\right),$$

while the second one results from:

$$\sin(a) \leq a.$$

The only thing left to check is that the function defined by (3.4) satisfies the differential equation (3.3). It is rather obvious for $t = 0$, then for $t \geq 0$, we get:

$$\begin{aligned}
\dot{x}(t) &= \frac{d}{dt}\left(\Phi(t,0)x_0 + \sum_{i=1}^{N}\lambda_i\left(\int_0^t \Phi(t,t')b_i(t')\sin\left(\omega_i c_i(t')x(t') + \varphi_i^*(t')\right)dt'\right) + \lambda_0\int_0^t \Phi(t,t')b_0(t')dt'\right)\\
&= A(t)\left(\Phi(t,0)x_0 + \sum_{i=1}^{N}\lambda_i\left(\int_0^t \Phi(t,t')b_i(t')\sin\left(\omega_i c_i(t')x(t') + \varphi_i^*(t')\right)dt'\right) + \lambda_0\int_0^t \Phi(t,t')b_0(t')dt'\right)\\
&\qquad + \sum_{i=1}^{N}\lambda_i\left(\Phi(t,t)b_i(t)\sin\left(\omega_i c_i(t)x(t) + \varphi_i^*(t)\right)\right) + \lambda_0\Phi(t,t)b_0(t)\\
&= A(t)x + \sum_{i=1}^{N}\lambda_i b_i(t)\sin\left(\omega_i c_i(t)x(t) + \varphi_i^*(t)\right) + \lambda_0 b_0(t),
\end{aligned}$$

which ends proving this theorem.

3.2.2 Qualitative analysis of the solutions

The equation (3.4) might be used to have a little bit more qualitative insight into the solution of the system (3.3). To this end, we bound $\|x\|$ from above by:

$$\forall t \geq 0, \quad \|x(t)\| \leq Ke^{-\alpha t}\|x_0\| + \sum_{i=0}^{N}\lambda_i\int_0^t \|\Phi(t,t')b_i(t')\|\,dt',$$

where the exponential stability of the matrix Φ is used to derive this equation. Note that every term of the summation is bounded since:

$$\forall i,\ 1 \leq i \leq N, \quad \forall t \geq 0, \quad \int_0^t \|\Phi(t,t')b_i(t')\|\,dt' \leq Kb_i^\star\int_0^t e^{-\alpha(t-t')}dt' \leq Kb_i^\star/\alpha.$$

It is relevant to give the following definitions:

$$\forall i,\ 0 \leq i \leq N, \quad \beta_i = \sup_{t \geq 0} \left(\int_0^t \|\Phi(t, t')b_i(t')\|\, dt' \right), \tag{3.5}$$

so that if ε is defined by:

$$\varepsilon = (N+1) \max_{0 \leq i \leq N} \lambda_i \beta_i, \tag{3.6}$$

the norm of the state vector x is eventually bounded from above by:

$$\forall t \geq 0, \quad \|x(t)\| \leq K e^{-\alpha t} \|x_0\| + \varepsilon. \tag{3.7}$$

With the previous elements, the discussion initiated in the introductory example can be pursued by now making use of the $\mathcal{L}_1$-norm. According to the expression (3.7), the solution is made up of two main components. First, the influence of the initial conditions is exponentially vanishing as t is indefinitely growing, while, second, the state-periodic perturbations persistently prevent the state from reaching the origin. The asymptotic bound on $\|x\|$ depends on two radically different kinds of physical parameters:

- the λ_i, the magnitudes of the components of the truncated Fourier series expansion of the function $\Lambda(x, t)$,
- the β_i expressing the influence of the inputs on the whole state through the vectors b_i, namely the $\mathcal{L}_1$-norm of the transfer from the perturbation $\lambda_i \sin(\omega_i c_i x + \varphi_i^*)$ to the whole state.

From a practical point of view, the λ_i cannot be changed in any way, for they are directly related to the considered perturbations. Nonetheless, if we suppose that the matrix A models the evolution of an electrical motor in closed loop, namely driven by a given controller, it might be possible to design and tune this controller to minimize the β_i expressing the sensitivity of the state x to the different perturbations. Under this assumption, the value of the parameter ε given by the equation (3.6) may be controlled to some extend, and ε may take a small value. However, for some technological and physical reasons, some β_i cannot be changed by appropriate controller design and tuning. In such situations, provided the λ_i are not too large, ε may still take a small value.

Under the conditions raised in the previous discussion, the origin is only slightly perturbed by the state-periodic functions. They generate small magnitude deviations of the vector x. In the following, we address the in-depth study of these particular situations where the parameter ε takes small value. Yet, the periodic functions of the state play a significant role in that they make the system deviate from its desired state (namely the origin) but they are not the more dominating for it. Let's express the equation (3.3) in a way that clearly suggests the dependency of the solution on ε. To this end, let's first define:

$$\forall i,\ 0 \leq i \leq N, \quad \bar{b}_i = \lambda_i b_i \Big/ \left((N+1) \max_{0 \leq n \leq N} \beta_n \lambda_n \right) = \lambda_i b_i / \varepsilon, \tag{3.8}$$

so that (3.3) is equivalently given by:

$$\dot{x} = Ax + \varepsilon \sum_{i=1}^{N} \bar{b}_i \sin(\omega_i c_i x + \varphi_i^*) + \varepsilon \bar{b}_0, \tag{3.9}$$

which is the equation we propose to integrate in the following.

3.3 Power series expansion of the state

The Cauchy theorem (presented in appendix C.1.1) claims the solution of the differential equation (3.9) may be expressed as a convergent power series in ε. The so-called Cauchy method, exposed in the appendix C.1.2, material in both Poincaré and Lyapunov work, is used to derive the different terms of such an expansion, thus leading to the solution of (3.9). The main contribution of this part is the introduction of the *Bell polynomials of the second kind* in this method. They are presented in the appendix appendix B. They turn out to be a most appropriate tool to explicitly compute the terms of the expansion. They are pretty useful to generalize the somehow tedious task of computing the n-th order derivative of the composition of two functions. Since the terms of the expansion are nicely given in closed form, we estimate their magnitudes through an extensive use of some properties of the Bell polynomials. It is showed that a very accurate approximation of the solution is obtained by only allowing for the first components of the expansion. Thanks to the analysis, one also estimates the maximum value of the small parameter for the power series to converge. The bound we obtain is not conservative which highlights that the proposed approach may cope with most physical situations where the origin is perturbed by state-periodic functions.

3.3.1 Cauchy method

Let's define the following functions $x^{(n)} : \mathbb{R}_+ \to \mathbb{R}^n$, of prime interest to integrate the equation (3.9):

$$\begin{aligned}
\dot{x}^{(0)} &= Ax^{(0)} \\
\dot{x}^{(1)} &= Ax^{(1)} + \sum_{i=1}^{N} \bar{b}_i \sin\left(\omega_i c_i x^{(0)} + \varphi_i^*\right) + \bar{b}_0 \\
\dot{x}^{(n+1)} &= Ax^{(n+1)} + (n+1)\sum_{i=1}^{N} \bar{b}_i \left(\sum_{r=1}^{n} \mathcal{B}_{n,r}\left(c_i x^{(1)}, \ldots, c_i x^{(n-r+1)}\right) \omega_i^r \sin\left(\omega_i c_i x^{(0)} + \varphi_i^* + \frac{r\pi}{2}\right)\right).
\end{aligned} \tag{3.10}$$

For each of them, consider the following initial conditions:

$$x^{(0)} = x_0 \text{ and } x^{(n)} = 0, \quad \forall n \geq 1, \tag{3.11}$$

The functions $\mathcal{B}_{n,r}$ in the equation (3.10) are the Bell polynomials of the second kind presented in appendix B.1. We prove the following theorem.

Theorem 3.2

Considering the functions $x^{(n)}$ defined by (3.10), there exists $\varepsilon^* > 0$ such that, if $\varepsilon < \varepsilon^*$, the power series $\sum_{n\geq 0} x^{(n)} \frac{\varepsilon^n}{n!}$ converges and its limit is the solution of the differential equation (3.9). Let $\rho = \max_{1\leq i\leq N} (\omega_i c_i^\star)$ and e the Neperian constant, the following relations hold:

$$\varepsilon^* = \frac{1}{\rho e} \quad \textit{and} \quad \forall n \geq 1, \quad \left\| x^{(n)} \right\|_\infty \leq (n\rho)^{n-1}. \tag{3.12}$$

Lemma 3.1 *Given the functions $x^{(n)}$ defined by* (3.10) *and the initial conditions* (3.11)*, the power series $\sum_{n\geq 0} x^{(n)}\frac{\varepsilon^n}{n!}$ converges and solves the equation* (3.9) *provided ε is small enough.*

PROOF:

The right-hand side of (3.9) is linear and thus analytical in ε. Moreover, the sine function is analytical, thus the right-hand side of (3.9) is analytical in x for any time t. The Cauchy theorem given in appendix C.1.1 guarantees the existence of functions $x^{(n)}$ $(n \geq 0)$ such that the following series $\sum_{n\geq 0} x^{(n)}\frac{\varepsilon^n}{n!}$ has a non-zero radius of convergence and is the solution of the equation (3.9).

The functions $x^{(n)}$ are derived by applying the so-called Cauchy method (presented in appendix C.1.2) which consists in first substituting x by $\sum_{n\geq 0} x^{(n)}\frac{\varepsilon^n}{n!}$ in equation (3.9) and then expanding the right-hand side in power of ε. For none of the b_i depends on the state x, only the following terms have to be expanded:

$$\forall i,\ 1 \leq i \leq N, \quad s_i = \sin\left(\omega_i c_i \sum_{n\geq 0} x^{(n)}\frac{\varepsilon^n}{n!} + \varphi_i^*\right). \tag{3.13}$$

If we use the Faa dì Bruno formula (presented in the appendix C.2) to get the general term of the composition of two power series expansions, the resulting expression depends on the Bell polynomials of the second kind, indeed:

$$\forall i,\ 1 \leq i \leq N, \quad s_i = f_{i,0}\left(c_i x^{(0)}, t\right) + \sum_{n\geq 1}\left(\sum_{r=1}^{n} \mathcal{B}_{n,r}\left(c_i x^{(1)}, \ldots, c_i x^{(n-r+1)}\right) f_{i,r}\left(c_i x^{(0)}, t\right)\right)\frac{\varepsilon^n}{n!}, \tag{3.14}$$

where the functions $f_{i,r}$ are given by:

$$\forall n \geq 0, \quad \forall i,\ 1 \leq i \leq N, \quad f_{i,n}(\xi_0, t) = \omega_i^n \sin\left(\omega_i \xi_0 + \varphi_i^* + \frac{n\pi}{2}\right). \tag{3.15}$$

To get the equation (3.14), observe that s_i results from the composition of the function f_i:

$$\forall i,\ 1 \leq i \leq N, \quad f_i\left(\xi, \xi_0, t\right) = \sin\left(\omega_i \xi + \omega_i \xi_0 + \varphi_i^*\right), \tag{3.16}$$

by $\sum_{n\geq 0} x^{(n)}\frac{\varepsilon^n}{n!}$ according to:

$$\forall i,\ 1 \leq i \leq N, \quad s_i = f_i\left(c_i \sum_{n\geq 1} x^{(n)}\frac{\varepsilon^n}{n!}, \quad c_i x^{(0)}, \quad t\right), \tag{3.17}$$

with f_i admitting the following expansion:

$$\begin{aligned} \forall i,\ 1 \leq i \leq N, \quad f_i &= \sum_{n\geq 0}\left(\frac{\partial^n f_i}{\partial \xi^n}\right)\frac{\xi^n}{n!} \\ &= \sum_{n\geq 0} \omega_i^n \sin\left(\omega_i \xi_0 + \varphi_i^* + \frac{n\pi}{2}\right)\frac{\xi^n}{n!} \\ &= \sum_{n\geq 0} f_{i,n}(\xi_0, t)\frac{\xi^n}{n!}, \end{aligned} \tag{3.18}$$

The expression (3.14) is thus readily obtained by applying the Faa dì Bruno formula (equation (C.6)) to the equation (3.17).

Let finally use the equation (3.14) in (3.9) to get:

$$\begin{aligned}\sum_{n\geq 0}\dot{x}^{(n)}\frac{\varepsilon^n}{n!} =& A\sum_{n\geq 0}x^{(n)}\frac{\varepsilon^n}{n!}+\varepsilon\left(\sum_{i=1}^{N}\bar{b}_i f_{i,0}\left(c_i x^{(0)},t\right)+\bar{b}_0\right)+\\ &\varepsilon\sum_{n\geq 1}\left(\sum_{i=1}^{N}\bar{b}_i\sum_{r=1}^{n}\mathcal{B}_{n,r}\left(c_i x^{(1)},\ldots,c_i x^{(n-r+1)}\right)f_{i,r}\left(c_i x^{(0)},t\right)\right)\frac{\varepsilon^n}{n!}.\end{aligned} \tag{3.19}$$

If we identify the terms of the same order in ε for both sides of the previous expression, the set of equations (3.10) is easily derived. The initial conditions x_0 of the system (3.9) do not depend on ε, thus, the relation (3.11) is an immediate consequence of (C.3) in appendix C.1.1.

Lemma 3.2 *The functions $x^{(n)}$ given by* (3.10) *are bounded, and, the series $\{\gamma_n\}_{n\geq 1}$ defined by:*

$$\gamma_1 = 1 \text{ and } \forall n\geq 1,\quad \gamma_{n+1} = (n+1)\sum_{r=1}^{n}\rho^r\mathcal{B}_{n,r}\left(\gamma_1,\ldots,\gamma_{n-r+1}\right), \tag{3.20}$$

satisfies $\left\|x^{(n)}\right\|_\infty \leq \gamma_n$, $\forall n\geq 1$, where ρ is defined in theorem 3.2.

Proof:

Let's prove this statement by induction. It is obvious that $x^{(0)}$ is bounded in virtue of the exponential stability of the autonomous system $\dot{x}=Ax$. Let $\mathcal{H}_n$ be the following induction assumption:

($\mathcal{H}_n$) *For all integer k between 1 and n, the function $x^{(k)}$ defined by* (3.10) *is bounded and $\left\|x^{(k)}\right\|_\infty$ satisfies $\left\|x^{(k)}\right\|_\infty \leq \gamma_k$.*

Proving $\mathcal{H}_1$ is carried out by first integrating the second line of (3.10). This is a casual linear system whose input is known, and, given the initial conditions (3.11), one eventually gets (see [11]):

$$\forall t\geq 0,\quad x^{(1)} = \sum_{i=1}^{N}\left(\int_0^t \Phi(t,t')\bar{b}_i(t')\sin\left(\omega_i c_i x^{(0)}+\varphi_i^*\right)dt'\right)+\int_0^t\Phi(t,t')\bar{b}_0(t')dt',$$

which is bounded as follows:

$$\begin{aligned}\left\|x^{(1)}\right\| &\leq \sum_{i=1}^{N}\left\|\sin\left(\omega_i c_i x^{(0)}+\varphi_i^*\right)\right\|_\infty\left(\int_0^t\left\|\Phi(t,t')\bar{b}_i(t')\right\|dt'\right)+\int_0^t\left\|\Phi(t,t')\bar{b}_0(t')\right\|dt'\\ &\leq \sum_{i=0}^{N}\lambda_i\beta_i/\varepsilon \leq 1.\end{aligned} \tag{3.21}$$

Let's now assume ($\mathcal{H}_n$) is fulfilled, we have to prove ($\mathcal{H}_{n+1}$). It simply amounts to proving

$$\left\|x^{(n+1)}\right\|_\infty \leq \gamma_{n+1}.$$

As previously, we integrate (3.10) and carry out computations similar to those necessary to prove ($\mathcal{H}_1$). Let's first note:

$$\forall n\geq 1,\quad \forall t\geq 0,\quad x^{(n+1)} = (n+1)\sum_{i=1}^{N}\sum_{r=1}^{n}\int_0^t\Phi(t,t')\bar{b}_i(t')\mathcal{B}_{n,r}\left(c_i x^{(1)},\ldots,c_i x^{(n-r+1)}\right)f_{i,r}\left(c_i x^{(0)},t'\right)dt'. \tag{3.22}$$

Given the definition (3.15) of the functions $f_{i,r}$, the following hold:

- $\forall i, 1 \leq i \leq N, \quad \forall r \geq 0, \quad \left\| f_{i,r}\left(c_i x^{(0)}, t\right) \right\|_\infty \leq \omega_i^r,$
- $\forall i, 1 \leq i \leq N, \quad \sup_{t \geq 0} \left(\int_0^t \left\| \Phi(t,t') \bar{b}_i(t') \right\| dt' \right) \leq \lambda_i \beta_i / \varepsilon \leq 1/(N+1).$

These relations are used in the equation (3.22), this leads us to $\forall n \geq 1$ and $\forall t \geq 0$:

$$\left\| x^{(n+1)} \right\| \leq \frac{n+1}{N+1} \sum_{i=1}^{N} \sum_{r=1}^{n} \omega_i^r \left\| \mathcal{B}_{n,r}\left(c_i x^{(1)}, \ldots, c_i x^{(n-r+1)}\right) \right\|_\infty . \tag{3.23}$$

Let's now make use of the different properties reported in appendix B.2 concerning the Bell polynomials $\mathcal{B}_{n,r}$. We particularly make the most of the polynomial $\mathcal{B}_{n,r}$ being homogeneous of degree r and having only positive coefficients:

$$\begin{aligned}
\left\| \mathcal{B}_{n,r}\left(c_i x^{(1)}, \ldots, c_i x^{(n-r+1)}\right) \right\|_\infty &\leq \mathcal{B}_{n,r}\left(\left\| c_i x^{(1)} \right\|_\infty, \ldots, \left\| c_i x^{(n-r+1)} \right\|_\infty \right) \\
&\leq \mathcal{B}_{n,r}\left(c_i^\star \left\| x^{(1)} \right\|_\infty, \ldots, c_i^\star \left\| x^{(n-r+1)} \right\|_\infty \right) \\
&\leq (c_i^\star)^r \mathcal{B}_{n,r}\left(\left\| x^{(1)} \right\|_\infty, \ldots, \left\| x^{(n-r+1)} \right\|_\infty \right) \\
&\leq (c_i^\star)^r \mathcal{B}_{n,r}\left(\gamma_1, \ldots, \gamma_{n-r+1}\right),
\end{aligned} \tag{3.24}$$

the last inequality resulting from the induction assumption $(\mathcal{H}_n)$. Let's use (3.24) together with (3.23), to get:

$$\begin{aligned}
\left\| x^{(n+1)} \right\|_\infty &\leq \frac{n+1}{N+1} \sum_{i=1}^{N} \sum_{r=1}^{n} \mathcal{B}_{n,r}\left(\gamma_1, \ldots, \gamma_{n-r+1}\right) \left(c_i^\star \omega_i\right)^r \\
&\leq (n+1) \sum_{r=1}^{n} \rho^r \mathcal{B}_{n,r}\left(\gamma_1, \ldots, \gamma_{n-r+1}\right) = \gamma_{n+1},
\end{aligned}$$

which proves $\mathcal{H}_{n+1}$.

Lemma 3.3 *Let γ_n be defined by* (3.20)*, the numerical series $\sum_{n \geq 1} \gamma_n \frac{\varepsilon^n}{n!}$ converges if ε is no larger than $\varepsilon^* = \frac{1}{\rho e}$, moreover, γ_n is explicitly given by $\gamma_n = (n\rho)^{n-1}$, $\forall n \geq 1$.*

Proof:

We shall prove this lemma in two steps:

1. We assume that the series $\sum_{n \geq 0} \gamma_n \frac{\varepsilon^n}{n!}$ converges and show that its limit solves an algebraic equation depending on ε.
2. The Lagrange inversion theorem presented in the appendix C.3 tells us that the equation we arrived at in the previous step has a unique and analytical root which can be expanded in a

power series of ε. The expression of ε^* and γ_n can also be deduced from this theorem.

Suppose $\sum_{n\geq 1}\gamma_n\frac{\varepsilon^n}{n!}$ converges for some ε and let γ be its limit. If we multiply both sides of the equation (3.20) by $\frac{\varepsilon^{n+1}}{(n+1)!}$, we get:

$$\forall n \geq 1, \quad \gamma_{n+1}\frac{\varepsilon^{n+1}}{(n+1)!} = \varepsilon\left(\sum_{r=1}^{n}\rho^r\mathcal{B}_{n,r}\left(\gamma_1,\ldots,\gamma_{n-r+1}\right)\right)\frac{\varepsilon^n}{n!} \tag{3.25}$$

Looking carefully at the right-hand side of this equation and keeping in mind the Faa dì Bruno formula (see equation (C.6) in the appendix), we recognize the n-th term of the power series expansion resulting from the composition of the function:

$$h(y) = e^{\rho y}$$

by the series $y = \gamma = \sum_{n\geq 1}\gamma_n\frac{\varepsilon^n}{n!}$ assumed convergent so far. Let's detail this statement. Since h is analytical on $\mathbb{R}$, the following expansion is derived and valid for any $y \in \mathbb{R}$:

$$h(y) = 1 + \sum_{n\geq 1}\rho^n\frac{y^n}{n!}$$

According to the Faa dì Bruno formula:

$$h\left(\sum_{n\geq 1}\gamma_n\frac{\varepsilon^n}{n!}\right) = 1 + \sum_{n\geq 1}\left(\sum_{r=1}^{n}\rho^r\mathcal{B}_{n,r}\left(\gamma_1,\ldots,\gamma_{n-r+1}\right)\right)\frac{\varepsilon^n}{n!}.$$

If we use the equation (3.25) together with the previous relation where we multiply both sides by ε, we eventually get:

$$\begin{aligned}\varepsilon\, h\left(\sum_{n\geq 1}\gamma_n\frac{\varepsilon^n}{n!}\right) &= \varepsilon\gamma_1 + \sum_{n\geq 1}\gamma_{n+1}\frac{\varepsilon^{n+1}}{(n+1)!} \\ &= \sum_{n\geq 1}\gamma_n\frac{\varepsilon^n}{n!}.\end{aligned}$$

Therefore, if $\sum_{n\geq 1}\gamma_n\frac{\varepsilon^n}{n!}$ converges, its limit γ solves the following equation:

$$\gamma = \varepsilon e^{\rho\gamma}. \tag{3.26}$$

Let's now move on to the second part of this proof. The right-hand side of the equation (3.26) fulfills the prerequisites of the Lagrange inversion theorem reported in the appendix C.3. Since the exponential function is analytical for any real number, the root γ of (3.26) may be expanded in power of ε for ε no larger than:

$$\frac{x^*}{\sup_{x=x^*}\left(N\exp\left(\rho x\right)\right)} = \frac{x^*}{N\exp\rho x^*}, \quad \forall x^* > 0.$$

The maximum value of the previous quantity is derived by canceling the derivative of $\frac{x}{N\exp\left(\rho x\right)}$ with respect to x. This results in setting $x^* = 1/\rho$. According to our approach, the largest ε for which the

equation (3.26) has an analytical root is given by:

$$\varepsilon^* = 1/(\rho e)\,.$$

As a consequence, the power series $\sum_{n\geq 1} \gamma_n \frac{\varepsilon^n}{n!}$ converges for $\varepsilon < 1/(\rho e)$. Moreover, the Lagrange inversion theorem makes it possible to explicitly compute the terms involved in the expansion of the consider root, thus:

$$\forall n \geq 1, \quad \gamma_n = \frac{d^{n-1}}{dy^{n-1}}\big(\exp(n\rho y)\big)\Big|_{y=0} = (n\rho)^{n-1}\,,$$

which ends the proof of this lemma.

Proof of the theorem 3.2:

The existence of a solution expressed as a power series expansion $\sum_{n\geq 0} x^{(n)} \frac{\varepsilon^n}{n!}$ is guaranteed by the Cauchy theorem given in the appendix C.1.1, and, according to the lemma 3.1, an immediate consequence of the Cauchy's method is the definitions of the functions $x^{(n)}$ by the equation (3.10). Furthermore, the functions $x^{(n)}$ are bounded by γ_n (see lemma 3.2), the numerical series $\sum_{n\geq 1} \gamma_n \frac{\varepsilon^n}{n!}$ converges when $\varepsilon \leq \frac{1}{\rho e}$ (see lemma 3.3), therefore the considered power series $\sum_{n\geq 0} x^{(n)} \frac{\varepsilon^n}{n!}$ also converges as soon as $\varepsilon \leq \varepsilon^* = \frac{1}{\rho e}$. The γ_n are recursively defined in the lemma 3.2 and the closed form is given in the lemma 3.3.

Remark 3.5 *The lemmas 3.1, 3.2 and 3.3 can be regarded in a slightly different way. In the previous proof, the convergence of the series* $\sum_{n\geq 0} x^{(n)} \frac{\varepsilon^n}{n!}$ *was a direct consequence of the the Cauchy's theorem and method. Actually, the previous lemmas completely prove the Cauchy's theorem for systems* (3.9)*. Let's make this new interpretation according to the appendices C.1.2 and C.1.3.*

According to the appendix C.1.2, suppose a power series $\sum_{n\geq 0} x^{(n)} \frac{\varepsilon^n}{n!}$ *formally satisfies the equation* (3.9)*, the functions* (3.10) *are thus built. Part of the work left to do consists in checking that the previously defined series is actually the solution of the differential equation* (3.9) *when* ε *is small enough. This amounts to checking the different convergence assumptions reported in the appendix C.1.3.*

According to the lemmas 3.2 and 3.3, the series $\sum_{n\geq 0} x^{(n)} \frac{\varepsilon^n}{n!}$ *is normally and thus uniformly converging. We furthermore use the equations* (3.10)*, the relations* $\left\| x^{(n)} \right\|_\infty \leq \gamma_n$ *as well as some of the properties*

of the Bell polynomials of the second kind to conduct the following computations:

$$\begin{aligned}\forall n \geq 1, \quad \left\| \dot{x}^{(n+1)} \right\|_\infty &\leq A^\star \left\| x^{(n+1)} \right\|_\infty + (n+1) \sum_{i=1}^{N} \bar{b}_i^\star \left(\sum_{r=1}^{n} \mathcal{B}_{n,r} \left(\left\| x^{(1)} \right\|_\infty, \ldots, \left\| x^{(n-r+1)} \right\|_\infty \right) (\omega_i c_i^\star)^r \right) \\ &\leq A^\star \gamma_{n+1} + (n+1) \left(\sum_{r=1}^{n} \rho^r \mathcal{B}_{n,r} \left(\gamma_1, \ldots, \gamma_{n-r+1} \right) \right) \left(\sum_{i=1}^{N} \bar{b}_i^\star \right) \\ &\leq \left(A^\star + \sum_{i=1}^{N} \bar{b}_i^\star \right) \gamma_{n+1}.\end{aligned}$$

This ends proving that the series $\sum_{n \geq 0} \dot{x}^{(n)} \frac{\varepsilon^n}{n!}$ *is also uniformly converging for* $\varepsilon < \frac{1}{\rho e}$ *and gives a constructive proof of the Cauchy's theorem at the same time.*

3.3.2 Practical considerations

The set of equations (3.10) defining the solution of (3.3), though infinite, is still triangular. The zero order term is computed by solving an autonomous linear differential equation, and is the only term of the expansion to take the initial conditions x_0 into account. Once $x^{(0)}$ is derived, the recursive process is initiated and higher order terms can easily be computed. Actually, at each iteration, one has to solve a first order linear system whose inputs are known since they only depend on lower order components.

The theorem 3.2 allows us to estimate the magnitudes of the successive approximations and also to determine the maximum value of ε so that the expansion remains convergent. The smallness of the parameter ε, required for the expansion to converge, may be expressed in terms of the physical variables of the model (3.3). We now have a better understanding of the roles played by the magnitudes λ_i and the pulsations ω_i, namely through the following constraint:

$$\max_{1 \leq i \leq N} \left(\omega_i c_i^\star \right) \max_{0 \leq i \leq N} \left(\lambda_i \beta_i \right) \leq \frac{1}{(N+1)e}. \tag{3.27}$$

The discussion initiated in the section 3.2.2 can now be pursued and a little bit more detailed. We previously had no idea on the roles of the ω_i. For a given system (3.3) with fixed β_i, the power series expansion of the solution remains valid for rapidly changing perturbations (large ω_i) provided their magnitudes is not too large. Conversely slowly varying (small ω_i) periodic functions of the state may have quite large magnitudes. From a technological point of view, this constraint is always satisfied. Actually, rapidly varying perturbations are mostly caused by interpolation errors with a couple microns spatial period while the magnitude of this phenomenon is a dozen of nanometers (see the remark 1.1). Some perturbations forces such as cogging have pretty significant magnitudes but they vary on larger scales, namely a couple of millimeters (refer to the remark 1.5).

The theorem 3.2 is thus relevant as it copes with most physical situations involving state-periodic perturbations. It allows us to integrate the equation (3.3) with an infinite series expansion which one may truncate as the magnitudes of the successive approximations rapidly tail away. Only the very first components of the series bring substantial information. Neglect the initial conditions x_0 only acting on $x^{(0)}$,

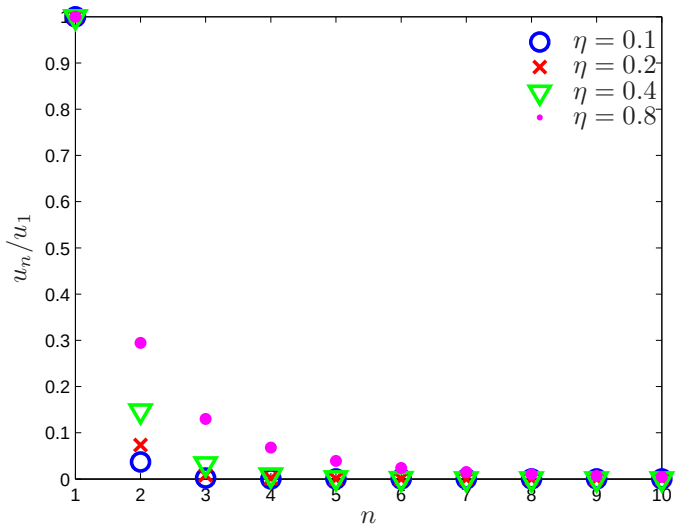

Figure 3.2: Convergence to zero of the power series expansion components derived by the Cauchy's method.

each term of the series expansion may be bounded as follows:

$$\forall n \geq 1, \quad \left\| x^{(n)} \right\|_\infty \frac{\varepsilon^n}{n!} \quad \leq \quad u_n = \frac{\varepsilon \left(\varepsilon \rho n\right)^{n-1}}{n!}.$$

The parameter ε is varied between 0 and ε^* by setting $\varepsilon = \eta\varepsilon^*$ and $0 \leq \eta \leq 1$. We focus on the convergence speed to zero of the series u_n by plotting $\frac{u_n}{u_1}$ on figure 3.2. This rate emphasizes the relative magnitude of the expansion terms with respect to the first order approximation. According to the figure 3.2, the smaller ε, the more dominating the very first terms of the expansion as the norm $\left\| x^{(n)} \right\|_\infty$ fastly converges to zero. It turns out that a pretty accurate approximation of the solution of (3.3) is obtained by summing the very first terms that are simply given by:

$$\begin{aligned}
\dot{x}^{(0)} &= Ax^{(0)} \\
\dot{x}^{(1)} &= Ax^{(1)} + \sum_{i=1}^{N} \bar{b}_i \sin\left(\omega c_i x^{(0)} + \varphi_i^*\right) + \bar{b}_0 \\
\dot{x}^{(2)} &= Ax^{(2)} + \sum_{i=1}^{N} \bar{b}_i \left(\omega_i c_i x^{(1)}\right) \cos\left(\omega_i c_i x^{(0)} + \varphi_i^*\right) \\
\dot{x}^{(3)} &= Ax^{(3)} + \sum_{i=1}^{N} \bar{b}_i \left(\left(\omega_i c_i x^{(2)}\right) \cos\left(\omega_i c_i x^{(0)} + \varphi_i^*\right) - \left(\omega_i c_i x^{(1)}\right)^2 \sin\left(\omega_i c_i x^{(0)} + \varphi_i^*\right)\right)
\end{aligned} \tag{3.28}$$

3.4 Global stability of the origin

3.4.1 Presentation

Thanks to the theorem 3.2, we found out to what extent the state-periodic perturbations cause deviations of the state around the origin. We are now concerned with deriving sufficient conditions under which the origin is stable in spite of the perturbations. A first approach consists in making use of the first Lyapunov method [29]. Consider the following system where the evolution of the constant parameter ε is added:

$$\begin{aligned} \dot{x} &= Ax + \varepsilon \sum_{i=1}^{N} \bar{b}_i \sin\left(\omega_i c_i x + \varphi_i^*\right) + \varepsilon \bar{b}_0 \\ \dot{\varepsilon} &= 0. \end{aligned}$$

Linearizing this system around the origin $x = 0$ and $\varepsilon = 0$ yields:

$$\begin{aligned} \dot{x} &= Ax + \varepsilon \sum_{i=1}^{N} \bar{b}_i \sin\left(\varphi_i^*\right) + \varepsilon \bar{b}_0 \\ \dot{\varepsilon} &= 0, \end{aligned}$$

or, in a more compact manner:

$$\dot{x} = Ax + \sum_{i=1}^{N} \lambda_i b_i \sin\left(\varphi_i^*\right) + \lambda_0 b_0. \tag{3.29}$$

If the first order linearized system is asymptotically stable, we can draw a conclusion toward the local stability of the original system (3.9). In other words, both the initial conditions on the state x_0 and the parameter ε have to be small enough for the previous conclusion to apply.

3.4.2 Global stability of the origin

The previous result is not entirely satisfactory and we propose to derive conditions yielding global asymptotic stability of the origin for the system (3.9) despite the presence of the perturbations.

Theorem 3.3

If the solutions of the system (3.29) *asymptotically converges to zero, the origin of the system* (3.9) *is globally asymptotically stable for* $\varepsilon < \varepsilon^*$.

PROOF:

Let's first show that, under the assumption of the theorem, the function $x^{(1)}$ given by (3.10) asymptotically reaches 0 as t goes to infinity irrespective of the initial conditions x_0.

Denote by x^* the solution of the system (3.29) and $\Delta = x^* - \varepsilon x^{(1)}$ so that:

$$\dot{\Delta} = A\Delta + 2\sum_{i=1}^{N} \lambda_i b_i \sin\left(\omega_i c_i x^{(0)}/2\right) \cos\left(\omega_i c_i x^{(0)}/2 + \varphi_i^*\right).$$

Since the transition matrix Φ is exponentially stable, we know that $x^{(0)}$ goes to zero as t goes to infinity for any initial conditions x_0. Since Δ is the solution of an exponentially stable linear system with vanishing input, Δ asymptotically converges to zero, see [11]. As a consequence, for any value x_0, the function $x^{(1)} = (x^* - \Delta)/\varepsilon$ also converges to zero.

According to the lemma 3.5, for any $n \geq 2$, the n-th order components of the power series expansion vanishes. Thus, for any $n \geq 0$ and $x_0 \in \mathbb{R}^n$, $x^{(n)}$ asymptotically converges to zero. According to lemma 3.4, it implies that the solution of the original system (3.3) is asymptotically stable whatever value x_0 may take, and, such a conclusion holds provided $\varepsilon < \varepsilon^*$.

Lemma 3.4 *If, for all $n \geq 0$, $x^{(n)}$, defined by* (3.10)*, asymptotically converges to zero, the series $\sum_{n\geq 0} x^{(n)} \frac{\varepsilon^n}{n!}$ solution of* (3.9) *asymptotically tends to zero for $\varepsilon \leq \varepsilon^*$.*

Proof:

Define X_M as the truncated series as follows:

$$X_M = \sum_{m=0}^{M} x^{(m)} \frac{\varepsilon^m}{m!}.$$

Let's prove that X_M is normally converging. Actually, according to lemma 3.2:

$$\forall M \geq 1, \quad \|X_M\|_\infty \leq K \|x_0\| + \sum_{m=1}^{M} \gamma_m \frac{\varepsilon^m}{m!},$$

and the series $\sum_{m\geq 1} \gamma_m \frac{\varepsilon^m}{m!}$ converges as suggested by lemma 3.3. As a conclusion, the series X_M is well normally and thus uniformly converging. For all M, using the assumption of this lemma, $X_M(t)$ asymptotically tends to zero for t growing indefinitely. Thanks to the uniform convergence, inverting the limit and summation operations is allowed for $\varepsilon < \varepsilon^*$. We have just proved that the solution of (3.9), namely:

$$\sum_{n\geq 0} x^{(n)} \frac{\varepsilon^n}{n!} = \lim_{M\to\infty} X_M$$

is asymptotically stable.

Lemma 3.5 *Consider the functions $x^{(n)}$ defined by* (3.10)*, if $x^{(1)}$ is asymptotically converging to zero, for all $n \geq 2$, $x^{(n)}$ is also asymptotically converging.*

Proof:

Let's prove this by induction, basing our reasoning on the following assumption:

($\mathcal{H}'_n$) *For all integer $k \leq n$, $x^{(k)}$ tends asymptotically towards zero.*

Under the conditions of this lemma, the assumption $\mathcal{H}'_1$ is obvious. Suppose $\mathcal{H}'_n$ valid, proving $\mathcal{H}'_{n+1}$ boils down to showing that $x^{(n+1)}$ (equation (3.10)) tends towrds zero. For any r between 1 and

n, $\mathcal{B}_{n,r}\left(c_i x^{(1)}, \ldots, c_i x^{(n-r+1)}\right)$ is a homogeneous polynomial with degree r, implying $\mathcal{B}_{n,r}$ has no constant term. According to $\mathcal{H}'_n$, $\mathcal{B}_{n,r}\left(c_i x^{(1)}, \ldots, c_i x^{(n-r+1)}\right)$ asymptotically tends to zero. The input of the exponentially stable linear system defining $x^{(n+1)}$ is asymptotically converging to zero since it results from the product of the previously mentioned polynomials and the bounded functions $\sin\left(\omega_i c_i x^{(0)} + \varphi_i^* + \frac{r\pi}{2}\right)$. We thus check that $x^{(n+1)}$ is converging to zero (see [11]) which ends proving $\mathcal{H}'_{n+1}$.

3.5 Partial expansion of the state

So far, we have addressed the expansion of the whole state in a power series. We pointed out a parameter ε which turns out to be small enough to guarantee the convergence of the expansion when the perturbations only have limited effects on the entire state x. However, it may sometimes happen that perturbations slightly affect only a partition of the state while the remaining components of the vector x are significantly affected by these perturbations. In such a situation, the previously defined parameter ε may not take arbitrarily small values. In this part, the expansion of the least perturbed components of the state is solely undertaken. To this end, we define a better suited parameter in that it only reflects the effect of the perturbations on the considered partition of the state. This newly defined parameter yields less conservative convergence conditions in the considered applications.

3.5.1 Example

To illustrate this, we rewrite the introductory example (3.2) a in way similar to (3.3) while neglecting viscous friction:

$$\dot{x} = \begin{pmatrix} 0 & 1 \\ -\omega_0^2 & -2\zeta_0\omega_0 \end{pmatrix} x + \begin{pmatrix} 0 \\ 1 \end{pmatrix} \lambda \sin(\omega c x) = Ax + b\lambda \sin(\omega c x + \omega \xi^*),$$

with $c = \begin{pmatrix} 1 & 0 \end{pmatrix}$.

This is a stationary example, and the computation of β defined by (3.5) is doable. Setting $\zeta_0 = 1$ and $\omega_0 = 2\pi \times 20\text{rad/s}$, we find $\beta \approx 6e^{-3}$ which is neither more nor less than the $\mathcal{L}_1$-norm of the transfer function $(sI - A)^{-1} b$. Rewriting the equation (3.27) for this example, the theorems 3.2 and 3.3 may only be applied if:

$$\lambda \leq \frac{1}{e\omega\beta} \approx \frac{160}{e\omega}. \tag{3.30}$$

The input $\lambda \sin(\omega c \xi)$ does not have the same impact on the first component of x (the position tracking error) as on its second component (the velocity tracking error). We compute the $\mathcal{L}_1$-norm of the associated transfer functions, respectively noted $H_1(s)$ and $H_2(s)$ and defined as follows:

$$\begin{aligned} \mu_1 &= \left\| \begin{pmatrix} 1 & 0 \end{pmatrix} (sI - A)^{-1} b \right\|_1 = \left\| \frac{1}{s^2 + 2\xi_0\omega_0 s + \omega_0^2} \right\|_1 = \|H_1(s)\|_1 \approx 6e^{-5} \\ \mu_2 &= \left\| \begin{pmatrix} 0 & 1 \end{pmatrix} (sI - A)^{-1} b \right\|_1 = \left\| \frac{s}{s^2 + 2\xi_0\omega_0 s + \omega_0^2} \right\|_1 = \|H_2(s)\|_1 \approx 6e^{-3} \end{aligned} \tag{3.31}$$

The perturbation influences the position tracking error approximately one hundred times less than it influences the velocity tracking error. Also note that β turns out to be large because of the effect of the perturbation on the second component of x (compare β and μ_2).

In this part, we shall expose the necessary elements to prove that the position tracking error may be expanded in powers of $\mu_1\lambda$ and the resulting series is converging if:

$$\lambda \leq \frac{1}{e\omega\mu_1} \approx \frac{16000}{e\omega}, \tag{3.32}$$

which enables this approach to cope with much larger perturbations when compared to (3.30). As generalized hereafter, the key point is the use of the $\mathcal{L}_1$-norm of the transfer from the perturbations to the considered partition of the state.

3.5.2 Preliminaries

Let $y = \left(y_1, \ldots, y_N, y_{N+1}, \ldots, y_M\right) \in \mathbb{R}^M$ be a function of the state x (see (3.3)) such as $y_i = c_i x$ with the c_i defined as follows:

- for i between 1 and N, c_i is given by the definition 3.1,
- for i between $N+1$ and M, c_i is an arbitrary row vector of size n featuring the same properties as the vector c_i of the definition 3.1.

The row vector c_i are stacked up in $C = \left(c_1^T, \ldots, c_M^T\right)^T$ and the definition $C^\star = \sup_{t\geq 0} \|C(t)\|$ is relevant. We now define the impulse responses h_i from any of the scalar inputs to the output $y = Cx$ as well as the formal input-output operators H_i as follows:

$$\forall i,\ 0 \leq i \leq N, \quad h_i(t,t') = C(t)\Phi(t,t')b_i(t') \quad \text{and} \quad H_i u = \int_0^t h_i(t,t')u(t')dt'. \tag{3.33}$$

We also define the $\mathcal{L}_1$-norm of the impulse responses $h_i(t,t')$ by:

$$\forall i,\ 0 \leq i \leq N, \quad \|h_i\|_1 = \sup_{t\geq 0} \left(\int_0^t \|h_i(t,t')\|\, dt' \right). \tag{3.34}$$

The previous parameter is well defined since the transition matrix is exponentially stable and the functions b_i and C are supposed to be bounded.

Using the previous definitions together with (3.4) yields an implicit equation for the output y:

$$y = C\Phi(t,0)x_0 + \sum_{i=1}^{N} \lambda_i H_i \sin\left(\omega_i C_i y + \varphi_i^*\right) + \lambda_0 H_0, \tag{3.35}$$

with C_i an M-dimensional row vector whose i-th entry is the only non-zero element and equals 1. In a way similar to (3.7), we also get:

$$\forall t \geq 0, \quad \|y(t)\| \leq KC^\star e^{-\alpha t}\|x_0\| + \mu, \tag{3.36}$$

with μ given by:

$$\mu = (N+1) \max_{0\leq i\leq N} \left(\lambda_i \|h_i\|_1\right). \tag{3.37}$$

The parameter μ directly quantifies the effect of the perturbations on the output, and is strongly related to the $\mathcal{L}_1$-norm of the transfer functions from the perturbations to y. In the following, the output y is expressed as a power series $\sum_{n\geq 0} y^{(n)} \frac{\mu^n}{n!}$.
To this end, we first define the reduced input-output operators:

$$\forall i,\ 0 \leq i \leq N, \quad \bar{H}_i = \lambda_i H_i/\mu, \tag{3.38}$$

and we rewrite (3.35) into:

$$y = C\Phi(t,0)x_0 + \mu \sum_{i=1}^{N} \bar{H}_i \sin\left(\omega_i C_i y + \varphi_i^*\right) + \mu \bar{H}_0. \tag{3.39}$$

We look for the solutions of the previous equation by formally replacing y by $\sum_{n\geq 0} y^{(n)} \frac{\mu^n}{n!}$.

3.5.3 Expansion and convergence towards zero of the output

Let's still make use of the Bell polynomials of the second kind and define the functions $y^{(n)}$ by:

$$\begin{aligned}
y^{(0)} &= C\Phi(t,0)x_0 \\
y^{(1)} &= \sum_{i=1}^{N} \bar{H}_i \sin\left(\omega_i C_i y^{(0)} + \varphi_i^*\right) + \bar{H}_0 \\
y^{(n+1)} &= (n+1) \sum_{i=1}^{N} \bar{H}_i \left(\sum_{r=1}^{n} \mathcal{B}_{n,r}\left(C_i y^{(1)}, \ldots, C_i y^{(n-r+1)}\right) \omega_i^r \sin\left(\omega_i C_i y^{(0)} + \varphi_i^* + \frac{r\pi}{2}\right)\right).
\end{aligned} \tag{3.40}$$

This set of functions is used to adapt the results of the theorems 3.2 and 3.3 to te current study concerning the output y. Given the different elements reported so far, the two following theorems are readily obtained.

Theorem 3.4

Given the functions $y^{(n)}$ defined by (3.40), there exists a scalar $\mu^* > 0$ such that, if $\mu \leq \mu^*$, the series $\sum_{n\geq 0} y^{(n)} \frac{\mu^n}{n!}$ converges and its limit is the solution of the equation (3.35). Furthermore, if we denote $\omega = \max_{1\leq i\leq N} \omega_i$ and e the Neperian constant:

$$\mu^* \leq \frac{1}{\omega e}, \quad \text{and} \quad \forall n \geq 1, \quad \left\| y^{(n)} \right\|_\infty \leq (\omega n)^{n-1} \tag{3.41}$$

PROOF:

We first formally replace y by $\sum_{n\geq 0} y^{(n)} \frac{\mu^n}{n!}$ in (3.35). To expand the sine functions where y appears, we simply use the equation (3.14) where we replace c_i by C_i. By doing so, the equations (3.40) defining

the $y^{(n)}$ are readily derived. According to the theorem 3.2 where the parameter ρ was used, let ω be:

$$\omega = \max_{1\leq i\leq N}(\omega_i C_i) \quad \text{thus} \quad \omega = \max_{1\leq i\leq N}\omega_i$$

since the only non-zero entry of C_i equals 1. The equation (3.41) matches the equation (3.12). The only thing left to prove is that the series we arrived at solves the equation (3.39). Let's use the functions $f_{i,n}$ (see equation (3.15)), the following relation holds:

$$\begin{aligned}\sum_{n\geq 0} y^{(n)}\frac{\mu^n}{n!} &= C\Phi(t,0)x_0 + \mu\bar{H}_0 + \\ &\mu\sum_{i=1}^{N}\left(\bar{H}_i f_{i,0}\left(C_i y^{(0)},t\right) + \sum_{n\geq 1}\bar{H}_i\left(\sum_{r=1}^{n}\mathcal{B}_{n,r}\left(C_i y^{(1)},\ldots,C_i y^{(n-r+1)}\right) f_{i,r}\left(C_i y^{(0)},t\right)\right)\frac{\mu^n}{n!}\right).\end{aligned} \tag{3.42}$$

By a reasoning similar to the proof of the lemma 3.3, the following series:

$$\sum_{i=1}^{N}\bar{H}_i\left(\sum_{r=1}^{n}\mathcal{B}_{n,r}\left(C_i y^{(1)},\ldots,C_i y^{(n-r+1)}\right) f_{i,r}\left(C_i y^{(0)},t\right)\right)\frac{\mu^n}{n!}$$

is showed to be normally converging. Integration (operators $\bar{H}_i$) and series summation operators may well be inverted in (3.42). Provided μ is small enough, the series $\sum_{n\geq 0} y^{(n)}\frac{\varepsilon^n}{n!}$ is the solution of (3.39).

Theorem 3.5

If the function y^* defined by:

$$y^* = \sum_{i=1}^{N} H_i \sin\left(\varphi_i^*\right) + H_0 \tag{3.43}$$

asymptotically tends to zero, the function y solution of (3.35) *also converges to zero if $\mu \leq \mu^*$ (defined by* (3.41)*) irrespective of the initial condition x_0.*

PROOF:

If y^* tends to zero, considering $y^* - \mu y^{(1)}$, it can be showed that $y^{(1)}$ is asymptotically converging to zero for any initial conditions x_0. The Bell polynomials of the second kind are homogeneous of degree r. When looking at (3.40), it is obvious to conclude that, for all $n \geq 2$, the functions $y^{(n)}$ are also vanishing. Note that $y^{(0)}$ is exponentially vanishing. Since the series $\sum_{n\geq 0} y^{(n)}\frac{\mu^n}{n!}$ converges normally, the output y, solving (3.39), turns out to be vanishing as t grows indefinitely.

Remark 3.6 *The expression giving the expansion of the output y is quite similar to the one pertaining to the expansion of the whole state x. Simply compare the equations* (3.10) *and* (3.40)*. The practical discussion of the section 3.3.2 may be adapted for the ongoing study, especially concerning the decay to*

zero of the terms of the series, namely

$$\left\| y^{(n)} \right\|_\infty \frac{\mu^n}{n!} \leq \frac{\mu \left(\mu\omega n\right)^{n-1}}{n!} = v_n.$$

By analogy with the approach of the section 3.3.2, suppose $\mu = \eta\mu^*$ *and* $0 \leq \eta \leq 1$*. The plot of* $\frac{v_n}{v_1}$ *as a function of* η *is readily similar to the one of the figure 3.2.*
The same conclusion may thus be drawn:

- *The smaller* μ*, the faster the decay rate to zero of* $\left\| y^{(n)} \right\|_\infty$ *with respect to* $y^{(1)}$*.*
- *The required smallness of* μ *for the expansion to converge can be translated into physical considerations. Namely:*

$$\max_{1\leq i\leq N}\left(\omega_i\right) \max_{0\leq i\leq N}\left(\lambda_i \left\|h_i\right\|_1\right) \leq \frac{1}{(N+1)e}.$$

3.5.4 Conclusion

We now get back to the introductory example and end this study. According to the previous remark, the convergence condition first exposed by the equation (3.32) is proved. The equation (3.31) defines $H_1(s)$, the transfer function from the perturbation to the tracking error cx. In view of the undisputable similarities between the expansion a sole output and of the whole state, we shall take advantage of the first terms of the expansion of the latter. They are given by the equation (3.28). We also assume that the steady state is reached, so that $y^{(0)}$ is neglected. We eventually get:

$$\begin{aligned} y^{(1)} &= \bar{H}_1(s)\sin\left(\omega\xi^*\right) \\ y^{(2)} &= \bar{H}_1(s)\left(\omega y^{(1)}\right)\cos\left(\omega\xi^*\right) \\ y^{(3)} &= \bar{H}_1(s)\left(\left(\omega y^{(2)}\right)\cos\left(\omega\xi^*\right) - \left(\omega y^{(1)}\right)^2 \sin\left(\omega\xi^*\right)\right), \end{aligned} \tag{3.44}$$

where, according to the remark 3.1, $\omega\xi^*$ is the forcing phase to allow for, and is substituted to the φ_i^*.
We may pursue the calculations a little bit further to unveil an interesting structure when the system is constrained to track a constant speed trajectory $\xi^* = \nu^* t$. We look for an explicit expression of the first terms $y^{(n)}\frac{\mu^n}{n!}$ in steady state ($y^{(0)} \to 0$):

$$\begin{aligned} y^{(1)}\mu &= \left(\lambda H_1(s)\right)\sin\left(\omega\nu^* t\right) \\ y^{(2)}\frac{\mu^2}{2!} &= \left(\lambda H_1(s)\right)^2 \omega \sin\left(\omega\nu^* t\right)\cos\left(\omega\nu^* t\right)/2 \\ y^{(3)}\frac{\mu^3}{3!} &= \left(\lambda H_1(s)\right)^3 \omega^2\left(\sin\left(\omega\nu^* t\right)\cos^2\left(\omega\nu^* t\right) - \sin^3\left(\omega\nu^* t\right)\right)/6. \end{aligned} \tag{3.45}$$

The regular perturbation analysis is informative. It shows that, when a brushless motor is operated at constant velocity, it oscillates around its desired trajectory. Several pulsations may be found even if the perturbation force is purely sinusoidal with the position. The figure 3.3 illustrates this point when

$\nu^* = 100\text{mm/s}$, $\omega = \frac{2\pi}{20}\text{rad/mm}$ and $\lambda = 10e^3\text{mm/s}^2$. The frequency peaks witnessed on this figure are more specifically explained as follows:

- The first order term generates the frequency peak located at $\frac{\omega\nu^*}{2\pi} = 5\text{Hz}$ and whose magnitude is directly related to $|H_1(i\omega\nu^*)|$.
- The second order term generates the frequency peak located at $\frac{2\omega\nu^*}{2\pi} = 10\text{Hz}$ and whose magnitude is directly related to $|H_1(2i\omega\nu^*)|^2$.
- The third order term brings the frequency peak located at $\frac{3\omega\nu^*}{2\pi} = 15Hz$ and is even more attenuated by $|H_1(s)|^3$.

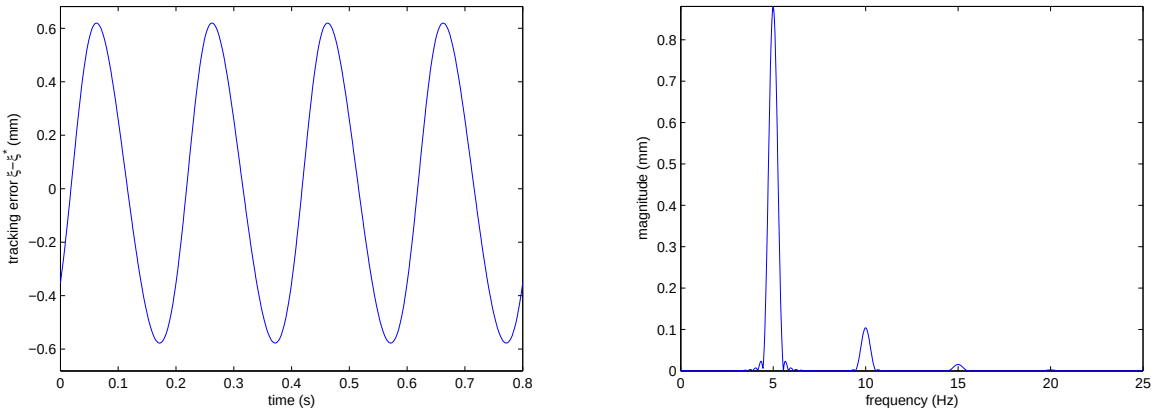

(a) Tracking error.

(b) FFT of the tracking error.

Figure 3.3: Simulation of the introductory example (3.1) with $\xi^* = 100t$, $\lambda = 1e^4\text{mm/s}^2$ and $\omega = \frac{2\pi}{20}\text{rad/mm}$.

CHAPTER 4

An Observer-Based Control Scheme Including Perturbations Modeling for High-Precision Trajectory Tracking

4.1 Presentation

This chapter is concerned with getting brushless motors tracking reference trajectories of any kind with stringent accuracy specifications (related to the applications presented in chapter 1) in spite of cogging forces and interpolation errors. The situation is illustrated by the figure 4.1.

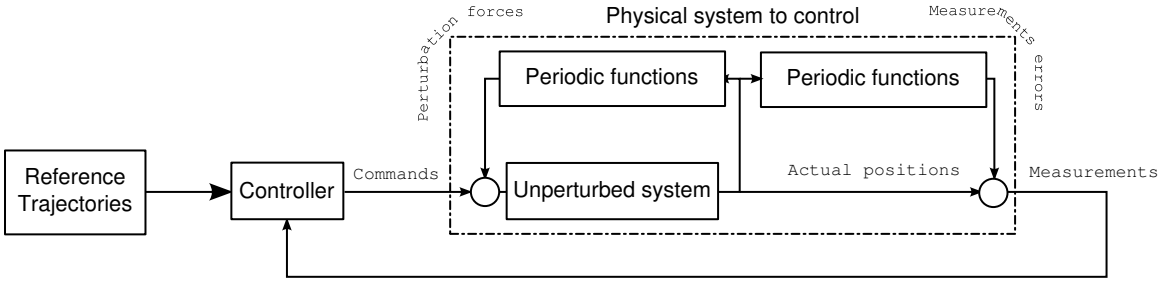

Figure 4.1: Design of a controller for high-end trajectory tracking despite state-periodic perturbations.

Great technological efforts have been made to minimize the, though natural, limitations considered so far. For cogging forces specifically pertaining to ironcore motors, the underlying idea consists in using the free design parameters, like the shapes of the magnets, the spacing in between slots, or the length of the rotor to analytically or numerically find out which configuration actually minimizes cogging forces. All these techniques generally lead to very complex designs, such as skewed magnets layouts, which, in the end, do not manage to completely get rid of cogging forces (see [25]). For ironless motors, despite the attention paid to the design of the circuits in charge of producing the electrical currents, there always remain some slowly time-varying offsets, responsible for cogging-like forces (see the equation (1.8)). The issue is similar

for interpolation errors mainly due to the thermal drift of electrical circuits.

Driving a production model brushless motor with a PID controller yields satisfactory results for some applications, but, when stringent accuracy specifications are at stake, a dedicated controller is required to get rid of these residual state-periodic perturbations. It might be tempting to perform this cancellation from a preliminary analytical or numerical analysis together with a feedforward compensation scheme. However, note that modeling these perturbations turn out to be tough (see [25] for cogging forces). The task is even more complicated in the case of interpolation errors. Imagine the huge amount of memory required to get a mapping of an optical rule.

The previous analysis makes definitely lean toward an online identification and cancellation scheme. In the existing literature, cogging forces and interpolation errors are not tackled simultaneously. Let's give a review of the existing solutions for cogging compensation. For repetitive tasks, it is possible to estimate the cogging forces affecting the motion during one run, and, directly compensate for them during the next run. This iterative method can obviously cope with perturbations of arbitrary shape and takes several tries to yield satisfactory results. It is either referred to as *learning feedforward* [40] or *iterative learning control* [51, 36, 12].

Some other existing solutions, dedicated to spatially periodic perturbations, express cogging forces as a spatial Fourier series expansion. Adaptive controllers may be designed to estimate both the magnitude and phase of each of the Fourier series expansion components and achieve position tracking thanks to cogging compensation, see [1, 48] for instance. Observer-based controllers can also be derived considering an extended system made up of the motor mechanics and the perturbations using an internal model. In [13], this approach is implemented for mechanical pure sine perturbations and can be adapted to remove the fundamental component of the cogging forces Fourier series, but the extension to higher order harmonics does not seem to be straightforward.

Both adaptive and observer-based methods reported so far suppose the velocity available, either by direct measurements or numerical differentiation of the position. For the high precision positioning applications previously mentioned, assuming the position directly measured is rather sensible and common, but numerical computation of the velocity may generate undesirable noise affecting the whole system performances.

The method central to the interpolation errors cancellation is known as the Heydemann's correction (see [24]). This approach was first intended to deal with interferometers, but, given the undisputable similarities between the functioning of interferometers and optical position errors, the approach has widely been extended to the latter. The core idea is to calibrate online the parameters of the sinusoidal pair delivered by the sensor (see the equation (1.3)). Several implementations exist, in the end, they all boil down to an online optimization either by classical iterative techniques [2] or, for example, neural networks [49].

In this chapter, an observer-based controller only relying on position measurements is designed. The framework is common to both cogging forces and interpolation errors. Our solution steers the tracking

error to zero by canceling cogging forces and filtering the position measurements to access the actual positions. These perturbations are defined by an arbitrary number of spatial periods, assumed known throughout this chapter. This rather strong assumption is loosened in the chapter 5, where it is showed that these parameters may be obtained from appropriate experiments.
As depicted on the figure 4.1, the proposed context generalizes the modelings of the equations (1.11) and (1.12). Namely, we consider a linear MIMO system, which can be regarded as the unperturbed plant. Its inputs can be viewed as forces, and, we suppose they are made up of commands and additive cogging forces, obviously periodic with respect to some positions. Moreover, the outputs of the unperturbed plant are assumed to be the considered tracking errors. The corresponding measurements are affected by interpolation errors. Practically speaking, we do not have access to the actual values of the positions and, perturbations are added to any commands computed by the controller.
After a part devoted to modeling, we derive the equations of the observer-based controller (section 2). The novelty of our approach lies in the use of the regular perturbation expansion of the chapter 3 to build the observer. We shall prove the relevancy of considering only the first-order approximation of the perturbed system to design the observer. The great advantage of doing so is clear for the gains tuning issue. Despite the nonlinearities of the plants (see figure 4.1), we eventually come up to a solution where the tuning has to be performed for a linear system. We shall see that it can be cast into some LMI optimization problems, see [10]. The final control architecture requires little online computation, especially since the gains are constant and computed offline.

4.1.1 Modeling

The systems considered hereafter obey the following definition and are illustrated on figure 4.2.

Definition 4.1 *Consider the system featuring p commands u_i and q measured outputs y_i such that:*

$$\begin{aligned} \dot{x} &= Ax + \sum_{i=1}^{p} b_i \left(u_i + \sum_{j \in \mathcal{I}_i} d_{i,j}\left(\xi_j\right) \right) \\ y_i &= c_i x + w_i\left(\xi_i\right), \quad 1 \leq i \leq q \end{aligned} \tag{4.1}$$

with the following notations:

- *x is an n-dimensional vector, A a square matrix of size n with constant entries. For all i between 1 and p, let b_i be a constant n-dimensional column vector, and, for all j between 1 and q, c_j a constant n-dimensional row vector.*

- *$c_i x$ is regarded as the tracking error between a spatial variable ξ_i and its reference trajectory ξ_i^*:*

$$\forall i,\ 1 \leq i \leq q, \quad \xi_i = c_i x + \xi_i^*. \tag{4.2}$$

- *The sets $\mathcal{I}_j$ are made up of integers from 1 to q:*

– *The functions $d_{i,j}$ are periodic with respect to the positions ξ_j and aim at modeling perturbation forces:*

$$\forall i,\ 1 \leq i \leq p, \quad \forall j \in \mathcal{I}_i, \quad d_{i,j}\left(\xi_j\right) = \sum_{n=1}^{N_{i,j}} \lambda_{i,j,n} \sin\left(\omega_{i,j,n}\xi_j + \varphi_{i,j,n}\right). \tag{4.3}$$

Note that the $\omega_{i,j,n}$ are supposed known while the magnitudes $\lambda_{i,j,n}$ and phases $\varphi_{i,j,n}$ are not. Let moreover $P_{i,j,n}$ be the spatial period associated to $\omega_{i,j,n} = \dfrac{2\pi}{P_{i,j,n}}$.

– *The functions w_i are periodic with respect to the positions ξ_i and aim at modeling measurement errors:*

$$\forall i,\ 1 \leq i \leq q, \quad w_i\left(\xi_i\right) = \sum_{n=1}^{N_i} \lambda'_{i,n} \sin\left(\omega'_{i,n}\xi_i + \varphi'_{i,n}\right). \tag{4.4}$$

Note that the $\omega'_{i,n}$ are supposed to be known while the magnitudes $\lambda'_{i,n}$ and phases $\varphi'_{i,n}$ are not. Let moreover $P'_{i,n}$ be the spatial period associated to $\omega'_{i,n} = \dfrac{2\pi}{P'_{i,n}}$.

Remark 4.1 *As suggested on figure 4.2, the unperturbed part of* (4.1) *is described by a linear stationary system with p inputs, comparable to torques or forces, and q outputs, regarded as tracking errors, such that:*

$$\begin{aligned} \dot{x} &= Ax + \sum_{i=1}^{p} b_i v_i \\ e_i &= c_i x, \quad 1 \leq i \leq q. \end{aligned} \tag{4.5}$$

Each input v_j is affected by cogging forces periodic in certain positions ξ_i (collected in the set $\mathcal{I}_j$). Moreover, the measurements of the deviations around the desired trajectories are corrupted by interpolation errors.

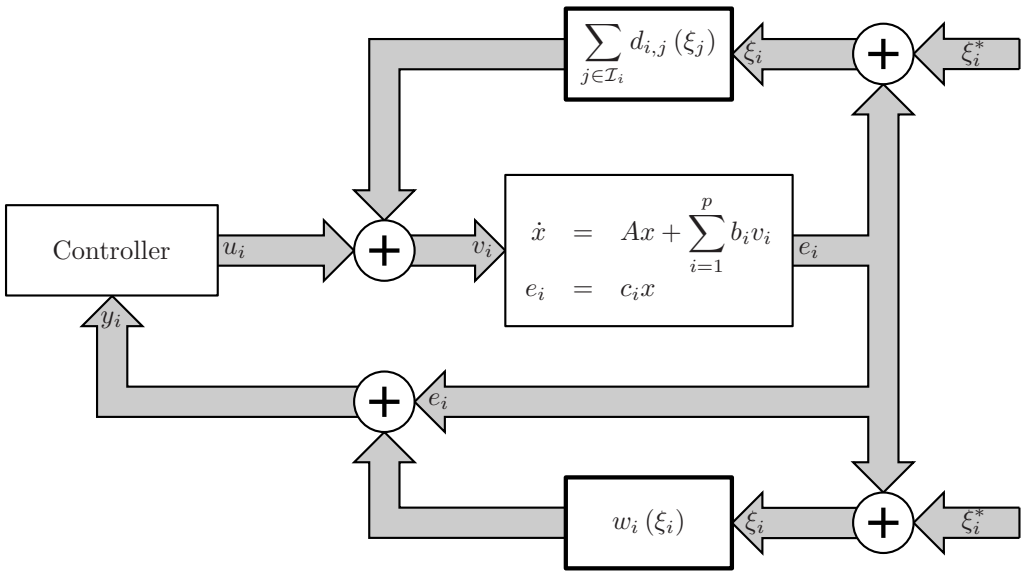

Figure 4.2: Systems under spatially periodic disturbances.

Remark 4.2 *One may assume that the unperturbed system* (4.5) *is derived from a mechanical analysis, it is justified to assume that the velocity tracking errors are present in the vector x, they are noted $\dot{e}_i = c_i' x$ with c_i' an n-dimensional constant row vector. Let ν_i be the derivative of the position ξ_i and $\nu_i^* = \dot{\xi}_i^*$ the corresponding reference velocity which is continuous and bounded. The following relations hold:*

$$\forall i,\ 1 \leq i \leq q, \quad \nu_i = c_i' x + \nu_i^* \quad \text{and} \quad \underline{\nu_i} \leq \nu_i^* \leq \overline{\nu}_i, \tag{4.6}$$

with $\overline{\nu}_i^*$ (respectively $\underline{\nu_i^*}$) the upper (respectively lower) bound on the reference velocity. The row vectors c_i' are collected in:

$$C' = \left((c_1')^T \quad \dots \quad (c_q')^T \right)^T \in \mathbb{R}^{q \times n}. \tag{4.7}$$

To give a compact view of the system (4.1), we make use of the internal model principle to describe the different perturbations (4.3) and (4.4). A sketch of this approach is given by the remarks 4.5 and 4.6. In the end, we arrive at the following state-space equation:

$$\begin{array}{rcl} \dot{\chi} & = & \mathcal{A}(\nu_1, \dots, \nu_q)\,\chi + \mathcal{B}u \\ y & = & \mathcal{C}\chi \end{array} \tag{4.8}$$

with the notations:

- Define $\chi = \begin{pmatrix} x^T & z^T \end{pmatrix}^T$ with z defined by (4.20) (in remark 4.6). The dimension of the vector χ is $n' = n + 2N$, with N defined by (4.19).

- Let u and y be the vectors where the commands and measurements are collected:

$$u = \begin{pmatrix} u_1 & \dots & u_p \end{pmatrix}^T, \quad y = \begin{pmatrix} y_1 & \dots & y_q \end{pmatrix}^T. \tag{4.9}$$

- The matrices B and C are defined as:

$$B = \begin{pmatrix} b_1 & \dots & b_p \end{pmatrix} \in \mathbb{R}^{n \times p}, \quad C = \begin{pmatrix} c_1^T & \dots & c_q^T \end{pmatrix}^T \in \mathbb{R}^{q \times n}, \tag{4.10}$$

  and, using the elements of the remark 4.6, two matrices $D \in \mathbb{R}^{p \times 2N}$ and $W \in \mathbb{R}^{q \times 2N}$ may be found such that:

$$\begin{pmatrix} \sum_{j \in \mathcal{I}_1} d_{1,j}(\xi_j) \\ \vdots \\ \sum_{j \in \mathcal{I}_p} d_{p,j}(\xi_j) \end{pmatrix} = Dz, \quad \begin{pmatrix} w_1(\xi_1) \\ \vdots \\ w_q(\xi_q) \end{pmatrix} = Wz. \tag{4.11}$$

- $\mathcal{A} \in \mathbb{R}^{n' \times n'}$, $\mathcal{B} \in \mathbb{R}^{n' \times p}$ and $\mathcal{C} \in \mathbb{R}^{q \times n'}$ are matrices defined as follows:

$$\mathcal{A}(\nu_1, \dots, \nu_q) = \begin{pmatrix} A & BD \\ \mathbf{0} & M(\nu_1, \dots, \nu_q) \end{pmatrix}, \quad \mathcal{B} = \begin{pmatrix} B \\ \mathbf{0} \end{pmatrix}, \quad \mathcal{C} = \begin{pmatrix} C & W \end{pmatrix}. \tag{4.12}$$

Remark 4.3 *According to the regular perturbation expansions presented in chapter 3, the equations* (4.1) *and* (4.5) *with the periodic functions $d_{i,j}$ and w_i evaluated along the reference trajectories ξ_i^* will play a role of prime interest in this chapter:*

$$\begin{aligned} \dot{x}^* &= Ax^* + \sum_{i=1}^{p} b_i \left(u_i^* + \sum_{j \in \mathcal{I}_i} d_{i,j}\left(\xi_j^*\right) \right) \\ y_i^* &= c_i x^* + w_i\left(\xi_i^*\right), \end{aligned} \tag{4.13}$$

and

$$\begin{aligned} \dot{\chi}^* &= \mathcal{A}\left(\nu_1^*, \ldots, \nu_q^*\right)\chi^* + \mathcal{B}u^* \\ y^* &= \mathcal{C}\chi^*, \end{aligned} \tag{4.14}$$

with $\chi^* = \begin{pmatrix} (x^*)^T & (z^*)^T \end{pmatrix}^T$. The previous two systems represent the first order approximation (in view of the theorem 3.2) of the system (4.1)*, though in open loop.*

Remark 4.4 *Since the matrix M (see equation* (4.20)*) is a linear function in the ν_i, the same result holds for the matrix $\mathcal{A}(\nu_1, \ldots, \nu_q)$ that may be expressed as:*

$$\mathcal{A}(\nu_1, \ldots, \nu_q) = \mathcal{A}_0 + \sum_{i=1}^{q} \nu_i \mathcal{A}_i = \begin{pmatrix} A & BD \\ \mathbf{0} & \mathbf{0} \end{pmatrix} + \sum_{i=1}^{q} \nu_i \begin{pmatrix} \mathbf{0} & \mathbf{0} \\ \mathbf{0} & M_i \end{pmatrix}. \tag{4.15}$$

Remark 4.5 *Each of the periodic functions previously used may be described using the internal model principle. To illustrate this, consider:*

$$\Lambda(\xi) = \sum_{k=1}^{K} \lambda_k \sin\left(\omega_k \xi + \varphi_k\right), \tag{4.16}$$

If we call $\nu = \dot{\xi}$ and

$$\zeta_k = \begin{pmatrix} \lambda_k \sin\left(\omega_k \xi + \varphi_k\right) & \lambda_k \cos\left(\omega_k \xi + \varphi_k\right) \end{pmatrix}^T,$$

observe that:

$$\dot{\zeta}_k = \nu \omega_k \begin{pmatrix} 0 & 1 \\ -1 & 0 \end{pmatrix} \zeta_k, \tag{4.17}$$

Stacking up the ζ_k in $\zeta = \begin{pmatrix} \zeta_1^T & \ldots & \zeta_K^T \end{pmatrix}$, the function Λ is given as the output of the following dynamical system:

$$\begin{aligned} \dot{\zeta} &= \nu \Theta \zeta \\ \Lambda &= \theta \zeta, \end{aligned} \tag{4.18}$$

with the notations:

- *Θ is a block diagonal matrix, made up of the elementary matrices $\omega_k \begin{pmatrix} 0 & 1 \\ -1 & 0 \end{pmatrix}$ for k varying from 1 to K,*
- *θ is a row vector of size $2K$ similar to $\begin{pmatrix} 1 & 0 & \ldots & 1 & 0 \end{pmatrix}$.*

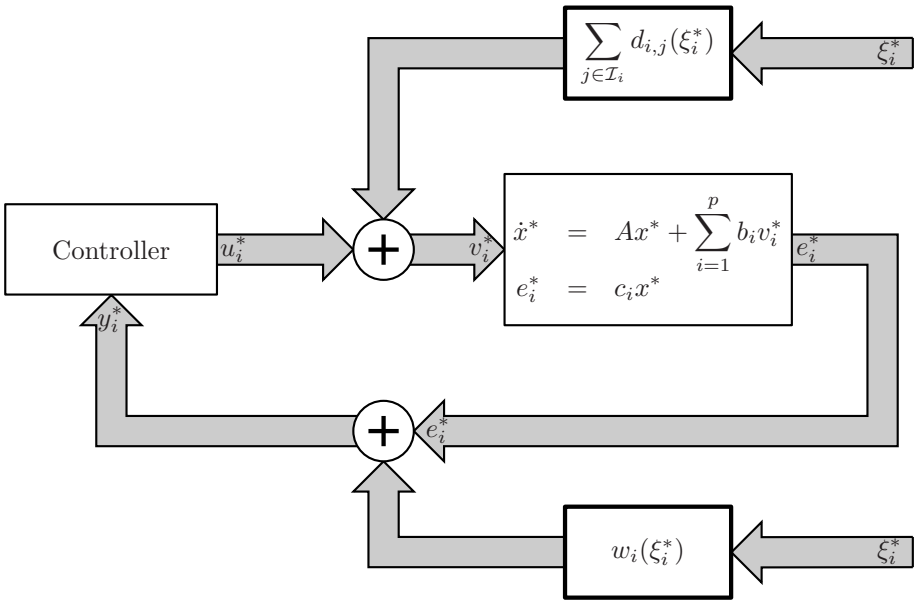

Figure 4.3: First order approximation resulting from the regular perturbation analysis.

Remark 4.6 *Let's collect in z the vectors ζ obtained when applying the method of the remark 4.5 to each periodic function ($d_{i,j}$ or w_i). If N denotes the number of elementary sine functions necessary to describe all these functions, namely, given the definitions* (4.3) *and* (4.4)*:*

$$N = \sum_{i=1}^{q} N_i + \sum_{j=1}^{p} \sum_{i\in\mathcal{I}_j} N_{j,i}, \tag{4.19}$$

z is of size $2N$ and there exists a square matrix $M(\nu_1, \ldots, \nu_q)$ of size $2N$ such that:

$$\dot{z} = M(\nu_1, \ldots, \nu_q)\, z. \tag{4.20}$$

M is block diagonal, each of these blocks being similar to $\nu\Theta$ (see (4.18)*). For this reason, $M(\nu_1, \ldots, \nu_q)$ is linear in the ν_i and may be expanded as:*

$$M(\nu_1, \ldots, \nu_q) = \sum_{i=1}^{q} \nu_i M_i. \tag{4.21}$$

4.2 Design of the control scheme

4.2.1 Presentation

Our goal is to design a command to get the tracking errors asymptotically converging to zero despite the spatially periodic perturbations and irrespective of the initial conditions. For a given control architecture, the analysis of the resulting closed loop may be undertaken performing the regular perturbation expansion developed in the theorem 3.2. Moreover, the Lyapunov-like theorem 3.3 states that, if the first order approximation of the closed loop is asymptotically stable, the tracking errors globally converge to zero. In the following, we propose to conceive an observer-based controller. We shall prove it is sufficient to design

the observer from the equations describing the first order approximation of the open loop (see (4.13) or (4.14)). We eventually come up with a solution entirely based on the first order approximation, which is definitely suited to cancel the effects of the perturbations for the original system. Controlling the latter with this architecture yields global asymptotical stability of the origin.

A Luenberger-like observer for the system (4.14) requires a likely time dependent matrix $\mathcal{K} \in \mathbb{R}^{n' \times q}$, such that:

$$\begin{aligned} \dot{\widehat{\chi}}^* &= \mathcal{A}\left(\nu_1^*, \ldots, \nu_q^*\right) \widehat{\chi} + \mathcal{B}u^* - \mathcal{K}\left(\widehat{y}^* - y^*\right) \\ \widehat{y}^* &= \mathcal{C}\widehat{\chi}^*. \end{aligned} \tag{4.22}$$

The goal of the control law is twofold:

- canceling the effects of the perturbations z^* altering the dynamics of the mechanical variables x^*,
- choosing the poles for x^*.

The following choice suits these expectations:

$$u^* = -\mathcal{L}\widehat{\chi}^* = -L\widehat{x}^* - D\widehat{z}^*. \tag{4.23}$$

We denote the observation errors by $\widetilde{\chi}^* = \widehat{\chi}^* - \chi^*$. The first order approximation in closed loop, when u^* gets applied, admits the following representation:

$$\begin{pmatrix} \dot{x}^* \\ \dot{\widetilde{\chi}}^* \end{pmatrix} = \begin{pmatrix} A - BL & -B\mathcal{L} \\ \mathbf{0} & \mathcal{A}\left(\nu_1^*, \ldots, \nu_q^*\right) - \mathcal{K}\mathcal{C} \end{pmatrix} \begin{pmatrix} x^* \\ \widetilde{\chi}^* \end{pmatrix}. \tag{4.24}$$

The matrices L and $\mathcal{K}$ may be tuned independently:

- If the pair (A, B) is assumed to be controllable, L is obviously tuned for the poles of $A - BL$ to all have negative real parts.
- $\mathcal{K}$ has to be such that $\mathcal{A}\left(\nu_1^*, \ldots, \nu_q^*\right) - \mathcal{K}\mathcal{C}$ defines an exponentially stable autonomous system.

By doing so, the origin of the first order approximation (see equation (4.14)) in closed loop is globally exponentially stable. We shall show that if L and $\mathcal{K}$ are tuned according to the previous constraints, and, if the observer (4.22) and the controller (4.23) are adapted to the original system (4.8), one eventually gets an observer-based controller that globally asymptotically stabilizes the original nonlinear system (4.8).

4.2.2 Observer-based controller

The sole change to the equations (4.22) consists in feeding them with the actual measurements y defined by (4.9). From now on, the observation are collected in the vector $\widehat{\chi}$ computed as:

$$\begin{aligned} \dot{\widehat{\chi}} &= \mathcal{A}\left(\nu_1^*, \ldots, \nu_q^*\right) \widehat{\chi} + \mathcal{B}u - \mathcal{K}\left(\widehat{y} - y\right) \\ \widehat{y} &= \mathcal{C}\widehat{\chi}. \end{aligned} \tag{4.25}$$

Let's mimic the equation (4.23). The command u is still designed to get rid of perturbations and place the mechanical poles, thus:

$$u = -\mathcal{L}\widehat{\chi} = -L\widehat{x} - D\widehat{z}. \tag{4.26}$$

We now look for a representation of the system (4.8) controlled by the command (4.26), itself resorting to the observations (4.25). Let $\widetilde{\chi} = \widehat{\chi} - \chi$ represent the observation errors such that:

$$\dot{\widetilde{\chi}} = \mathcal{A}\left(\nu_1^*, \ldots, \nu_q^*\right)\widehat{\chi} - \mathcal{A}\left(\nu_1, \ldots, \nu_q\right)\chi - \mathcal{K}\mathcal{C}\widetilde{\chi}.$$

We turn to best account $\mathcal{A}\left(\nu_1, \ldots, \nu_q\right)$ being linear in each of its arguments (see (4.15)) together with the equations (4.6):

$$\mathcal{A}\left(\nu_1, \ldots, \nu_q\right) = \mathcal{A}\left(\nu_1^*, \ldots, \nu_q^*\right) + \mathcal{A}\left(c_1'x, \ldots, c_q'x\right).$$

In the end, the observation errors are given by the following differential equation:

$$\dot{\widetilde{\chi}} = \left(\mathcal{A}\left(\nu_1^*, \ldots, \nu_q^*\right) - \mathcal{K}\mathcal{C}\right)\widetilde{\chi} + \mathcal{F}\left(x\right), \tag{4.27}$$

with the matrix $\mathcal{F}(x)$ given by:

$$\mathcal{F}(x) = -\sum_{i=1}^{q}\left(c_i'x\right)\mathcal{A}_i. \tag{4.28}$$

The system (4.8) in closed loop is actually described by:

$$\begin{pmatrix} \dot{x} \\ \dot{\widetilde{\chi}} \end{pmatrix} = \begin{pmatrix} A - BL & -B\mathcal{L} \\ \mathbf{0} & \mathcal{A}\left(\nu_1^*, \ldots, \nu_q^*\right) - \mathcal{K}\mathcal{C} \end{pmatrix}\begin{pmatrix} x \\ \widetilde{\chi} \end{pmatrix} + \begin{pmatrix} \mathbf{0} \\ \mathcal{F}(x) \end{pmatrix}, \tag{4.29}$$

where the evolution of the non controllable part (namely the perturbation z) has been omitted. The following theorem gives necessary conditions for the system (4.29) to be globally asymptotically stable.

Theorem 4.1

If the gain matrices $\mathcal{K}$ and L are tuned so that the system (4.24) *is exponentially stable, the origin of the system* (4.29) *is globally asymptotically stable.*

Proof:

The proof is organized as follows:

1. we first define an auxiliary dynamical system for which the stability findings of the chapter 3 apply,

2. the stability of the origin of (4.29) is then deduced.

We shall make use of the first order approximation of the open loop given by (4.14) and the structure of the matrix $\mathcal{A}$ in (4.12). Let's use the following notations:

$$\bar{z} = \widehat{z} - z^*, \quad \bar{\chi} = \begin{pmatrix} \widetilde{x}^T & \bar{z}^T \end{pmatrix}^T \quad X = \begin{pmatrix} x^T & \bar{\chi}^T \end{pmatrix}^T.$$

Studying the evolution of X defined by blocks yields:

$$\begin{aligned}\dot{x} &= (A-BL)\,x - B\mathcal{L}\bar{\chi} - BD\,(z^*-z)\\ \dot{\widetilde{x}} &= A\widetilde{x} + BD\bar{z} - K_x\mathcal{C}\bar{\chi} + BD\,(z^*-z) - K_xW\,(z^*-z)\\ \dot{\bar{z}} &= M\left(\nu_1^*,\ldots,\nu_q^*\right)\bar{z} - K_z\mathcal{C}\bar{\chi} - K_zW\,(z^*-z)\,.\end{aligned}$$

The previous equations may be collected as follows:

$$\dot{X} = \begin{pmatrix} A-BL & -B\mathcal{L} \\ \mathbf{0} & \mathcal{A}\left(\nu_1^*,\ldots,\nu_q^*\right)\end{pmatrix} X + \sum_{i=1}^{p}\mathcal{S}_i\sum_{j\in\mathcal{I}_i}\left(d_{i,j}(\xi_j) - d_{i,j}(\xi_j^*)\right) + \sum_{i=1}^{q}\mathcal{T}_i\left(w_i(\xi_i) - w_i(\xi_i^*)\right), \tag{4.30}$$

with:

- $\mathcal{S}_i = \begin{pmatrix} b_i^T & -b_i^T & \mathbf{0}\end{pmatrix}^T, \quad 1\le i\le p,$
- $\mathcal{K}_i$ is the i-th column of the observer gains matrix $\mathcal{K}$,
- $\mathcal{T}_i = \begin{pmatrix} \mathbf{0} & -\mathcal{K}_i^T\end{pmatrix}^T, \quad 1\le i\le q.$

Let $\Phi(t,t')$ be the transition matrix associated to (4.24), recall that such a matrix may be defined since the right-hand side of the linear differential equation is a continuous function of time, see [11]. Moreover, the following quantities are well defined:

$$\forall,\ 1\le i\le p,\quad \sigma_i = \sup_{t\ge 0}\left(\int_0^t \left\|\begin{pmatrix}C & 0\end{pmatrix}\Phi(t,t')\mathcal{S}_i\right\|\,dt'\right),\quad \tau_i = \sup_{t\ge 0}\left(\int_0^t \left\|\begin{pmatrix}C & 0\end{pmatrix}\Phi(t,t')\mathcal{T}_i\right\|\,dt'\right). \tag{4.31}$$

Using the previous equation, if we keep in mind the definition of the functions $d_{i,j}$ and w_i (equations (4.3) and (4.4)), let μ be defined by analogy with the equation (3.37):

$$\mu = 2N\max\left(\sigma_i\lambda_{i,j,n},\ \tau_i\lambda'_{i,n}\right) \tag{4.32}$$

If μ takes a sufficiently small value, the theorem 3.5 applies. Practically speaking, to know whether the output Cx converges to zero, one has to evaluate the functions $w_i(\xi_i)$ and $d_{i,j}(\xi_j)$ along the reference trajectories, namely replacing ξ_i (respectively $\xi_{i,j}$) by ξ_i^* (respectively $\xi_{i,j}^*$) in the equation (4.30). By doing so, the inputs of this system are canceled. Recall that this system is assumed exponentially stable according to the theorem. The output $Cx = \begin{pmatrix}C & \mathbf{0}\end{pmatrix}X$ of the system (4.30) asymptotically converges to zero (see [11]), provided μ is small enough.

Since all the terms c_ix go to zero and that the functions $d_{i,j}$ and w_i are continuous, the following relations hold:

$$\begin{aligned}\lim_{t\to\infty}\left(w_i - w_i^*\right) &= \lim_{t\to\infty}\left(w_i\left(\xi_i^* + c_ix\right) - w_i\left(\xi_i^*\right)\right) = 0, \quad \forall i,\ 1\le i\le q,\\ \lim_{t\to\infty}\left(d_{i,j} - d_{i,j}^*\right) &= \lim_{t\to\infty}\left(d_{i,j}\left(\xi_j^* + c_jx\right) - d_{i,j}\left(\xi_j*\right)\right) = 0, \quad 1\le i\le p,\ j\in\mathcal{I}_i.\end{aligned}$$

As an immediate consequence and according to the terms of the theorem, if μ is small enough, (4.30) is an exponentially stable system with vanishing inputs. The whole state x converges to zero as t grows indefinitely.

The only thing left to do is proving that $\widetilde{z} = \bar{z} + z^* - z$ converges to zero. The vector z is made up of blocks similar to (4.17), and z^* features the same block structure apart from the fact that the considered positions are replaced by their references. The conclusion is rather easily obtained by noting that:

$$\lim_{t\to\infty} \widetilde{z} = \lim_{t\to\infty} \bar{z} + \lim_{t\to\infty} (z^* - z) = \lim_{t\to\infty} \begin{pmatrix} \vdots \\ \lambda \sin(\omega\xi^* + \varphi) - \lambda \sin(\omega\xi^* + \omega c x + \varphi) \\ \lambda \cos(\omega\xi^* + \varphi) - \lambda \cos(\omega\xi^* + \omega c x + \varphi) \\ \vdots \end{pmatrix} = \begin{pmatrix} 0 \\ \vdots \\ \vdots \\ 0 \end{pmatrix},$$

with $x \to 0$.

Remark 4.7 *For the findings of this theorem to apply, the smallness of the parameter μ (defined by* (4.32)*) has to be taken into account. This constraint is actually satisfied in most physical situations, as discussed hereafter.*

As previously suggested, the magnitudes $\lambda_{i,j,n}$ of the perturbation forces $d_{i,j}$ may take arbitrarily large values. In the equation (4.31) *defining μ, they are combined with σ_i which is neither more nor less than the sensitivity of the closed to perturbations acting on the tracking errors from the input of the unperturbed system (given by the equation* (4.8)*). Practically speaking, when the system* (4.5) *is driven by the observer-based controller, making the first-order approximation* (4.24) *the faster yields sensitivities σ_i the smaller. Given the context of high-precision and high performance positioning, such a tuning may be carried out. As a result, the terms $\sigma_i \lambda_{i,j,n}$ may be controlled and do not have much impact on the magnitude of μ.*

Let's move on the terms $\tau_i \lambda'_{i,n}$ appearing in the equation (4.32)*. τ_i depicts the influence of the measurement errors on the tracking error. This value is usually close to the unity while the corresponding $\lambda'_{i,n}$ used in the modeling of spatially periodic measurements errors are usually very small (a few dozens nanometers), especially in our context where the resolutions of the sensors matter since the overall precision is at stake.*

Remark 4.8 *The previous proof relies on the regular perturbation analysis based on an input-output description. An expansion of the whole state (through the theorem 3.3) would yield too conservative results, namely such an expansion would only be valid for very small magnitude perturbations. Given the structure of the equation* (4.30)*, it is not conceivable to expect all the inputs to have only a slight influence on the whole state X in the equation* (4.30)*.*

The theorem 3.5 is then best suited to have a converging expansion of the output despite significantly large perturbations. Furthermore, the previously considered output $y = \mathcal{C}\chi = Cx$ is zero-state detectable. Its convergence to zero implies the convergence of the whole state X toward zero. This property is material to justify that the observation errors are also asymptotically reaching zero, and that the observation scheme, initially designed for the first order approximation, is also suited for the observation of the original nonlinear system.

4.2.3 Interpretation

One has to keep in mind that the evolution of the observation errors is not autonomous (see (4.27)). This is due to the fact that our observation scheme is suited to the first-order approximation and not to the original system. To get these errors converging to zero, the system has to be driven by the observer-based command u of the equation (4.26).

In view of the remark 4.7, we may from now on assume that the tuning of the observer-based controller amounts to making the first-order approximation of the closed loop (the equation (4.24)) exponentially stable. It is noteworthy that, given the block triangular structure of this system, the controller (L) and observer ($\mathcal{K}$) gains may be tuned independently even if the original system (4.1) is nonlinear. Replacing the actual positions by their references allows us to get rid of the different loops involving periodic functions of the actual positions. An immediate consequence is that we now have to deal with a linear time-varying system to conduct gain tuning.

While the tuning of L for $A - BL$ to be exponentially stable is rather obvious when the pair (A, B) is controllable, one still has to find $\mathcal{K}$ for the following system:

$$\dot{\widetilde{\chi}}^* = \left(\mathcal{A}\left(\nu_1^*, \ldots, \nu_q^*\right) - \mathcal{K}\mathcal{C}\right)\widetilde{\chi}^*$$

to be exponentially stable. This task is far from being as straightforward as the tuning of L and we suggest to address it in the following.

4.3 Observer gains tuning

This issue may be undertaken in different ways. First, imagine that the first-order approximation (see figure 4.3) is observable [45], namely the observation matrix associated with the pair $\left(\mathcal{A}\left(\nu_1^*, \ldots, \nu_q^*\right), \mathcal{C}\right)$ is invertible. A Lyapunov transformation may be found to rewrite the matrix $\mathcal{A}\left(\nu_1^*, \ldots, \nu_q^*\right)$ into canonical phase-variable form (see [44, 56]). In this new base, the poles of the equivalent system may be set to arbitrary constant values with negative real parts so as to satisfy a certain decay-rate to zero α. Rewriting the system in the original base yields the corresponding observer gains. The decay-rate to zero of the resulting autonomous system:

$$\dot{\widetilde{\chi}}^* = \left(\mathcal{A}\left(\nu_1^*, \ldots, \nu_q^*\right) - \mathcal{K}\mathcal{C}\right)\widetilde{\chi}^*$$

is also guaranteed to be α. By doing so, the observer gains are time-varying functions depending on the reference velocities.

In this part, we propose a method yielding constant observer gains $\mathcal{K}$. To this end, we use the very specific structure of the matrix $\mathcal{A}\left(\nu_1^*, \ldots, \nu_q^*\right)$. This matrix is linear with respect to the reference velocities ν_i^* (see (4.15)) which are bounded functions of time (see (4.6)). When the ν_i^* vary in between their bounds, the matrix $\mathcal{A}$ belongs to a polytope whose vertices are given by:

$$\mathbb{A} = \left\{ \mathcal{A}^{(i)} \in \mathbb{R}^{n' \times n'}, 1 \leq i \leq 2^q \quad \middle/ \quad \mathcal{A}^{(i)} = \mathcal{A}\left(x_1, \ldots, x_q\right), \quad \forall j,\, 1 \leq j \leq q, \quad x_j = \overline{\nu}_j \text{ or } \underline{\nu}_j \right\}. \quad (4.33)$$

At any time, $\mathcal{A}\left(\nu_1^*,\ldots,\nu_q^*\right)$ belongs to the convex hull of the set whose vertices are the elements of $\mathbb{A}$ and the following relation holds:

$$\mathcal{A}\left(\nu_1^*(t),\ldots,\nu_q^*(t)\right)=\sum_{i=1}^{2^q}\mu_i(t)\mathcal{A}^{(i)} \quad \text{and} \quad \sum_{i=1}^{2^q}\mu_i(t)=1. \tag{4.34}$$

The previous property is crucial for the proposed tuning method. One actually has to design an observer for the polytopic system $\dot{\widetilde{\chi}}=\mathcal{A}\left(\nu_1^*,\ldots,\nu_q^*\right)\widetilde{\chi}$ from the measurements $\mathcal{C}\chi$, see [10]. We derive two LMI problems in the following, the latter enabling to set the decay-rate to zero of both the positioning and observations errors for the original nonlinear system in closed loop described by the equation (4.29). Provided these LMI problems are feasible, the derived gains are constant and the LMI optimization phase is carried out offline only once.

4.3.1 Quadratic stabilization

LMI formulation

The following theorem brings an answer to the question of tuning $\mathcal{K}$ for the matrix $\mathcal{A}\left(\nu_1^*,\ldots,\nu_q^*\right)-\mathcal{K}\mathcal{C}$ to be exponentially stable.

Theorem 4.2

Given the definition of the matrices $\mathcal{A}^{(i)}$ by (4.33), if there exist two matrices $\mathcal{P}\in\mathbb{R}^{n'\times n'}$ and $\mathcal{Q}\in\mathbb{R}^{n'\times q}$ such that:

(i) $\mathcal{P}=\mathcal{P}^T$ *and* $\mathcal{P}>0$,

(ii) $\left(\mathcal{A}^{(i)}\right)\mathcal{P}+\mathcal{P}\left(\mathcal{A}^{(i)}\right)^T-\mathcal{C}^T\mathcal{Q}^T-\mathcal{Q}\mathcal{C}+2\alpha\mathcal{P}<0, \quad \forall i,\ 1\leq i\leq 2^q$,

by setting $\mathcal{K}=\mathcal{P}^{-1}\mathcal{Q}$, the matrix $\mathcal{A}\left(\nu_1^*,\ldots,\nu_q^*\right)-\mathcal{K}\mathcal{C}$ defines an exponentially stable system with decay-rate to zero at least α.

Proof:

Suppose the previous conditions *(i)* and *(ii)* are met, we first show that $V(\chi)=\chi^T\mathcal{P}\chi$ is a Lyapunov function for the system:

$$\dot{\chi}=\left(\mathcal{A}\left(\nu_1^*,\ldots,\nu_q^*\right)-\mathcal{P}^{-1}\mathcal{Q}\mathcal{C}\right)\chi.$$

In virtue of *(i)*, this function is positive definite, let's compute its derivative with respect to time:

$$\begin{aligned}\dot{V}(\chi) &= \dot{\chi}^T\mathcal{P}\chi+\chi^T\mathcal{P}\dot{\chi}\\ &= \chi^T\left(\left(\mathcal{A}-\mathcal{P}^{-1}\mathcal{Q}\mathcal{C}\right)^T\mathcal{P}+\mathcal{P}\left(\mathcal{A}-\mathcal{P}^{-1}\mathcal{Q}\mathcal{C}\right)+\dot{\mathcal{P}}\right)\chi\\ &= \chi^T\left(\mathcal{A}^T\mathcal{P}+\mathcal{P}\mathcal{A}-\mathcal{C}\mathcal{Q}^T-\mathcal{Q}\mathcal{C}\right)\chi\end{aligned}$$

As suggested by (4.34), since $\sum_{i=1}^{2^q} \mu_i = 1$, the last line together with the condition *(ii)* is rewritten in:

$$\begin{aligned}
\dot{V}(\chi) &= \chi^T \left(\sum_{i=1}^{2^q} \mu_i \left(\left(\mathcal{A}^{(i)} \right)^T \mathcal{P} + \mathcal{P} \left(\mathcal{A}^{(i)} \right) \right) - \mathcal{C}^T \mathcal{Q}^T - \mathcal{Q}\mathcal{C} \right) \chi \\
&= \chi^T \left(\sum_{i=1}^{2^q} \mu_i \left(\left(\mathcal{A}^{(i)} \right)^T \mathcal{P} + \mathcal{P} \left(\mathcal{A}^{(i)} \right) - \mathcal{C}^T \mathcal{Q}^T - \mathcal{Q}\mathcal{C} \right) \right) \chi \\
&\leq -2\alpha V(\chi).
\end{aligned}$$

This point guarantees the stability of the solutions whose decay-rate to zero may be bounded from above as follows. Let's first divide both sides of the previous equation by the strictly positive quantity $V(\chi)$ if $\chi \neq 0$:

$$\frac{\dot{V}(t)}{V(t)} \leq -2\alpha.$$

and integrate it from 0 to any $t > 0$:

$$V(\chi) \leq V(\chi(0))\, e^{-2\alpha t}.$$

Since $\mathcal{P}$ is strictly definite positive, there exists a constant value $\delta > 0$ such that $\mathcal{P} \geq \delta I$. As a consequence, $\|\chi\| \leq V(\chi(0))\, e^{-\alpha t}/\delta$ and the result of the theorem holds.

Interpretation

A quadratic Lyapunov function with a constant matrix $\mathcal{P}$ is obtained in the previous theorem. A more general issue consists in finding a time-varying $\mathcal{P}$ such that:

$$\mathcal{A}^T\mathcal{P} + \mathcal{P}\mathcal{A} - \mathcal{C}\mathcal{Q}^T - \mathcal{Q}\mathcal{C} + \dot{\mathcal{P}} \leq -2\alpha\mathcal{P}.$$

This is though an infinite dimensional problem, and the proposed theorem yields sufficient conditions in finite dimension to this issue. The polytopic nature of the system allows to enforce negativity conditions only on the vertices of the set described by the matrix $\mathcal{A}\left(\nu_1^*, \ldots, \nu_q^*\right)$. One still has to keep in mind that the number of constraints to fulfill is exponentially increasing with the number of outputs q, namely the positions in which the perturbation are periodic.

Once the LMI problem given in the theorem 4.2 is solved, the theorem 4.1 allows to conclude to the global asymptotic stability of the closed loop (4.29), but, nothing can be said regarding its decay-rate to zero. However, if L is such that the poles of $A - BL$ are located on the left of $-\alpha$, the zero and first order approximations of the system in closed loop have decay-rate to zero α. In the following, we propose a slightly different LMI problem that endows all the terms of the regular perturbation analysis with the same decay-rate to zero.

4.3.2 Small gains theorem

General problem

Let's have a closer look at the closed loop (4.29), and interpret it as the input-output interconnection of two dynamical systems. The state of the first is x while the state of the second is $\widetilde{\chi}$:

$$\begin{aligned} \dot{x} &= (A - BL)\, x - B\mathcal{L}u_1 \\ z_1 &= \sum_{i=1}^{q} (c_i' x)\, \mathcal{A}_i \chi, \end{aligned} \tag{4.35}$$

and:

$$\begin{aligned} \dot{\widetilde{\chi}} &= \left(\mathcal{A}\left(\nu_1^*, \ldots, \nu_q^*\right) - \mathcal{K}\mathcal{C}\right) \widetilde{\chi} + u_2 \\ z_2 &= \widetilde{\chi}. \end{aligned} \tag{4.36}$$

The equation modeling the system in closed loop is obtained by setting $u_1 = z_2$ and $u_2 = -z_1$. The following theorem makes the most of this structure and establishes conditions under which this interconnection is stable with decay-rate to zero α.

Theorem 4.3

Suppose there exist:

(i) a function $V_1 : x \in \mathbb{R}^n \to \mathbb{R}_+$ strictly positive for $x \neq 0$, zero for $x = 0$, and a scalar $\gamma_1 > 0$ such that:

$$\dot{V}_1 \leq \gamma_1^2 u_1^T u_1 - x^T C'^T C' x - 2\alpha V_1,$$

(ii) a function $V_2 : \chi \in \mathbb{R}^{n'} \to \mathbb{R}_+$ strictly positive for $\chi \neq 0$, zero for $\chi = 0$, and a scalar $\gamma_2 > 0$ such that:

$$\dot{V}_2 \leq \gamma_1^2 u_2^T u_2 - \chi^T \chi - 2\alpha V_2,$$

then the solutions of the system (4.29) are exponentially converging to zero with decay-rate to zero at least α if the following constraint holds:

$$\gamma_1 \gamma_2 \max_{1 \leq i \leq q} \left(\sqrt{\sum_{n=1}^{N_i} \left(\lambda_{i,n}' \omega_{i,n}'\right)^2 + \sum_{j=1}^{p} \sum_{n=1}^{N_{j,i}} \left(\lambda_{j,i,n} \omega_{j,i,n}\right)^2} \right) \leq 1. \tag{4.37}$$

PROOF:

Let's exhibit a scalar $a > 0$ for $V = V_1 + aV_2$ to be a Lyapunov function for the system defined by (4.29). V satisfies all the basic assumptions of a Lyapunov function, we now compute its derivative

with respect to time when $u_1 = z_2 = \chi$ and $u_2 = -z_1 = -\sum_{i=1}^{q} (c_i' x)\, \mathcal{A}_i \chi$ (see (4.28)):

$$\dot{V} \leq \gamma_1 \chi^T \chi - x^T C'^T C' x + a\gamma_2 z_1^T z_1 - a\chi^T \chi - 2\alpha V$$

If we denote by:

$$\gamma = \max_{1 \leq i \leq q} \left(\sqrt{\sum_{n=1}^{N_i} \left(\lambda_{i,n}' \omega_{i,n}'\right)^2 + \sum_{j=1}^{p} \sum_{n=1}^{N_{j,i}} \left(\lambda_{j,i,n} \omega_{j,i,n}\right)^2} \right), \tag{4.38}$$

according to the lemma 4.1, we have:

$$z_1^T z_1 \leq \gamma x^T C'^T C' x,$$

thus:

$$\dot{V} \leq (\gamma_1 - a)\chi^T \chi + (a\gamma\gamma_2 - 1) x^T C'^T C' x - 2\alpha V.$$

Provided the condition (4.37) is satisfied, one may find a scalar $a > 0$ such that:

$$\gamma_1 \leq a \leq \frac{1}{\gamma\gamma_2},$$

and, in these conditions, $\dot{V} \leq -2\alpha V$, which, according to the elements reported in the proof of the theorem 4.2, yields the exponential convergence to zero with decay-rate at least α of both x and $\widetilde{\chi}$.

Lemma 4.1 *The norm of the vector z_1 defined by* (4.35) *is bounded by:*

$$z_1^T z_1 \leq \left(\max_{1 \leq i \leq q} \sqrt{\sum_{n=1}^{N_i} \left(\lambda_{i,n}' \omega_{i,n}'\right)^2 + \sum_{j=1}^{p} \sum_{n=1}^{N_{j,i}} \left(\lambda_{j,i,n} \omega_{j,i,n}\right)^2} \right) x^T C'^T C' x, \tag{4.39}$$

with C' given by the equation (4.6).

Proof:

Practically speaking, for $i > 0$, the terms $\mathcal{A}_i \chi$ are given by:

$$\mathcal{A}_i \chi = \begin{pmatrix} \mathbf{0} & \mathbf{0} \\ \mathbf{0} & M_i \end{pmatrix} \begin{pmatrix} x \\ z \end{pmatrix} = \begin{pmatrix} \mathbf{0} \\ M_i z \end{pmatrix},$$

where each M_i is a block diagonal matrix. These blocks are similar to the matrix appearing in (4.18) and aim at modeling some functions periodic in the only position ξ_i. For $i \neq j$, the terms $M_i^T M_j$ necessarily equal zero and thus:

$$\begin{aligned} z_1^T z_1 &= \left(\sum_{i=1}^{q} (c_i' x)\, \mathcal{A}_i \chi \right)^T \left(\sum_{i=1}^{q} (c_i' x)\, \mathcal{A}_i \chi \right) \\ &= \sum_{i=1}^{q} \sum_{j=1}^{q} (c_i' x) \left(c_j' x\right) \chi^T \mathcal{A}_i^T \mathcal{A}_j \chi \\ &= \sum_{i=1}^{q} \left(c_i' x\right)^2 z^T M_i^T M_i z. \end{aligned}$$

The non-zero terms of the vector $M_i z$ are of two kinds:

- some components are similar to:

$$\lambda'_{i,n}\omega'_{i,n}\cos\left(\omega'_{i,n}\xi_i+\varphi'_{i,n}\right) \quad \text{and} \quad -\lambda'_{i,n}\omega'_{i,n}\sin\left(\omega'_{i,n}\xi_i+\varphi'_{i,n}\right),$$

  for all n between 1 and N_i,

- when considering the system depicted on 4.2, for an input indexed by j (between 1 and p), if the position indexed by i influences the system through the input j (namely if $i \in \mathcal{I}_j$), some non-zero components of $M_i z$ actually look like:

$$\lambda_{j,i,n}\omega_{j,i,n}\cos\left(\omega_{j,i,n}\xi_i+\varphi_{j,i,n}\right) \quad \text{and} \quad -\lambda_{j,i,n}\omega_{j,i,n}\sin\left(\omega_{j,i,n}\xi_i+\varphi_{j,i,n}\right),$$

  for all n between 1 and $N_{j,i}$.

As a consequence, $z^T M_i^T M_i z$ is given by:

$$\forall i,\ 1\le i\le q, \quad z^T M_i^T M_i z = \sum_{n=1}^{N_i}\left(\lambda'_{i,n}\omega'_{i,n}\right)^2 + \sum_{j=1}^{p}\left(\sum_{\substack{n=1\\ i\in\mathcal{I}_j}}^{N_{j,i}}\left(\lambda_{j,i,n}\omega_{j,i,n}\right)^2\right) \tag{4.40}$$

and, in these conditions:

$$z_1^T z_1 \le \max_{1\le i\le q}\left(z^T M_i^T M_i z\right)\sum_{i=1}^{q}\left(c'_i x\right)^2 = \max_{1\le i\le q}\left(z^T M_i^T M_i z\right)\ x^T C'^T C' x,$$

which ends proving the equation (4.39).

LMI formulation

We still suppose L given by any *a priori* setting for which it is possible to compute the smallest γ_1 such that the condition (i) of the theorem 4.3 is fulfilled. From now on, we are solely concerned with computing $\mathcal{K}$ to minimize γ_2 according to the condition *(ii)* of the theorem 4.3. By doing so, for a predefined L, we derive the observer gains for our control architecture to withstand the largest perturbations. As illustrated by the following theorem, if the perturbations stick to a small gain condition, the system in closed loop remains stable with decay-rate to zero α.

Theorem 4.4

Consider a scalar $\alpha > 0$. Under the following conditions:

(i) Define $H(s) = C'\left(sI-(A-BL)\right)^{-1}B\mathcal{L}$ the transfer function of the system (4.35), all its poles are assumed to have negative real parts on the left of $-\alpha$,

(ii) Define the scalar γ_2^*, the matrices $\mathcal{P}^*$ and $\mathcal{Q}^*$ solutions of the following optimization problem under LMI constraints

$$\left((\gamma_2^*)^2,\, \mathcal{P}^*,\, \mathcal{Q}^*\right) = \arg\min_{\gamma_2^2, \mathcal{P}, \mathcal{Q}} \gamma_2^2$$

Subject to:

- $\exists \mathcal{P} = \mathcal{P}^T > 0$
- $\exists \mathcal{Q}$
- $$\begin{pmatrix} \left(\mathcal{A}^{(i)}\right)^T \mathcal{P} + \mathcal{P}\left(\mathcal{A}^{(i)}\right) - \mathcal{C}^T\mathcal{Q}^T - \mathcal{Q}\mathcal{C} + I + 2\alpha\mathcal{P} & \mathcal{P} \\ \mathcal{P} & -\gamma_2^2 I \end{pmatrix} \leq 0, \quad \forall i,\, 1 \leq i \leq 2^q, \tag{4.41}$$

by letting $\mathcal{K} = \mathcal{P}^{-1}\mathcal{Q}$, the closed loop system (4.29) is exponentially stable with decay-rate to zero α if:

$$\gamma_2^* \left\|H(s-\alpha)\right\|_\infty \max_{1\leq i\leq q} \left(\sqrt{\sum_{n=1}^{N_i} \left(\lambda'_{i,n}\omega'_{i,n}\right)^2 + \sum_{j=1}^{p}\sum_{n=1}^{N_{j,i}} \left(\lambda_{j,i,n}\omega_{j,i,n}\right)^2} \right) \leq 1. \tag{4.42}$$

PROOF:

This theorem entirely relies on the following two lemmas and the theorem 4.3:

- According to the lemma 4.2, for a given L, the smallest scalar γ_1, provable by quadratic stabilization, satisfying the condition *(i)* of the theorem 4.3 is given by $\left\|H(s-\alpha)\right\|_\infty$,
- According to the lemma 4.3, solving the optimization problem (4.41) leads to the smallest value γ_2^*, provable by quadratic stabilization, so that the conditions *(ii)* of the theorem 4.3 are fulfilled.

Thanks to the small gain theorem 4.3, the closed loop is exponentially stable, the decay-rate to zero of its solutions is α as long as the condition (4.42) holds.

Lemma 4.2 *Under the assumptions (i) of the theorem 4.4, if γ_1^* is the smallest value γ_1 such that the conditions (i) of the theorem 4.3 are satisfied, then:*

$$\gamma_1^* \leq \left\|H(s-\alpha)\right\|_\infty. \tag{4.43}$$

PROOF:

Let's look for a quadratic Lyapunov function satisfying the conditions *(i)* of the theorem 4.3. In other words, a matrix $P = P^T > 0$ defining $V = x^T P x$. We are thus looking for γ_1 and P such that:

$$x^T\left((A-BL))^T P + P\left(A-BL\right) + 2\alpha P + C'^T C\right) x - x^T\left(PB\mathcal{L}\right) u_1 - u_1^T\left(\mathcal{L}^T B^T P\right) x - \gamma_1^2 u_1^T u_1 \leq 0,$$

which is equivalent to the following matrix being negative:

$$\begin{pmatrix} (A+\alpha I-BL)^T+(A+\alpha I-BL)^T+C'^TC' & -PB\mathcal{L} \\ -(PB\mathcal{L})^T & -\gamma_1^2 \end{pmatrix} \leq 0.$$

Minimizing γ_1 while satisfying both the previous negativity condition and $P = P^T > 0$ is an LMI problem boiling down to computing the H_∞ norm of the following transfer function:

$$C'\left(sI-(A+\alpha I-BL)^{-1}B\mathcal{L}\right. = C'\left((s-\alpha)I-(A-BL)^{-1}B\mathcal{L}\right. = H(s-\alpha).$$

If the poles of $H(s)$ are all located to the left of $-\alpha$, $H(s-\alpha)$ is stable, and $\|H(s-\alpha)\|_\infty$ is well defined, which ends proving this lemma.

Lemma 4.3 *Given the notations of the theorem 4.4, if we let $\mathcal{K} = (\mathcal{P}^*)^{-1}\mathcal{Q}^*$, the quadratic function $V_2 = \widetilde{\chi}^T\mathcal{P}^*\widetilde{\chi}$ meets the requirements of the point (ii) of the theorem 4.3.*

PROOF:

The function V_2 previously defined meets the basic requirements of a potential Lyapunov candidate function. For the sake of clarity, we omit the dependencies of $\mathcal{A}\left(\nu_1^*,\ldots,\nu_q^*\right)$ on the ν_i^* and we compute $\dot{V}_2$

$$\dot{V}_2 = \widetilde{\chi}^T\left(\mathcal{A}^T\mathcal{P}^*+\mathcal{A}\mathcal{P}^*-(\mathcal{Q}^*\mathcal{C})^T-(\mathcal{Q}^*\mathcal{C})\right)\widetilde{\chi}+\widetilde{\chi}^T\mathcal{P}^*u_2+u_2^T\mathcal{P}^*\widetilde{\chi}.$$

Recalling that $\mathcal{A}\left(\nu_1^*,\ldots,\nu_q^*\right)$ may be expressed as a function of the vertices $\mathcal{A}^{(i)}$ (see the equation (4.34)), we rewrite the previous equation into:

$$\dot{V}_2 = \sum_{i=1}^{2^q}\mu_i\begin{pmatrix}\widetilde{\chi}^T & u_2^T\end{pmatrix}\begin{pmatrix}\left(\mathcal{A}^{(i)}\right)^T\mathcal{P}^*+\left(\mathcal{A}^{(i)}\right)\mathcal{P}^*-(\mathcal{Q}^*\mathcal{C})^T-(\mathcal{Q}^*\mathcal{C}) & \mathcal{P}^* \\ \mathcal{P}^* & \mathbf{0}\end{pmatrix}\begin{pmatrix}\widetilde{\chi} \\ u_2\end{pmatrix}$$

where we make use of the equality $\sum_{i=1}^{2^q}\mu_i = 1$. If we now use the LMI constraints appearing in the optimization problem (4.41):

$$\begin{aligned}\dot{V}_2 &\leq \sum_{i=1}^{2^q}\mu_i\begin{pmatrix}\widetilde{\chi}^T & u_2^T\end{pmatrix}\begin{pmatrix}I+2\alpha\mathcal{P}^* & \mathbf{0} \\ \mathbf{0} & -(\gamma_2^*)^2\end{pmatrix}\begin{pmatrix}\widetilde{\chi} \\ u_2\end{pmatrix} \\ &\leq -(\gamma_2^*)^2u_2^Tu_2-\widetilde{\chi}^T\widetilde{\chi}-2\alpha V_2,\end{aligned}$$

which eventually proves the point *(ii)* of the theorem 4.3.

CHAPTER 5

High-Precision Trajectory Tracking: Experimental Results

5.1 Introduction

We now move on to the implementation of the observer-based control scheme presented in chapter 4. We provide experimental results that illustrate the performances of the previous design. Our work sets a unified framework allowing to get rid of any of the state-periodic perturbations listed in the chapter 1, thus yielding extremely accurate trajectory tracking compared to a casual PID controller. The following figures 5.1(a), 5.1(b) and 5.1(c) illustrate this point, we shall anyway comment them later on.

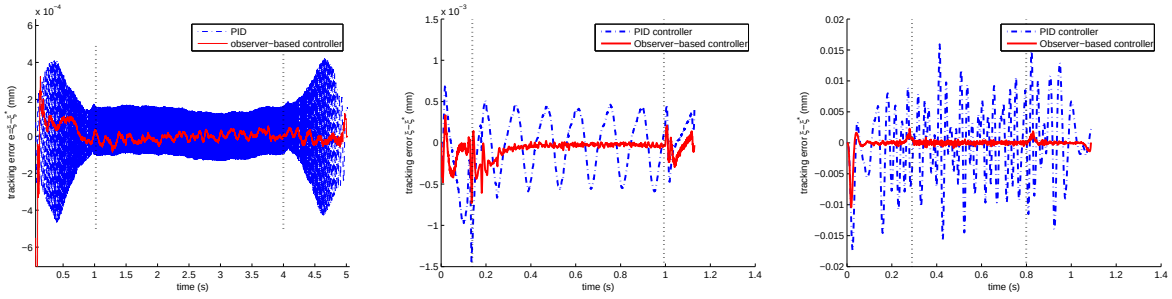

(a) Interpolation errors. (b) Forces created by currents offsets. (c) Cogging forces.

Figure 5.1: Tracking errors obtained with a PID controller and the observer-based design in presence of miscellaneous state-periodic perturbations.

On the top of highlighting the efficiency of the method, we shall also give a technical answer to two questions left open, so far. Namely, the determination of the spatial pulsations of the perturbations (given in the equations (4.3) and (4.4)), as well as some hints to carry out the gains tuning through the LMI optimization of the theorems 4.4 and 4.2.

These two issues are addressed by considering a brushless linear motor mounted on a fixed frame. We shall

show that the estimations of the pulsations of the spatially periodic forces ($\omega_{i,j,n}$ in the equation (4.3)) and the position measurements errors ($\omega_{i,n}$ in the equation (4.4)) are derived from Fourier transforms performed on experimental data. We also give a slightly modified version of the LMI optimization problem of the equation (4.41) to enable rest to rest trajectories. We then give the experimental results related to an ironless motor. The perturbation forces acting on this ironless motor clearly fulfill the truncated Fourier series considered so far. We shall then consider an ironcore motor and see that cogging forces, to which this motor is subjected, are far from being so close to the modeling. However, our method still exhibits outstanding performances despite the context.

5.2 Observer-based controller tuning

5.2.1 Experimental setup

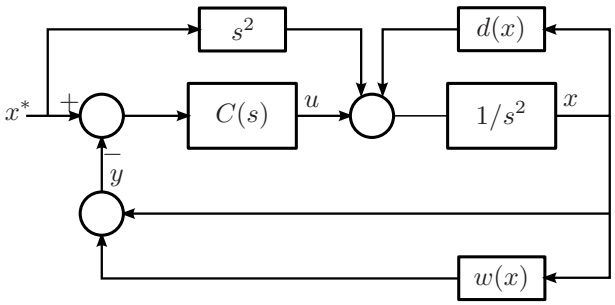

Figure 5.2: Ironless motor driven by PID controller.

A brushless linear motor, whose load is much lighter than the base on which it is mounted, is modeled by the equation (1.11). Furthermore assume that high quality ball bearings are used, viscous friction is neglected and:

$$\begin{aligned} \ddot{\xi} &= u + d(\xi) - \frac{f}{m}\text{sign}\left(\dot{\xi}\right) \\ y &= \xi + w(\xi), \end{aligned} \tag{5.1}$$

with two ξ-periodic functions d and w respectively modeling forces and interpolation errors. According to the chapter 4, suppose they are given by:

$$d(\xi) = \sum \lambda_n \sin\left(\omega_n \xi + \varphi_n\right) \quad \text{and} \quad w(\xi) = \sum \lambda'_n \sin\left(\omega'_n \xi + \varphi'_n\right). \tag{5.2}$$

The magnitudes and phases are still unknown, and, from now on, so are the pulsations ω_n and ω'_n.
Observe the same example was treated as an illustration throughout the chapter 3, except it was driven by a PD controller and we only took into account a pure sine perturbation force. In the presence of dry friction, it is though more suited to drive this motor with a casual PID controller together with a feedforward term on the reference acceleration, as illustrated on the figure 5.2. Let ξ^* denote the reference trajectory, $e = \xi - \xi^*$ the tracking error and $C(s)$ the transfer function of the PID controller, the command u is given by:

$$u = C(s)(\xi^* - y) + s^2\xi^* = C(s)(e + w) + s^2\xi^*. \tag{5.3}$$

According to the figure 5.2, open the loops involving the nonlinear functions d and w, and, in these conditions, one defines $\mathcal{S}$ (respectively $\mathcal{T}$) the transfer function from the output of the block $d(\xi)$ (respectively the block $w(\xi)$) to the tracking error $e = \xi - \xi^*$. In other words, $\mathcal{S}$ matches the sensitivity of the closed loop to perturbation forces, and $\mathcal{T}$ the sensitivity to measurement errors:

$$\mathcal{S}(s) = \frac{1}{s^2 + C(s)} \quad \text{and} \quad \mathcal{T}(s) = \frac{C(s)}{s^2 + C(s)}. \tag{5.4}$$

For a representative setting of the PID controller, the magnitudes of the transfer functions $\mathcal{S}$ and $\mathcal{T}$ are plotted on figure 5.3.

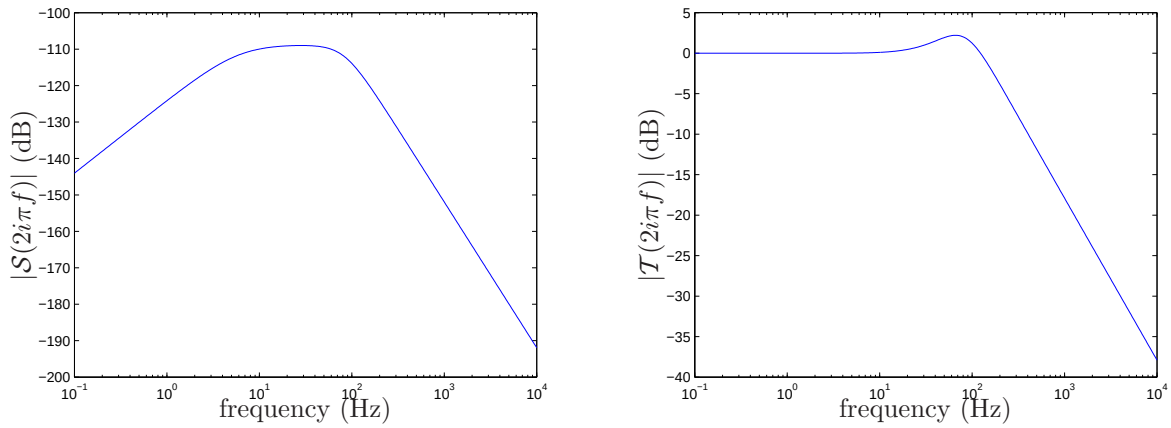

(a) (b)

Figure 5.3: Magnitudes of $\mathcal{S}$ (a) and $\mathcal{T}$ (b) for a recommended setting $K_p = 300e^3$, $K_i = 10e^6$ and $K_d = 800$.

5.2.2 Spatial pulsations estimation

As illustrated in the section 3.5.4, when the motor is required to track a constant velocity trajectory $x^* = \nu^* t$, the spatially periodic functions generate oscillations around the desired trajectory. The corresponding frequencies may be measured from Fourier transforms of the tracking error e, and the spatial pulsations may thus be easily obtained. Let's illustrate this point.

The tracking error e is the output of a system affected by two spatially periodic functions, as illustrated on figure 5.2. We mimic the equation (3.35) and e solves the following formal relation:

$$e = \mathcal{S}(s)d(\xi) + \mathcal{T}(s)w(\xi),$$

We neglect the term allowing for the initial conditions in (3.35), which simply amounts to supposing the system in steady state.

From the theorem 3.4, the first order term of the regular perturbation analysis is given by:

$$\mu e^{(1)} = \mathcal{S}(s)d(\xi^*) + \mathcal{T}(s)w(\xi^*),$$

where we recall $x^* = \nu t$.

According to the bode's diagrams of the figure 5.3, the perturbation force d is significantly softened by the transfer function $\mathcal{S}$. Moreover, as expected, the norm of $\mathcal{T}$ is close to 1, but w is a very small magnitude function. Thus, the parameter μ (as defined by the equation (3.37)) takes a very small value in comparison to its allowable upper value μ^* (defined by (3.41)). The remark 3.3.2 together with the figure 3.2 allows us to state that the high order terms of the expansion of the tracking error are probably insignificant compared to the first. Once the system is in steady state, it pretty relevant (and convenient) to assume:

$$\begin{aligned} e \approx \mu e^{(1)} = &\sum |\mathcal{S}(i\omega_n\nu^*)|\,\lambda_n \sin\Big(\omega_n\nu^* t + \varphi_n + \arg\left(\mathcal{S}(i\omega_n\nu)\right)\Big) \\ &+ \sum |\mathcal{T}(i\omega'_n\nu^*)|\,\lambda'_n \sin\Big(\omega'_n\nu^* t + \varphi'_n + \arg\left(\mathcal{T}(i\omega'_n\nu^*)\right)\Big). \end{aligned} \tag{5.5}$$

The pulsations of the force d and the measurement error w may be determined independently from each other by two successive experiments:

- Set $\nu \lll 1$. Observe on the figure 5.3 that, no matter how small λ'_n is with respect to λ_n, in the expression (5.5), if ν is set to a small enough value, the terms $|\mathcal{T}(i\omega_n\nu^*)|\,\lambda'_n$ dominate the terms $|\mathcal{S}(i\omega_n\nu^*)|\,\lambda_n$. We conclude that a Fourier transform of the tracking error at low speed allows to estimate the ω'_n.

- Set $\nu \ggg 1$. Since the ω'_n is approximately 1000 times larger than the ω_n, when the velocity is set to large values, the tracking error is mainly made up of components whose frequencies are located at $\omega_n\nu^*$. For instance, as mentioned in the chapter 1, it is very representative to suppose:

  $$\omega_n \approx \frac{2\pi}{10}\text{rad/mm},\ \lambda_n \approx 1000\text{mm/s}^2 \quad \text{and} \quad \omega'_n \approx \frac{2\pi}{10e^{-3}}\text{rad/mm},\ \lambda'_n \approx 100e^{-6}\text{mm}.$$

  When ν is set to 100mm/s, we actually have:

  $$|\mathcal{T}(i\omega'_n\nu)|\,\lambda'_n \approx 1\text{nm} \quad \text{and} \quad |\mathcal{S}(i\omega_n\nu)|\,\lambda_n \approx 1\mu\text{m}.$$

Remark 5.1 *The previous method yields satisfactory results in practice, however, when computing the Fourier transform of the tracking error, the results have to be cautiously interpreted. Recall the equations giving the first order approximations for a pure sine perturbation (see equation* (3.45)*). We may find a frequency (first order approximation) and its double (second order approximation), even if the perturbation features only one spectral component. If the perturbation has two components with pulsations ω and 2ω, a Fourier transform also leads to the same interpretation, except both are obtained from the first order term, and, none of them is significantly dominating the other.*

5.2.3 Gains tuning

Our observer-based controller is of prime interest for scanning motion, when the motor has to track a constant velocity trajectory. It enables to get rid of the undesirable oscillations highlighted in the section 3.5.4. Yet, this algorithm is also intended (and designed) to achieve precise trajectory tracking during

acceleration and deceleration phases. The case where ν^* is constant is solely interesting to determine the spatial pulsations. From now on, we suppose that ν^* is varying. To solve the LMI optimization problem (4.41), some bounds on the reference velocity have to be given, namely to construct the matrices $\mathcal{A}^{(i)}$ defined by the equation (4.33).

According to the notations of the chapter 4 (see the equation (4.6)), a first attempt would be to set $\underline{\nu}^*$ to zero and $\overline{\nu}^*$ to the desired scanning velocity. By doing so, the LMI optimization fails for it is unfeasible. The pair made up of the matrix $\mathcal{A}(0)$ and $\mathcal{C}$ (both defined by (4.12)) is unobservable.

To circumvent this issue, $\underline{\nu}^*$ is set to a small value close to zero. The experimental results will illustrate that no instability is witnessed when the reference speed varies from 0 to $\underline{\nu}^*$, although the stability is *a priori* not guaranteed. Also note that it takes little time for the reference speed to vary from 0 to a small $\underline{\nu}^*$ since the achievable acceleration are pretty high for the considered high-end motors.

To ease the LMI optimization, we also use the following hint. The pair $(\mathcal{A}(\underline{\nu}^*), \mathcal{C})$ is actually hardly observable. It may lead to numerical difficulties to expect the system to have the same decay-rate to zero for $\nu^* = \overline{\nu}^*$ and for $\nu^* = \overline{\nu}^*$. As a tentative explanation, consider linear stationary systems for which unobservability means that the poles cannot be placed arbitrarily. In the end, we basically solve the equation (4.41) by varying α according to the reference velocity. Indeed, for our example, for $\mathcal{A}^{(i)} = \mathcal{A}(\overline{\nu}^*)$, replace α by a quite large value $\overline{\alpha}$, while, for $\mathcal{A}^{(i)} = \mathcal{A}(\underline{\nu}^*)$, α is set to a rather close to zero value $\underline{\alpha}$. By doing so, the LMI formulation remains tractable and we also satisfies the implicit requirement of quickly rallying the reference trajectory during the constant velocity scanning phases.

We are using The Yalmip interface [28] to code these LMI problems. The Yalmip formalism is pretty convenient as it allows to test different LMI solvers, namely, we have tested CSDP [8, 9], DSDP [4, 5] and SeDuMi [47]. They all seem to perform the same.

5.3 Experimental results

For a PID controller, we have showed that interpolation errors are limiting only at low speed (say $<$ 10mm/s), whereas cogging forces are insignificant. The converse conclusion may be drawn for high velocity (say $>$ 100mm/s). We assume that it holds for the observer-based controller, which is tuned to cancel either forces or measurement errors. The parameters used for the following experimental results are listed in the tables 5.1(a) and 5.1(b).

5.3.1 Ironless motor

Interpolation errors cancellation

We first consider a low speed trajectory (plotted on figure 5.4(c)) to emphasize the efficiency of the interpolation errors cancellation. Measurements of the true tracking error is required for the purpose of this study. The motor is equipped with an external interferometer, while the standard optical scale is used to control the motor (according to the context depicted in the chapter 1).

motor	setting	ν^* bounds mm/s		decay-rate		spatial periods mm				
		$\overline{\nu}^*$	$\underline{\nu}^*$	$\overline{\alpha}$	$\underline{\alpha}$	P_1	P_2	P_3	P'_1	P'_2
ironless motor	*low velocity (a)*	0.1	1	50	1				$4e^{-3}$	
	low velocity (b)	0.1	1	50	1				$4e^{-3}$	$2e^{-3}$
	high velocity	300	10	20	0.1	42	21			
ironcore motor	*high velocity*	500	20	20	0.1	24	16	12		

(a) Observer-based controller.

motor	K_p	K_i	K_d
ironless motor	$300e^3$	$10e^6$	800
ironcore motor	$120e^3$	$15e^6$	800

(b) PID controller

Table 5.1: Controller parameters.

To determine the spatial periods of the interpolation error, on the figure 5.4(d), we plot the Fourier transform of the tracking error during the constant velocity phase while the motor is controlled by a PID. It seems there are two fundamental periods, namely $P'_1 = 4\mu$m and $P'_2 = 2\mu$m. It is also quite interesting to note that some peaks around 1.3μm and 1μm are also present in this Fourier transform. So far, given their magnitudes, it cannot be deduced whether they result from higher order terms of the expansion. This point is discussed in the following.

When the motor is driven by the observer-based controller allowing for only one pulsation ($P'_1 = 4\mu$m), a Fourier transform of the resulting tracking error shows that the peak around (2μm) is not canceled (see the figure 5.4(g)). This clearly confirms our first impression, $P'_2 = 2\mu$m is well a fundamental period and we move on to the observer-based setting of the table 5.1 allowing for both these fundamental periods. As witnessed on the figures 5.4(g) and 5.4(h), our solution manages to entirely get rid of these two peaks, while, looking at 5.4(f), the peak around 1.3μm remains. We thus have another fundamental period. Its influence is not significant enough to tune our observer-based scheme to cancel it.

Let's now have a look at the figure 5.4(a). The overall precision seen by the interferometer is dramatically improved. This figure also shows that the system quickly rallies its reference trajectory, even within the acceleration phase. On the detailed view of the figure 5.4(b), corresponding to he constant velocity phase, the gain is even more obvious. The high frequency remaining in the red curve matches the interpolation error of the interferometer itself. The command sent (figure 5.4(e)) is clearly filtered. It prevents the

motor from heating by avoiding unnecessary high frequency current references. It also quite noticeably removes the whistle sound caused by this motor at low speed.

Electrical currents offsets

The main state-periodic phenomenon affecting ironless motors operating at high velocity is generated by the electrical offsets. The interpolation errors are small enough to be neglected, and the position measurements are provided by the optical scale. There is no need for an interferometer.
For the reference trajectory presented on the figure 5.5(c), when using a PID controller, the resulting tracking error and its Fourier transform are plotted on the figures 5.5(a) and 5.5(b). The two peaks located at $P_1 = 42mm$ and $P_2 = 21mm$ are used to tune the observer gains. Note that these periods are strongly related to the magnetic pitch ($42mm$) of this motor. Our solution clearly outperforms the PID controller, during the constant velocity phase as well as during the acceleration phases. The tracking error is ten times smaller than the one resulting from the use of the PID controller. Quite interestingly, at first sight, the commands sent to the motor are almost identical (see the figure 5.5(d)). However, on the figure 5.5(e), though slight, the phase difference of the signals generated by the observer-based controller causes an important gain in terms of positioning precision.

5.3.2 Ironcore motor

We now move on to the control of an ironcore motor along a high speed trajectory (500mm/s). This motor is pretty sturdy and may thus withstand higher velocity motion. The most striking fact on the figure 5.6(a) is the pretty whimsical behavior of the tracking error when the motor is driven by the PID controller. The spectral content of the tracking error is pretty intricate as depicted by the figure 5.6(b). The oscillations generated by the electrical offsets were stationary, with constant magnitudes. We are now facing a completely different situation. The Fourier transform suggest to use three periods to tune the observer, namely $P_1 = 24mm$, $P_2 = 12mm$ and $P_3 = 16mm$. Note that the first two are once again related to the magnetic pitch of this motor (24mm).
The robustness of our control scheme to perturbations that do not entirely comply with the position periodic assumption is proved. The cogging forces are completely compensated for. The resulting tracking error is measured to be 20 times smaller than with the PID.

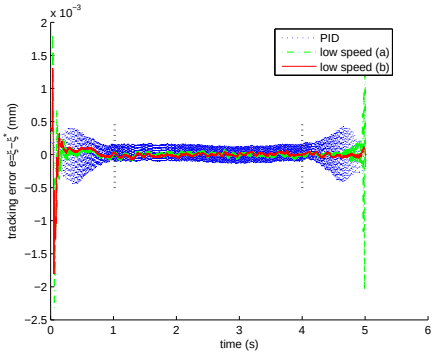

(a) Tracking error.

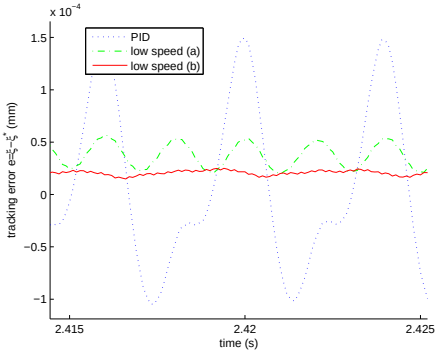

(b) Detailed View of the figure 5.4(a).

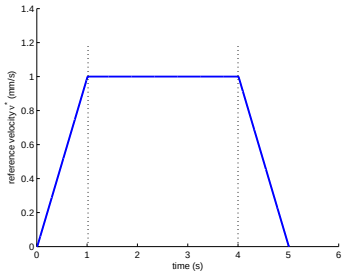

(c) Reference velocity ($\overline{\nu}^* = 1$mm/s).

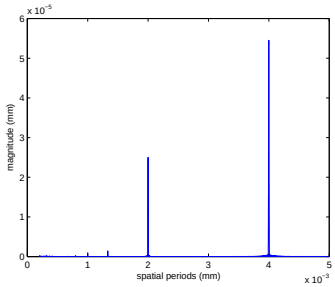

(d) Fourier transform wrt. spatial periods of the tracking error during the constant velocity motion with a PID controller.

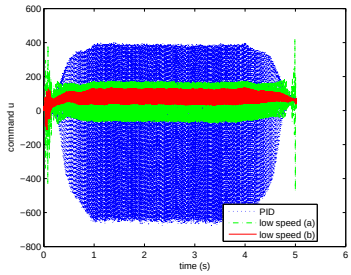

(e) Command u sent to the motor.

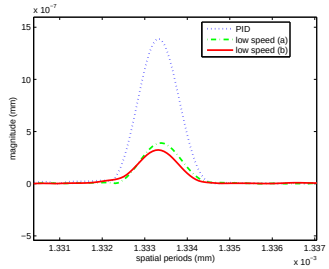

(f) Fourier transforms wrt. spatial periods, during the constant velocity motion, around 1.3μm.

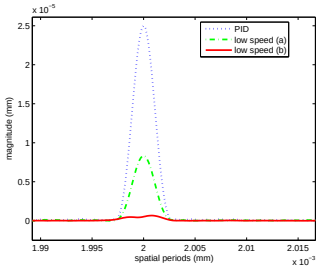

(g) Fourier transforms wrt. spatial periods, during the constant velocity motion, around 2μm.

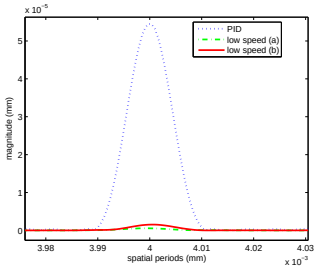

(h) Fourier transforms wrt. spatial periods, during the constant velocity motion, around 4μm.

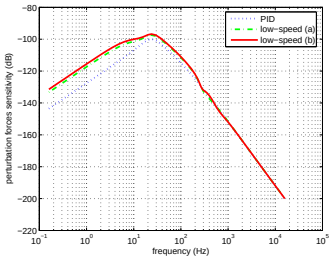

(i) Plant sensitivity to perturbation forces during the constant velocity phase.

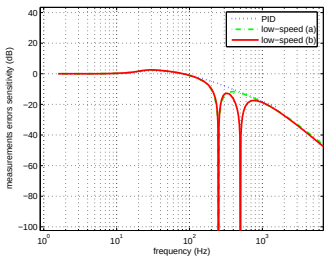

(j) Plant sensitivity to measurements errors during the constant velocity phase.

Figure 5.4: Experimental results for the ironless motor at low speed (1mm/s), successively driven by a PID controller (−), and the observer-based controller according to the *low speed (a)* (−) and *low speed (b)* (−) settings of the table 5.1.

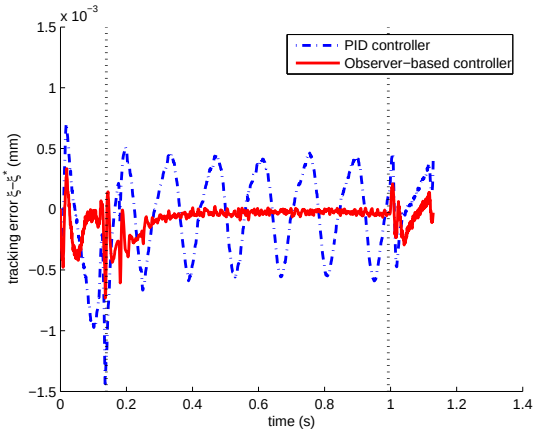

(a) Tracking error.

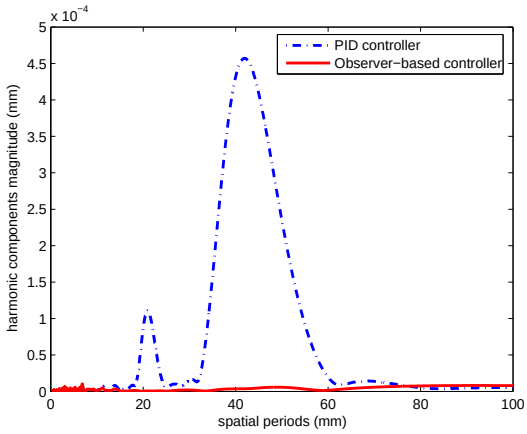

(b) Fourier transform wrt. spatial periods of the tracking error in the constant velocity phase.

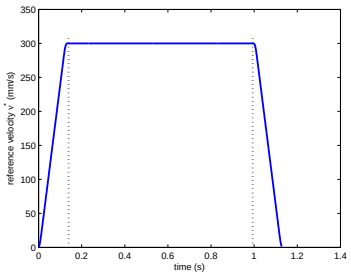

(c) Reference velocity $\overline{v}^* = 300$mm/s.

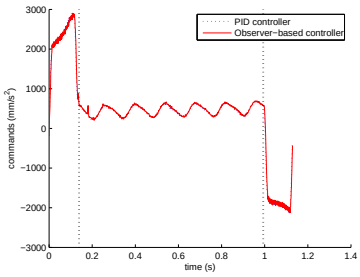

(d) Command u.

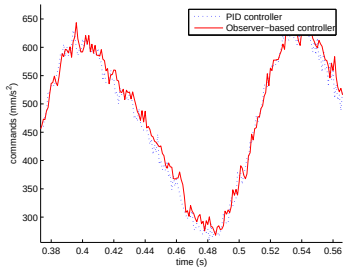

(e) Detailed view of the figure 5.5(d) during the constant velocity motion.

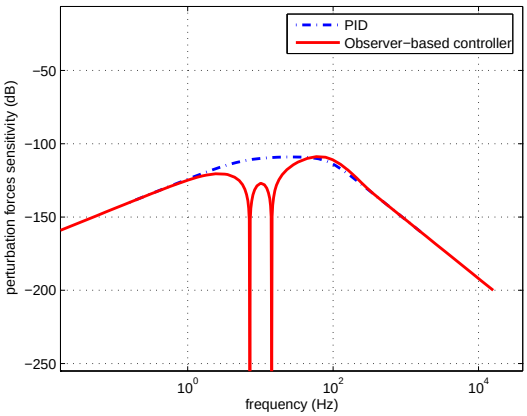

(f) Plant sensitivity to perturbation forces during the constant velocity phase.

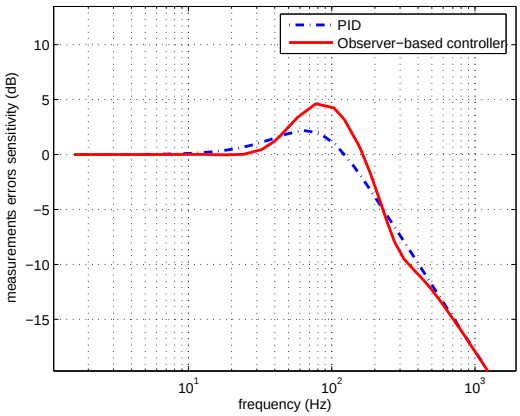

(g) Plant sensitivity to measurements errors during the constant velocity phase.

Figure 5.5: Experimental results for the ironless motor at high velocity (300mm/s) using a PID controller (−) and the observer-based controller for spatially periodic forces cancellation (−).

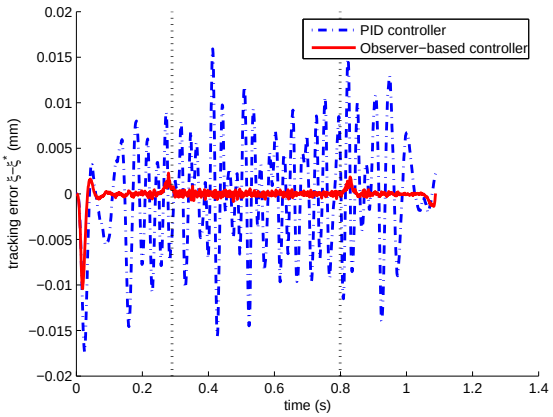

(a) Tracking error.

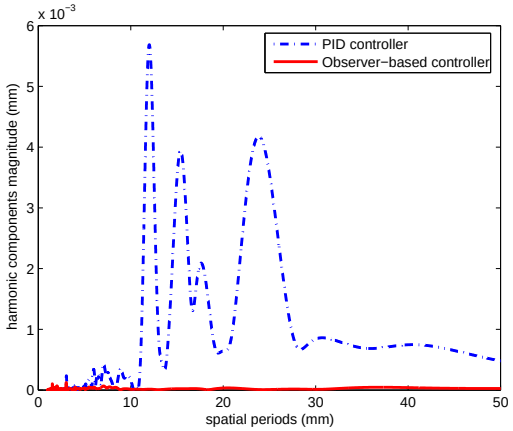

(b) Fourier transform wrt. spatial periods of the tracking error in the constant velocity phase.

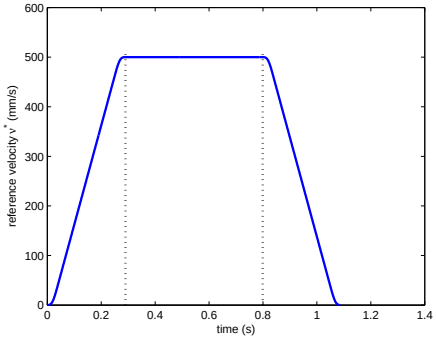

(c) Reference velocity $\overline{v}^* = 500$mm/s.

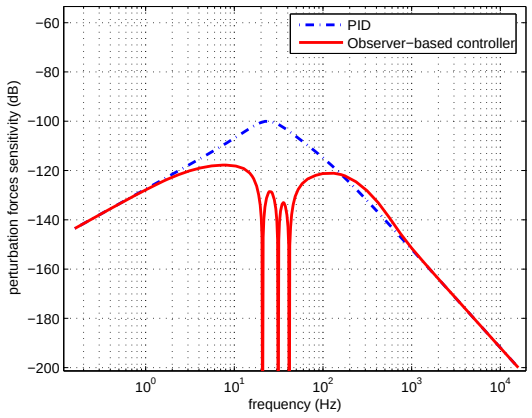

(d) Plant sensitivity to perturbation forces during the constant velocity phase.

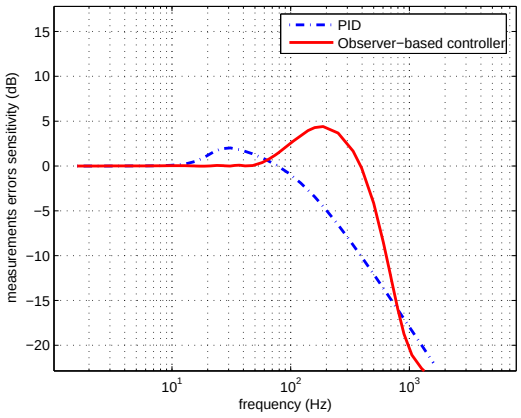

(e) Plant sensitivity to measurements errors during the constant velocity phase.

Figure 5.6: Experimental results for the ironcore motor at high velocity (500mm/s) using a PID controller (−) and the observer-based controller for spatially periodic forces cancellation (−).

Conclusion

Our work contains contributions to theoretical issues, whose technical implications constitute consistent solutions to several problems arising in the manufacturing machines used in the semiconductor industry. Let's draw up a conclusion in the same vein by first recalling the theoretical aspects and then their applications. Consider the theorem 2.1. At first sight, the initial problem consists in integrating twice a casual double integrator featuring dry friction and a periodic command. The study we carried out unveils a very intricate situation. The system reaches periodic orbits that are quite unusual, since some sliding motion phases may occur along them. The theorem states that the nature of the orbit depends upon a single parameter. This is in practice central to accurately initialize brushless motors from the only knowledge of the displacements. This is a material contribution to an unusual problem, as already discussed in the chapter 2.

The chapter 3 also brings several key theoretical elements, particularly the theorem 3.2 that introduces the *Bell polynomials of the second kind*. They are not so common in the control community, but they turn out to be convenient to conduct a full regular perturbation analysis. Any term of the expansion is given in closed form thanks to these polynomials, and, quite interestingly, the radius of convergence as well as the truncation error are estimated. This full regular perturbation analysis allows to derive sufficient conditions for the *global asymptotic stability* of the considered systems. For this reason, the theorem 3.3 may be seen as a generalization of the Lyapunov method for the systems altered by state-periodic disturbances.

This analysis is fruitfully used in the chapter 4 to design an observer-based control scheme. The approach is innovatory since the observer structure hinges upon the regular perturbation analysis. It is showed to match the required expectations in terms of trajectory tracking by making use of the Lyapunov-like theorem. The framework encompasses the cancellation of both measurements errors and perturbation forces affecting the positioning systems used in the semiconductor industry. The results presented in the chapter 5 clearly demonstrates the validity and the efficiency of the design.

No matter how simplistic the modeling used for the gains tuning may seem, the method yields extremely satisfactory results, as highlighted in the chapter 5. For slightly more complex systems, this rough modeling prevents us from tuning the observer-based controller as aggressively and easily. Basically, some unmodeled dynamics turn out to be limiting. For instance, when two linear motors are sandwiched together to move on a horizontal plane, the coupling generates high frequency modes. When they are not taken into account, it is not possible to hound the observer-based scheme into a corner. To circumvent this issue, the modeling has to supplemented with this information. Practically speaking, recall we consider plants made up of an unperturbed part on the one hand, and state-periodic perturbations on the other hand. To extent the validity of the approach, some mechanical modes must be added to the unperturbed part. It is noteworthy to point out that the LMI formalism is perfectly suited to cope with uncertain or time-varying modes. In view of the mechanical sandwiched structure previously mentioned, the damping ratio or, more presumably, the frequency of a given mode are likely to depend on the positions of the motors. It is also unrealistic that these estimated values be not corrupted. The theorems 4.2 and 4.4 require some negativity conditions to be met on the vertices defined by the bounds on the reference velocity. Thus, we may add new vertices depending on the frequencies of the modes. By doing so, the modeling remains valid on a wider frequency domain, and the resulting tuning do not put the stability of the closed into jeopardy.

Let's return to an assumption made in the chapter 1 concerning the currents controller. We assume it tuned in such a way that the currents perfectly rally their references. In practice [6, 7], it may be showed that the electrical windings are affected by back electromotive voltages $\varepsilon\dot{\xi}\sin\left(\frac{2\pi}{P}\xi+\varphi\right)$. To get rid of this voltage, one may design an observer-based controller, allowing for this voltage evaluated along the reference trajectory ξ^*. A proof could rely on a regular perturbation analysis, close to the one done in the chapter 3. However, this case is a little bit more complicated. To carry out a complete regular perturbation analysis, the Bell polynomials of the second kind are still of prime interest to expand the sine function of the position. The next step is to compute the Cauchy product of the previous expansion with the velocity expressed as a power series. It is rather obvious that a fully dedicated study is required given the noticeable complexity. Though, we think that an observer-based controller based on the first order approximation of the back-emf voltages does the job. Namely, replace the actual expression of the perturbation with $\varepsilon\dot{\xi}^*\sin\left(\frac{2\pi}{P}\xi^*+\varphi\right)$ to define the observer structure. Some slight technological changes may be required to allow the autonomous currents controller to be fed with the reference trajectory. Note the online computation burden is not that important.

As a concluding remark, we would like to lay the emphasis on some possible enhancements of the proposed control architecture. First, our observer tuning boils down to some LMI optimization problems. Their feasibility may be regarded as an observability test for the considered observation structure. They turn out to be feasible in most of the situations we considered. However, it may be worth going deeper

into this question, especially since some issues may arise when dealing with systems featuring several mechanical modes, as previously discussed. The gains of the controller L were chosen according to some settings known to yield satisfactory results. We simply supplement the control law with state-periodic perturbations cancellation. Determining the controller gains according to some new criteria may also be a fruitful avenue of research. Finally, the reference trajectory design is not addressed in our work. It may be worth considering existing anti-vibratory techniques of this kind [31, 46]. Actually, the considered motors are usually mounted on moving bases, it is possible to design reference trajectories taking this information into account, and preventing the system from undesired trajectories. The framework of our study allows to accurately track references of any kind. The overall performances may thus be improved by a parallel use of our disturbances rejection method and the reported anti-vibratory trajectory design techniques.

Bibliography

[1] Hyo-Sung Ahn, YangQuan Chen, and Huifang Dou. State-periodic adaptive compensation of cogging and coulomb friction in permanent-magnet linear motors. *IEEE Transactions on Magnetics*, 41(1), January 2005.

[2] Silvano Balemi. Automatic calibration of sinusoidal encoder signals. In *Proceedings of the 16th IFAC World Congress*, Prague, 2005.

[3] Carl M. Bender and Steven A. Orszag. *Advanced Mathematical Methods for Scientists and Engineers I, Asymptotic Methods and Perturbation Theory*. Springer, 1999.

[4] Steven J. Benson and Yinyu Ye. DSDP5: Software for semidefinite programming. Technical Report ANL/MCS-P1289-0905, Mathematics and Computer Science Division, Argonne National Laboratory, Argonne, IL, September 2005. Submitted to ACM Transactions on Mathematical Software.

[5] Steven J. Benson and Yinyu Ye. DSDP5 user guide — software for semidefinite programming. Technical Report ANL/MCS-TM-277, Mathematics and Computer Science Division, Argonne National Laboratory, Argonne, IL, September 2005.

[6] J. Boichot, E. Delaleau, N.V. Diep, J. Lévine, and E. Parzy. Modeling and control of a high-precision positioning system actuated by a linear synchronous motor. In *Proceedings of the IFAC World Congress*, Beijing, Chine, 1999.

[7] J. Boichot, E. Delaleau, N.V. Diep, J. Lévine, and E. Parzy. Modeling and control of a two D.O.F. high-precision positioning system. In *Proceedings of the European Conference on Control*, Karlsruhe, Allemagne, 1999.

[8] B. Borchers. A c library for semidefinite programming. *Optimization Methods and Software*, 11(1):597–611, 1999.

[9] B. Borchers. Csdp 2.3 user's guide. *Optimization Methods and Software*, 11(1):597–611, 1999.

[10] Stephen Boyd, Laurent El Ghaoui, Eric Feron, and Venkataramanan Balakrishnan. *Linear Matrix Inequalities in System and Control Theory*. SIAM, 1994.

[11] Roger W. Brockett. *Finite Dimensional Linear Systems*. John Wiley and Sons, Inc, 1970.

[12] B.H.M Bukkems, D. Kostic, A.G. de Jager, and Steinbuch Maarten. Learning-based identification and iterative learning control of direct-drive robots. *IEEE Transactions on Control Systems Technology*, 2005.

[13] Carlos Canudas de Wit and Laurent Praly. Adaptive eccentricity compensation. *IEEE Transactions on Control Systems Technology*, 8(5), September 2000.

[14] Augustin Louis Cauchy. Mémoire sur les intégrales des systèmes d'équations différentielles et aux dérivées partielles, et sur le développement de ces intégrales en séries ordonnées suivant les puissances ascendantes d'un paramètre que renferment les équations proposées. *Comptes Rendus Hebdomadaires des Séances de l'Académie des Sciences*, 14, 1841.

[15] Earl A. Coddington and Norman Levinson. *Theory of Ordinary Differential Equations*. McGraw-Hill Book Company, 1955.

[16] Louis Comtet. *Advanced Combinatorics: The Art of Finite and Infinite Expansion*. Reidel Publishing Company, 1974.

[17] J.C. Culioli. *Introduction à l'Optimisation*. Ellipses, 1994.

[18] R Dhaouadi, N. Mohan, and L. Norum. Design and implementation of an extended kalman filter for the state estimation of a permanent magnet synchronous motor. *IEEE, Transactions on Power Electronics*, 6:491 – 497, 1991.

[19] Jean Dieudonné. *Calcul Infinitésimal*. Hermann Paris, 1968.

[20] Jean Dieudonné. *Éléments d'Analyse*, volume 1. Fondements de l'Analyse Moderne. Gauthier-Villars, 1969.

[21] Francesco Faa dì Bruno. Note sur une nouvelle formule de calcul différentiel. *Quarterly Journal of Pure and Applied Mathematics*, 1:359 – 360, 1857.

[22] A.F. Filippov. *Differential Equations with Discontinuous Righthand Sides*. Kluwer Academic Publishers, 1988.

[23] John Guckenheimer and Philip Holmes. *Nonlinear oscillations, Dynamical Systems and Bifurcations of Vector Fields*. Springer-Verlag, 1986.

[24] P.L.M. Heydemann. Determination and correction of quadrature fringe measurement errors in interferometers. *Applied Optics*, 20(19):3382–3384, 1981.

[25] Mohammad S. Islam, Sayeed Mir, and Tomy Sebastian. Issues in reducing the cogging torque of mass-produced permanent-magnet brushless dc motor. *IEEE Transactions on Industry Applications*, 40(3), May/June 2004.

[26] Warren P. Jonhson. The curious history of faa dì bruno formula. *American Mathematical Monthly*, 109:217 – 234, 2002.

[27] A.B. Kulkarni and M. Ehsani. A noval position sensor elimination technique for the interior permanent magnet synchronous motor drive. *IEEE, Transactions on Industry Applications*, pages 144 – 150, 1992.

[28] J. Löfberg. Yalmip : A toolbox for modeling and optimization in MATLAB. In *Proceedings of the CACSD Conference*, Taipei, Taiwan, 2004.

[29] Alexandre Liapunoff. *Problème Général de la Stabilité du Mouvement*. Éditions Jacques Gabay, 1988.

[30] K.W. Lim, K.S. Low, and M.F. Rahman. Observers for sensorless control of permanent magnet synchronous motor drive. In *Proceedings of the IFAC World Congress*, pages 431 – 434, Sydney, Australia, 1993.

[31] Jean Lévine and Van Diep Nguyen. Flat output characterization for linear systems using polynomial matrices. *Systems and Control Letters*, 48(1):69–75, 2003.

[32] Jérémy Malaizé. Devices and methods for cogging force cancellation in linear motors, 2007.

[33] Jérémy Malaizé, Roger Desailly, Jean Lévine, Franck Duquenoy, and Daniel Gvero. Apparatus and method for estimation of initial phase of a brushless motor, 2006.

[34] Jérémy Malaizé and Jean Lévine. Active estimation of the initial phase for brushless synchronous motors. In *Proceedings of the 9th IEEE International Worshop on Advanced Motion Control*, Istanbul, Turkey, 2006.

[35] Jérémy Malaizé and Jean Lévine. Estimation active de la phase initiale des moteurs synchrones. In *Actes de la Conférence Internationale Française d'Automatique*, 2006.

[36] R.J.E. Merry, M.J.G van de Molengraft, and Maarten Steinbuch. Iterative learning control with wavelet filtering. *International Journal of Robust and Nonlinear Control*, 2007.

[37] T. Noguchi, K. Yamada, S. Kondo, and I. Takahashi. Initial rotor position estimation method of sensorless PM motor with no sensitivity to armature resistance. *IEEE, Transactions on Industrial Electronics*, 45:118 – 125, 1998.

[38] S. Ogasawara and H. Agaki. An approach to real time position estimation at zero and low speed for a PM motor based on saliency. In *IEEE, Proceedings of the Industry Applications Society Annual Meeting*, pages 29 – 35, 1996.

[39] S. Ostlund and M. Brokemper. Sensorless rotor-position detection from zero to rated speed for an integrated PM synchronous motor drive. *IEEE, Transactions on Industry Applications*, 32:1158 – 1165, 1996.

[40] Gerco Otten, J. A. Theo de Vries, Job van Amerongen, M. Adrian Rankers, and W. Erik Gall. Linear motor motion control using a learning feedforward controller. *IEEE/ASME transactions on mechatronics*, 2(3), September 1997.

[41] Henri Poincaré. *Mécanique Céleste, Tome I.* Librairie Scientifique et Technique Albert Blanchard, 1987.

[42] Henri Poincaré. *Mécanique Céleste, Tome II.* Librairie Scientifique et Technique Albert Blanchard, 1987.

[43] P.B. Schmidt, M.L. Gasperi, G. Ray, and A.H. Wijenayake. Initial rotor angle detection of a non-salient pole permanent magnet synchronous machine. In *IEEE, Proceedings of the Industry Applications Society Annual Meeting*, pages 459 – 463, 1997.

[44] L.M. Silverman. Transformation of time-variable systems to canonical (phase-variable) form. *IEEE Transaction on Automatic Control*, 1966.

[45] L.M. Silverman and H.E. Meadows. Controllability and observability in time-variable linear systems. *SIAM Journal on Control*, 1967.

[46] N. Singer, W. Singhose, and W. Seering. Comparison of filtering methods for reducing residual vibration. *European Journal of Control*, 5:208–218, 1999.

[47] Jos F. Sturm. Using sedumi 1.02, a matlab toolbox for optimization over symmetric cones. *Optimization Methods and Software*, pages 625–653, 1999.

[48] K. K. Tan, S. N. Huang, and T. H. Lee. Robust adaptive numerical compensation for friction anf force ripple in permanent-magnet linear motor. *IEEE Transactions on Magnetics*, 38(1), January 2002.

[49] Kok Kiong Tan and Kok-Zuea Tang. Adaptive online correction and interpolation of quadrature encoder signals using radial basis functions. *IEEE Transactions on Control Systems Technology*, 13(3):370 – 377, 2005.

[50] Eric Temple Bell. Partition polynomials. *Annals of Mathematics*, 19:38 – 46, 1927.

[51] K. van Berkel, I. Rotariu, and Maarten Steinbuch. Cogging compensating piecewise iterative learning control for variable setpoints with application to a wafer stage. In *Proceedings of the 26th American Control Conference*, New-York, 2007.

[52] Milton Van Dyke. *Perturbation Methods in Fluid Mechanics*. Academic Press, New York and London, 1964.

[53] Jiabin Wang, David Howe, and Geraint W. Jewel. Fringing in tubular permanent-magnet machines: Part I, magnetic field distribution, flux linkage, and thrust force. *IEEE Transactions on Magnetics*, 39(6), September 2003.

[54] Jiabin Wang, David Howe, and GeraintW. Jewel. Fringing in tubular permanent-magnet machines: Part II, cogging force and its minimization. *IEEE Transactions on Magnetics*, 39(6), November 2003.

[55] Xiuhe Wang, Yubo Yang, and Dajin Fu. Study of cogging torque in surface-mounted permanent magnet motors with energy method. *Journal of magnetism and magnetic materials*, 267, 2003.

[56] William A. Wolovich. On the stabilization of controllable systems. *IEEE Transaction on Automatic Control*, 1968.

APPENDIX A

Periodic orbits classification

A.1 Proof of the property 3

We first show that τ_0 is necessarily located between β and $1-\alpha$. Referring to the variations of the figure 2.6, f_λ is strictly increasing from α to β, then strictly decreasing beyond β. The only chance to solve $f_\lambda(\tau_0) = f_\lambda(\alpha)$ in τ_0 is to have τ_0 greater than β. On this domain, given the variations 2.6, showing that $\tau_0 < 1-\alpha$ is equivalent to proving $f_\lambda(\tau_0) - f_\lambda(1-\alpha) > 0$:

$$f_\lambda(\tau_0) - f_\lambda(1-\alpha) = f_\lambda(\alpha) - f_\lambda(1-\alpha) = v_0(\alpha) - \lambda\alpha - v_0(\alpha) - \lambda\alpha + \lambda = \lambda(1-2\alpha) > 0.$$

The previous inequality resulting from $\alpha \leq 1/2$, as witnessed on the figure 2.4.
For any x between β and $1-\alpha$, we compute the derivative of $f_\lambda(x) - f_\lambda(\alpha)$ with respect to λ. Recall that α depends on λ, while x is a fixed value:

$$\frac{d}{d\lambda}\left(f_\lambda(x) - f_\lambda(\alpha)\right) = -x - \left(\frac{d\alpha}{d\lambda}\left(u_0(\alpha) - \lambda\right) - \alpha\right) = -(x-\alpha) < 0. \tag{A.1}$$

We now have all the necessary elements to prove that τ_0 is decreasing with λ. Consider two scalars λ' and $\lambda'' > \lambda'$, α' and α'' (respectively β' and β'') the corresponding values of α (respectively β). Suppose also x' and x'' given by:

$$f_{\lambda'}(x') = f_{\lambda'}(\alpha') \quad \text{and} \quad f_{\lambda''}(x'') = f_{\lambda''}(\alpha''). \tag{A.2}$$

Thanks to the equation (A.1), since $f_{\lambda'}(x') - f_{\lambda'}(\alpha') = 0$, we eventually get:

$$f_{\lambda''}(x') - f_{\lambda''}(\alpha'') \leq 0. \tag{A.3}$$

If we use the definitions (A.2), we arrive at $f_{\lambda''}(x') \leq f_{\lambda''}(x'')$. Since $f_{\lambda''}$ is decreasing, $x'' \leq x'$ and this proves that τ_0 is a decreasing function in λ.

The property 1 states that for $\lambda = \lambda_1$, the curves of f_λ and h_λ intersects in $\tau^* = 1-\beta$ and so $f_\lambda(1-\beta) = h_\lambda(1-\beta)$. Since $\lambda_1 \leq \lambda_2$, according to the property 2, the relation $h_\lambda(1-\beta) = -f_\lambda(\beta) \leq f_\lambda(\alpha)$ holds and then:

$$f_{\lambda_1}(1-\beta) = h_{\lambda_1}(1-\beta) = -f_{\lambda_1}(\beta) \leq f_{\lambda_1}(\alpha) = f_{\lambda_1}(\tau_0),$$

Since f_λ is decreasing on $[\beta, 1]$, for $\lambda = \lambda_1$, $\tau_0 < 1-\beta$. It can be checked on the figure 2.4 that $1-\beta$ is an increasing function of λ, and it has just been showed that τ_0 is a decreasing function of λ. As a consequence, τ_0 remains in the interval $[\beta, 1-\beta]$ for all $\lambda \geq \lambda_1$.

A.2 Proof of the property 4

Checking that an interval $I_\lambda = [a, b]$ meets the point (iii) comes down to the both following properties:

- the image of the interval $[a, b]$ by the mapping h_λ is included in the image of the same interval by the mapping f_λ, since on $[1-\beta, 1-\alpha]$, h_λ is increasing and f_λ decreasing, this is basically equivalent to:

$$f_\lambda(b) \leq h_\lambda(a) \leq h_\lambda(b) \leq f_\lambda(a), \tag{A.4}$$

- the image of the set $[0, a] \cup [b, 1]$ by the mapping f_λ does not intersect the image of $[a, b]$ by the mapping h_λ.

Adopting the notations of the property 3, for $\lambda \leq \lambda_1$, τ_0 may belong either to $[1-\beta, 1-\alpha]$ or $[\beta, 1-\beta]$. These two cases are treated separately and depicted on the figure A.1:

- $\tau_0 \geq 1-\beta$: we have $f_\lambda(\tau_0) = f_\lambda(\alpha) \geq f_\lambda(\tau^*)$ and since f_λ is decreasing beyond β, τ_0 is necessarily smaller than τ^*. As a consequence, $h_\lambda(\tau_0) \leq f_\lambda(\tau_0)$, and according to the definition 2.3, we also have:

$$f_\lambda(\tau_0) = f_\lambda(\alpha) \leq 0 \leq -f_\lambda(\alpha) = h_\lambda(1-\alpha).$$

  Define $a = \tau_0$, there exists b between a and $1-\alpha$ such that $h_\lambda(b) = f_\lambda(a)$. The definition of b yields:

$$v_0(a) + v_0(b) = \lambda(1 + a - b).$$

  To check that a and b satisfies the equation (A.4), we use the previous equation to study the sign of $f_\lambda(b) - h_\lambda(a)$:

$$f_\lambda(b) - h_\lambda(a) = v_0(b) - \lambda b + v_0(a) + \lambda a - \lambda = 2\lambda\,(a - b) < 0.$$

  The inequality holds since $b > a = \tau_0$.

  We now prove that the images of $[a, b]$ by f_λ and h_λ do not intersect outside $[a, b]$. Consider any y such that $y < a = \tau_0$. We have $f_\lambda(y) > f_\lambda(\alpha) = f_\lambda(a) > h_\lambda(b)$. The function h_λ is increasing for any x in $[a, b]$, therefore $f_\lambda(y) > h_\lambda(b) > h_\lambda(x)$. Consider now any y such that $y > b$. We have

$f_\lambda(y) < f_\lambda(b) < h_\lambda(a) < h_\lambda(x)$ for all x in $[a, b]$. This ends proving the point (iii). Given the way the interval I_λ is built, (i) is also verified. Concerning (ii), since f_λ and h_λ are respectively decreasing and increasing, if the relations (A.4) are fulfilled, the plots of f_λ and h_λ necessarily intersects in $[a, b]$.

- $\tau_0 \leq 1 - \beta$: define $a = 1 - \beta$. According to the property 1, f_λ intersects h_λ in τ^* greater than $a = 1 - \beta$. An immediate consequence is:

$$f_\lambda(a) = f_\lambda(1 - \beta) > h_\lambda(1 - \beta) = h_\lambda(a). \tag{A.5}$$

Moreover, we have $1 - \beta = a > \tau_0$ and $f_\lambda(\tau_0) = f_\lambda(\alpha) < 0$. As f_λ is decreasing, we also have:

$$f_\lambda(a) < 0 < h_\lambda(1 - \alpha). \tag{A.6}$$

If we combine (A.5) and (A.6), we show that there exists $b > a$ between $1 - \beta$ and $1 - \alpha$ (the point (i) is then verified) such that $h_\lambda(b) = f_\lambda(a)$. Since f_λ and g are strictly monotone, we furthermore show that $\tau^* \in [a, b]$ ((ii) is also fulfilled). We check the conditions (A.4) by calculations similar to the case $\tau_0 > 1 - \beta$. Finally, for any x in $[a, b]$:

$$\begin{array}{rcl} \forall y,\ 0 \leq y \leq \alpha & , & f_\lambda(y) \geq f_\lambda(\alpha) = f_(\tau_0) \geq h_\lambda(b) \geq h_\lambda(x) \\ \forall y,\ \alpha \leq y \leq a & , & f_\lambda(y) \geq f_\lambda(a) \geq h_\lambda(b) \geq h_\lambda(x) \\ \forall y,\ b \leq y \leq 1 & , & f_\lambda(y) \leq f_\lambda(b) \leq h_\lambda(a) \leq h_\lambda(x), \end{array}$$

which ends proving (iii).

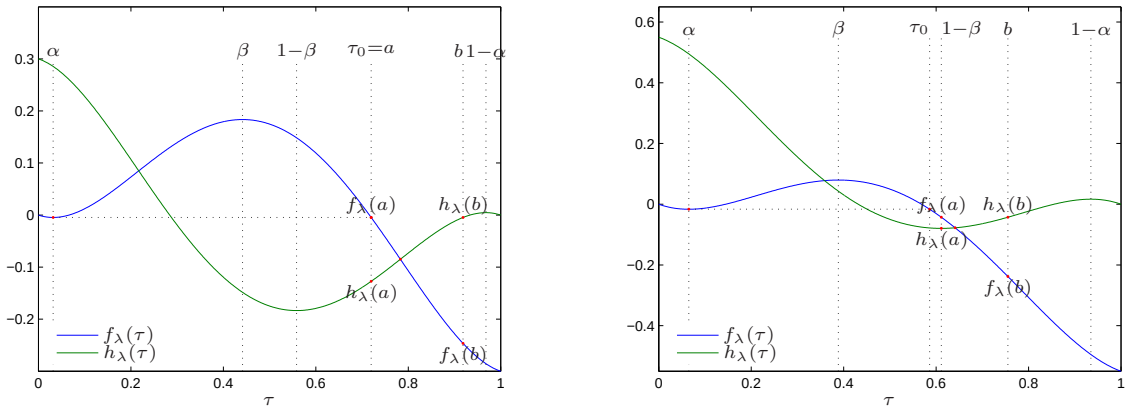

$1 - \beta \leq \tau_0 \leq 1 - \alpha$ $\qquad$ $\beta \leq \tau_0 \leq 1 - \beta$

Figure A.1: Construction of the intervals I_λ.

A.3 Proof of the property 5

For $\lambda \leq \lambda_1$, the property 4 is used to show that for any $u_n \in I_\lambda$, one may find u_{n+1} in the same interval such that $f_\lambda(u_{n+1}) = h_\lambda(u_n)$. This proves that if the first terms of the series belongs to I_λ, the next terms remain within I_λ.

For any interval I_λ defined by the property 4, the situation is similar to the one depicted on the figure A.2. f_λ is decreasing and h_λ increasing on I_λ and they intersect in $\tau^* \in I_\lambda$. Thus, if $u_n < \tau^*$, for any $u \in I_\lambda$ such that $u < \tau^*$, $f_\lambda(u) > h_\lambda(u_n)$, u_{n+1} is necessarily greater than τ^*. Conversely, if $u_n > \tau^*$, for any $u \in I_\lambda$ such $u > \tau^*$, $f_\lambda(u) < h_\lambda(u_n)$, u_{n+1} is necessarily less than τ^*. The terms of the series u_n are thus alternatively greater and less than τ^*.
Let's define $\tilde{v}_n = v_0(u_n) - v_0(\tau^*)$. The relation $f_\lambda(u_{n+1}) = h_\lambda(u_n)$ may also be expressed as:

$$v_0(u_{n+1}) - \lambda u_{n+1} = -v_0(u_n) - \lambda u_n + \lambda.$$

According to the definition of τ^* by the equation (2.6), the following substitution $\lambda = 2v_0(\tau^*)$ holds and thus, the previous equation is rewritten into:

$$\tilde{v}_{n+1} = -\tilde{v}_n + \lambda\,(u_{n+1} - u_n)\,. \tag{A.7}$$

Suppose $u_n > \tau^*$. Since v_0 is decreasing on I_λ (see figure 2.5), we have $v_0(u_n) < v_0(\tau^*) < v_0(u_{n+1})$. Therefore $\tilde{v}_n < 0 < \tilde{v}_{n+1}$ and $u_{n+1} < u_n$. The equation (A.7) may be rewritten in:

$$|\tilde{v}_{n+1}| = \tilde{v}_{n+1} = -\tilde{v}_n + \lambda\,(u_{n+1} - u_n) = |\tilde{v}_n| - \lambda|u_{n+1} - u_n| < |\tilde{v}_n|. \tag{A.8}$$

Now suppose than $u_n < \tau^*$. We now have $v_0(u_n) < v_0(\tau^*) < v_0(u_{n+1})$. This now implies $\tilde{v}_{n+1} < 0 < \tilde{v}_n$ and $u_{n+1} > u_n$ so that:

$$|\tilde{v}_{n+1}| = -\tilde{v}_{n+1} = \tilde{v}_n - \lambda\,(u_{n+1} - u_n) = |\tilde{v}_n| - \lambda|u_{n+1} - u_n| < |\tilde{v}_n|. \tag{A.9}$$

We have just proved through the equations (A.8) and (A.9) that $|\tilde{v}_n|$ is decreasing. We also know that $|\tilde{v}_n$ is bounded from below. It may be concluded that $|\tilde{v}_n$ converges. Since the u_n's belong to I_λ where v_0 is continuous and strictly monotone, the series u_{2p} and u_{2p+1} respectively converge to $\tau^* + l_+$ and $\tau^* + l_-$. The recurrence equations $f_\lambda(u_{2p+1}) = h_\lambda(u_{2p})$ and $f_\lambda(u_{2p+2}) = h_\lambda(u_{2p+1})$ may now be rewritten for $p \to \infty$:

$$v_0(\tau^* + l_-) - \lambda(\tau^* + l_-) = -v_0(\tau^* + l_+) - \lambda(\tau^* + l_+) + \lambda \tag{A.10}$$

$$v_0(\tau^* + l_+) - \lambda(\tau^* + l_+) = -v_0(\tau^* + l_-) - \lambda(\tau^* + l_-) + \lambda. \tag{A.11}$$

Subtracting the equation (A.11) to (A.10) yields that $l_+ = l_- = l$. If we then add the equation (A.11) to (A.10), l turns out to fulfill $v_0(\tau^* + l) = \lambda/2$. Necessarily $l = 0$ and $u_n \to \tau^*$.

A.4 Proof of the property 6

For any λ greater than λ_1, f_λ and h_λ intersects within $[\beta, 1-\beta]$ and thus:

$$h_\lambda(1-\beta) > f_\lambda(1-\beta). \tag{A.12}$$

Moreover, when λ is less than λ_2, from the property 2, it may be deduced that $h_\lambda(1-\beta) \leq f_\lambda(\alpha) \leq 0 \leq f_\lambda(\beta) = -h_\lambda(1-\beta)$, or, more interestingly:

$$h_\lambda(1-\beta) < f_\lambda(\beta). \tag{A.13}$$

If we combine the equations (A.12) and (A.13) together with f_λ being strictly monotone on $[\beta, 1-\beta]$, we conclude that the equation $f_\lambda(y) = h_\lambda(1-\beta)$ admits a unique roots y on the interval $[\beta, 1-\beta]$.

Moreover, for any y in $[0, \beta]$, $f_\lambda(y)$ is greater than $f_\lambda(\alpha)$, itself greater than $h_\lambda(1-\beta)$ according to the property 8. For any y in $[1-\beta, 1]$, f_λ, as a decreasing function, is less than $f_\lambda(1-\beta)$, the latter being also less than $h_\lambda(1-\beta)$ according to the property 7. This results into the equation $f_\lambda(y) = h_\lambda(1-\beta)$ having only one root y on $[0, 1]$ and y lies within $[\beta, 1-\beta]$.

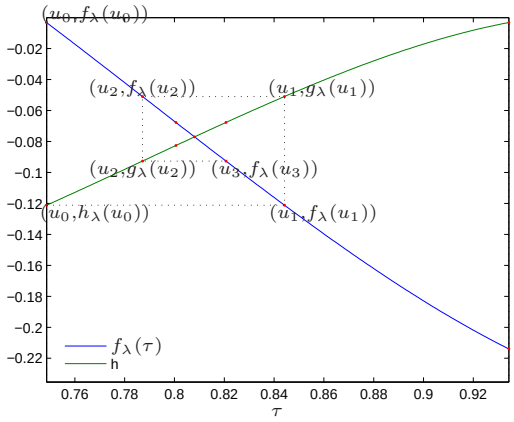

Figure A.2: Convergence of the series u_n to τ^*.

A.5 Proof of the property 7

Since g_λ is decreasing within $[1-\beta, 1-\alpha]$ and that I_λ lies within this interval, for any $x \in I_\lambda$ and any $y \in [x, 1-\alpha]$, $g_\lambda(y) < g_\lambda(x)$. If a solution y to the equation $g_\lambda(y) = g_\lambda(x)$, y lies necessarily between $1-\alpha$ and 1. However, for any $x \in I_\lambda$:

$$g_\lambda(x) = v_0(x) + \lambda x - \lambda + \lambda = -h_\lambda(x) + g_\lambda(1),$$

and I_λ is such that $h_\lambda(x) \leq 0$. This implies that $g_\lambda(x) > g_\lambda(1)$, and thus, for any y between $1-\alpha$ and α where g_λ is increasing,

$$g_\lambda(x) > g_\lambda(1) > g_\lambda(y),$$

which ends proving this property.

A.6 Proof of the property 8

For the same reasons as previously, if $g_\lambda(y) = g_\lambda(x)$ has a root y for any $x \in I_\lambda$, then y lies necessarily within $[1-\alpha, 1]$. For $\lambda \leq \lambda_2$, according to the property 2 and the definitions of the functions f_λ g_λ and h_λ by (2.5), $f_\lambda(\alpha) + f_\lambda(\beta) = f_\lambda(\alpha) - h_\lambda(1-\beta) \geq 0$ and then:

$$g_\lambda(1-\beta) - g_\lambda(1) = -h_\lambda(1-\beta) > -f_\lambda(\alpha) > 0.$$

We conclude than for any y in $[1-\alpha, 1]$ where g_λ is increasing, $g_\lambda(1-\beta) > g_\lambda(1) > g_\lambda(y)$.

A.7 Proof of the property 9

Suppose first that $h_\lambda(1-\beta) \leq 0$, since $\lambda \geq \lambda_2$, we get:

$$f_\lambda(\alpha) \leq h_\lambda(1-\beta) \leq 0 = f_\lambda(0).$$

We conclude about the existence of a unique y in $[0, \alpha]$ such that $f_\lambda(y) = h_\lambda(1-\beta)$. For reasons previously mentioned in the proof of the property 8, if $h_\lambda(1-\beta) \leq 0$, the equation $g_\lambda(z) = g_\lambda(1-\beta)$ has no root z lying within $[1-\beta, 1]$.
Let's suppose now that $h_\lambda(1-\beta) > 0$. For any y in $[0, \alpha]$, $f_\lambda(y) \leq 0 \leq h_\lambda(1-\beta)$, there is no root y in $[0, \alpha]$ to the equation $f_\lambda(y) = h_\lambda(1-\beta)$. We still use $h_\lambda(1-\beta) > 0$ to get:

$$g_\lambda(1) - g_\lambda(1-\beta) = h_\lambda(1-\beta) \geq 0.$$

Moreover $g_\lambda(1-\beta) > g_\lambda(1-\alpha)$ since g_λ is decreasing between $1-\beta$ and $1-\alpha$. Thus, we can find z lying within $[1-\alpha, 1]$ such that $g_\lambda(z) = g_\lambda(1-\beta)$.

APPENDIX B

Bell polynomials of the second kind

B.1 Definition

Consider two integers n and r such that $n \geq 1$ and $1 \leq r \leq n$. The Bell polynomial of the second kind $\mathcal{B}_{n,r}$, sometimes referred to as the incomplete Bell polynomial, is given by [50, 16]:

$$\mathcal{B}_{n,r}\left(x_1, \ldots, x_{n-r+1}\right) = \sum \frac{n!}{j_1! \ldots j_{n-r+1}!} \left(\frac{x_1}{1!}\right)^{j_1} \cdots \left(\frac{x_{n-r+1}}{(n-r+1)!}\right)^{j_{n-r+1}}, \tag{B.1}$$

with the summation extending for all non negative integers j_i such that:

$$j_1 + \ldots + j_{n-r+1} = r \quad \text{and} \quad j_1 + 2j_2 + \ldots + (n-r+1)j_{n-r+1} = n. \tag{B.2}$$

For two given n and r, to construct this polynomial, one first has to list the different ways of splitting the integer n into r non empty subsets. This yields a combination $(j_1, \ldots, j_{n-r+1})$ to be used in (B.1).
For instance, consider the case $n = 6$ and $r = 3$. The different partitions of the integer 6 in 3 parts are the followings:

- $6 = 4 + 1 + 1$, and for this combination the only non-zero j_i's are $j_1 = 2$ and $j_4 = 1$,
- $6 = 3 + 2 + 1$, and for this combination the only non-zero j_i's are $j_1 = 1$, $j_2 = 1$ and $j_3 = 1$,
- $6 = 2 + 2 + 2$, and for this combination the only non-zero j_i is $j_2 = 3$.

If we eventually apply the formula (B.1):

$$\mathcal{B}_{6,3}\left(x_1, x_2, x_3, x_4\right) = 15x_1^2x_4 + 60x_1x_2x_3 + 15x_2^3.$$

The coefficients of the Bell polynomials of the second kind may be proved to bear a combinatorial meaning. As can be checked on the previous example, the coefficient of the monomial $x_1^{j_1} x_2^{j_2} \ldots x_{n-r+1}^{j_{n-r+1}}$ corresponds

to the number of partitions of a set made up of n indistinguishable elements into r subsets with respectively j_i elements.

B.2 Properties

We now review some properties that do not depend on the choice of n and r:

1. $\mathcal{B}_{n,r}(x_1, \ldots, x_{n-r+1})$ is homogeneous of degree r in x_i.
2. The coefficients of the different monomials are positive.
3. $\forall \alpha > 0, \quad \mathcal{B}_{n,r}(\alpha x_1, \ldots, \alpha x_{n-r+1}) = \alpha^r \mathcal{B}_{n,r}(x_1, \ldots, x_{n-r+1})$.
4. $\forall i,\ 1 \leq i \leq n-r+1, \quad 0 \leq x_i \leq y_i \quad \Longrightarrow \quad \mathcal{B}_{n,r}(x_1, \ldots, x_{n-r+1}) \leq \mathcal{B}_{n,r}(y_1, \ldots, y_{n-r+1})$.
5. $\|\mathcal{B}_{n,r}(x_1, \ldots, x_{n-r+1})\| \leq \mathcal{B}_{n,r}(\|x_1\|, \ldots, \|x_{n-r+1}\|)$.

For any given n and r, the summation appearing in (B.1) extends over all elements of the set defined by (B.2), the property (i) is thus trivial. As an immediate consequence of (B.1), the coefficients of the monomials are strictly positive which yields the property (ii). According to the combinatorial interpretation previously mentioned, these coefficients can be proved to be integers. The property (iii) results from (i). Considering (iv), if the x_i's are positive and bounded by y_i, according to (ii), the conclusion is immediate. The property (v) is implied by both the triangle inequality and the Bell polynomials of the second kind having only positive coefficients.

APPENDIX C

Some results on analytical functions

C.1 Analyticity of the solutions of a differential equation

In both Poincaré [41] and Lyapunov [29] seminal works, the following theorem on the analyticity of the solution of a differential equation is attributed to Cauchy. It may be quite complicated to find some references by Cauchy directly presenting it. See however [14] for a sketch of the proof. A complete, though radically different, proof may be found in [15] and [20]. Note that these approaches are less informative than the genuine one suggested by Cauchy. They completely rely on tools of the complex functions analysis, and the expansion of the solution in power series is guaranteed by some high level theorems. On the other hand, according to the Cauchy's method, the series are directly showed to converge, almost by hand.

C.1.1 Cauchy's theorem

Theorem C.1: *Let $f(x, \varepsilon, t) : \mathbb{R}^n \times \mathbb{R} \times \mathbb{R}_+ \to \mathbb{R}^n$ be an analytical function with respect to x and ε for all time t in $[0, T]$, and any $T > 0$. For any initial conditions $x_0 \in \mathbb{R}^n$ in $t = 0$, the solution of the following differential equation*

$$\dot{x} = f(x, \varepsilon, t) \tag{C.1}$$

can be expressed as a power series in ε for all t in $[0, T]$ and ε small enough.

This theorem states the existence of functions $x^{(n)} : \mathbb{R}_+ \to \mathbb{R}^n$ such that the solution x of the equation (C.1) admits the following representation:

$$\forall t,\ 0 \leq t \leq T, \quad x(t) = \sum_{n \geq 0} x^{(n)}(t) \frac{\varepsilon^n}{n!}. \tag{C.2}$$

In order to fulfill the initial conditions, one gets:

$$\sum_{n\geq 0} x_n(0)\frac{\varepsilon^n}{n!} = x_0,$$

which, thanks to the uniqueness of power series expansions, readily yields

$$x^{(0)}(0) = x_0, \quad \forall n \geq 1,\ x^{(n)}(0) = 0. \tag{C.3}$$

We give a sketch of the corresponding proof:

1. Suppose that such functions $x^{(n)}$ exist, and that the series they define formally satisfies the equation (C.1) with initial conditions (C.3). It is possible to exhibit an *a priori* expression of the $x^{(n)}$'s.

2. One has to check *afterward* that the previously defined functions allow to build a power series satisfying the differential equation (C.1).

This is a rather classical way of proving such a theorem and we suggest to illustrate it in the following.

C.1.2 Cauchy's method

Suppose there exist some differentiable functions $x^{(n)}$ such that the series $\sum_{n\geq 0} x^{(n)}\frac{\varepsilon^n}{n!}$ formally satisfies the equation (C.1). This means it is possible to invert the series summation and the derivation operators. Basically, these assumptions have to be checked in a second time. Provided such a substitution may be performed, one gets:

$$\forall t, 0 \leq t \leq T, \quad \sum_{n\geq 0} \dot{x}^{(n)}\frac{\varepsilon^n}{n!} = f\left(\sum_{n\geq 0} x^{(n)}\frac{\varepsilon^n}{n!}, \quad \varepsilon, \quad t\right) = f^*(\varepsilon, t).$$

The function f^* results from the composition of two analytical functions. Therefore, f^* is analytical with respect to ε for any t and ε small enough. It may more precisely be showed that the following triangular structure is obtained:

$$f^*(\varepsilon, t) = \sum_{n\geq 0} f_n\left(x^{(n)}, \ldots, x^{(0)}, t\right)\frac{\varepsilon^n}{n!}. \tag{C.4}$$

Combining the equation (C.4) with the differential equation (C.1), one eventually gets

$$\sum_{n\geq 0} \dot{x}^{(n)}\frac{\varepsilon^n}{n!} = \sum_{n\geq 0} f_n\left(x^{(n)}, \ldots, x^{(0)}, t\right)\frac{\varepsilon^n}{n!}.$$

Using the uniqueness of the power series expansions yields:

$$\begin{aligned} \dot{x}^{(0)} &= f_0\left(x^{(0)}, t\right) \\ \dot{x}^{(1)} &= f_1\left(x^{(1)}, x^{(0)}, t\right) \\ \dot{x}^{(n)} &= f_n\left(x^{(n)}, \ldots, x^{(1)}, x^{(0)}, t\right), \quad \forall n \geq 2, \end{aligned} \tag{C.5}$$

together with the initial conditions (C.3).

C.1.3 Validation

The functions given by (C.5) have to fulfill certain properties for the series they define to be the solution of the equation (C.1). The initial conditions are obviously satisfied, but one needs some very strong properties to invert series summation and differentiation. Namely the series $\sum_{n\geq 0} x^{(n)}\frac{\varepsilon^n}{n!}$ has to converge and the series $\sum_{n\geq 0} \dot{x}^{(n)}\frac{\varepsilon^n}{n!}$ has to be uniformly converging. In these conditions:

$$\begin{aligned}\sum_{n\geq 0} \dot{x}^{(n)}\frac{\varepsilon^n}{n!} &= \sum_{n\geq 0} f_n\left(x^{(n)},\dots,x^{(0)},t\right)\frac{\varepsilon^n}{n!}\\ &= f\left(\sum_{n\geq 0} x^{(n)}\frac{\varepsilon^n}{n!},\varepsilon,t\right)\\ &= \frac{d}{dt}\left(\sum_{n\geq 0} x^{(n)}\frac{\varepsilon^n}{n!}\right),\end{aligned}$$

The last line is due to the uniform convergence of $\sum_{n\geq 0} \dot{x}^{(n)}\frac{\varepsilon^n}{n!}$. This ends proving that, under these assumptions related to series convergence, the series $\sum_{n\geq 0} x^{(n)}\frac{\varepsilon^n}{n!}$ solves equation (C.1).

C.2 Analytical functions composition

As previously mentioned, to compute the functions $x^{(n)}$, the composition of two analytical functions has to be expressed in power series. This can be done using the Faa dì Bruno formula [21], entirely based on the Bell polynomials of the second kind discussed in the appendix B. A complete survey of the different existing formulations may be found in [26].

Theorem C.2: *Consider the two following analytical functions:*

- *f analytical with respect to x such that $f(x)=\sum_{n\geq 0} f_n\frac{x^n}{n!}$,*
- *x analytical with respect to ε such that $x(\varepsilon)=\sum_{n\geq 1} x_n\frac{\varepsilon^n}{n!}$.*

The function resulting from the composition $f\circ x$ is analytical with respect to ε and, for ε small enough:

$$(f\circ x)(\varepsilon) = f_0 + \sum_{n\geq 1}\left(\sum_{r=1}^{n} f_r \mathcal{B}_{n,r}\left(x_1,\dots,x_{n-r+1}\right)\right)\frac{\varepsilon^n}{n!}, \tag{C.6}$$

where the $\mathcal{B}_{n,r}$'s are the Bell polynomials of the second kind given by (B.1).

C.3 Analyticity of the roots of an algebraic equation

We end this review with the expansion of the root of an algebraic equation in power series, namely the Lagrange's inversion theorem, that one may find in [19].

Theorem C.3: *Let $f : \mathbb{R} \to \mathbb{R}$ be a scalar function of x, analytical for $|x| \leq x^*$ and $M = \sup_{x=x^*} |f(x)|$. Thus, for all $\varepsilon \in \mathbb{R}$ such that $|\varepsilon| \leq \varepsilon^* = x^*/M$, the equation*

$$x = \varepsilon f(x)$$

has only one root $x = h(\varepsilon)$, with h analytical for $|\varepsilon| < \varepsilon^*$. Moreover the following expansion is converging for $|\varepsilon| < \varepsilon^*$:

$$\forall \varepsilon,\ |\varepsilon| < \varepsilon^*, \quad h(\varepsilon) = \sum_{n \geq 1} \frac{\varepsilon^n}{n!} \left(\frac{d^{n-1}}{dx^{n-1}} \left(f(x)^n \right) \right)_{x=0}. \tag{C.7}$$